UCLouvain

AGRO LOUVAIN

Faculty of Bioscience Engineering

Characterisation of a coating composed of LL-37-heparin complexes and study of its antibacterial activity

Master Thesis

Author: Alix Mertens de Wilmars

Supervisors: Prof. Christine Dupont

Ir. Cédric Vranckx

Readers: Prof. Sophie Demoustier

Prof. Françoise Van Bambeke

Academic Year: 2019-2020

Thesis presented in partial fullfilment of the requirements for the degree of Master in bioengineering: chemistry and bioindustries

Acknowledgements

While conducting this master thesis, I have received help and support from a number of people to whom I would like to express my gratitude.

First of all, I would like to thank Prof. Christine Dupont for allowing me to conduct my master thesis in her laboratory. It was a real opportunity to work in such a dynamic and instructive environment. I especially thank her for her precious and positive advice and help on many subjects, and her availability even during the more difficult period of sanitary crisis.

I would also like to thank my supervisor Cédric Vranckx, who was been there since day one to show me all the tips and tricks of the lab and guide me throughout my whole master thesis. His daily and precious help, availability and feedback were essential for the successful carry-out of this work. I wish him the best of luck for the rest of his thesis and for the future.

I also thank Prof. Sophie Demoustier and Prof. Françoise Van Bambeke for being part of my master thesis jury and taking the time to read and evaluate my work.

I would like to express my gratitude to Pierre Eloy, for his very didactive explanations and help with the XPS. I also thank Hervé Poilvache who welcomed me in Woluwe and helped me with all the bacterial tests. I also thank Naïma Sallem and Prof. Alain Jonas for their help with the ellipsometer.

Above all, a big thanks to the whole laboratory team who have always been eager to help and for their good vibes throughout the year. It was a great experience to work with you in the lab. Thanks to Benjamin, Thomas and Maxime for the good atmosphere and the breakfasts in the morning. I wish them all succes in their future projects!

Finally, I thank my father for the proofreading and the last useful advices.

Contents

List of Figures

List of Tables

List of abbreviations

AFM Atomic force microscopy

AMP Antimicrobial peptide

BEA Biofilm eradication agent

BSA Bovine serum albumin

CFU Colony Forming Unit

CHI Chitosan

DD Degree of deacetylation

DNA Deoxyribonucleic acid

ECM Extracellular matrix

ELISA Enzymatic-linked immunosorbent assay

EPS Extra polymeric substances

GAG Glycosaminoglycane

HEP Heparin

I Ionic strength

LBL Layer-by-layer

MHB Mueller Hinton Broth

MIC Minimal inhibitory concentration

PAH Poly(allylamine hydrochloride)

PBS Phosphate-buffered saline

PE Polyelectrolyte

PEG Polyethylene glycol

PET Poly(ethylene terephthalate)

PJI Prosthetic joint infection

PPC Protein-polyelectrolyte complex

PSS Poly(styrenesulfonate)

QCM-D Quartz crystal microbalance with dissipation

SAM Self-assembled monolayer

SDS Sodium dodecyl sulfate

THA Total hip arthroplasty

TSA Trypticase soy agar

XPS X-ray photoelectron spectroscopy

Part I

Motivation and context of the study

Joint replacement is a life-enhancing procedure for many people worldwide. Ageing of the population and the global rise in life quality result in an increasing incidence of hip and knee replacement surgeries. However, these surgeries can go along with complications which are a big burden for patients life quality and for the global health care industry. Infection of the replaced joint or loosening of the implant are examples of complications suffered by patients, and ongoing efforts are thus made to improve the properties of the devices implanted in our body.

Great attention must therefore be given to the manufacturing of the implant: the materials are selected for their high mechanical strength, good biocompatibility and bioactivity, the design and positioning of the different elements must be defined carefully, and the surface properties are important to control the response of the body to the newly implanted device. In this context, a thesis project has been developed by Cédric Vranckx in the laboratory of Prof. Christine Dupont (BSMA), that consists in improving the surface properties of implants with the final goal to reduce bacterial infections and promote the integration of the implant into the body by means of a coating. This coating integrates the antimicrobial peptide LL-37, which has proven to possess excellent antibacterial and antibiofilm properties against microorganisms involved in prosthetic joint infection.
This work is thus part of the ongoing thesis of C. Vranckx, and focuses on the LL-37 integration and activity inside the coating, the characterisation of the coating and its response to bacterial infection.

The multidisciplinary aspect of the subject combined with the concrete final biomedical utility and application motivated me to take part in this project. Life sciences and more particularly microbiology and biomolecular engineering have always awoken my interest and curiosity, and this project was the perfect opportunity to combine the microbiological and surface characterisation aspects, in a dynamic and well-equiped laboratory.

In the next section, the objectives of this work will be clearly defined through the formulation of the research questions, and the global strategy to conduct this research will be presented. Then, the state of the art of the subject will be exposed in order to have a better understanding of the biological and chemical context. In the following part, the experimental methods and the used materials are described, followed by the obtained results. These results will be discussed, interpreted and compared with literature, and in a general discussion, they will be replaced in the biological context and linked together in a more general overview. Finally, the main conclusions of this work will be drawn and future perspectives will be explored in the last section.

Part II

Objectives and strategy

Considering the rising incidence of bacterial infections after hip or knee replacement surgeries, new methods have been investigated to improve the implant properties and reduce the rate of post-operative infections. To this end, a PhD project was proposed by Cédric Vranckx that consists in developing a coating for titanium implants that would prevent bacterial adhesion and infection on the implant surface and promote osseointegration. The use of protein-polyelectrolyte complexes as building blocks for the immobilisation of the antimicrobial peptide LL-37 into the coating is investigated. The present master thesis was carried out in the context of this PhD project. More specifically, the objective of this work is to study the use of the antimicrobial agent LL-37 into the coating set-up developed by C. Vranckx, to measure its anti-bacterial activity and determine its efficiency.
Other aspects of the coating such as its integration into the body are also part of the global problematic and must thus be kept in mind but will not be discussed in detail in this work. The design of the coating and its construction have already been studied by C. Vranckx while its interaction with bone cells for optimal integration into the body has been covered previously by R. Hardy in his master thesis. [1].

Figure 1 depicts the set-up of the coating. The substrate on which the coating is constructed is the ELI titanium alloy, Ti6Al4V, which is a very common material for orthopaedic implant design. The designed coating is made of successively adsorbed layers of polyelectrolytes assembled following a method called layer-by-layer (LBL), which will be further detailed in this work. This LBL method allows the immobilisation of an antimicrobial peptide, the LL-37, by complexation with a polyelectrolyte to form a protein-polyelectrolyte complex (PPC). This peptide has proven to possess significant antimicrobial and antibiofilm activity against the main pathogens involved in prosthetic joint infection.
To improve the antibacterial activity and the osseointegration of the coating even more, chitosan and heparin are selected as the building polyelectrolytes of the multilayer.

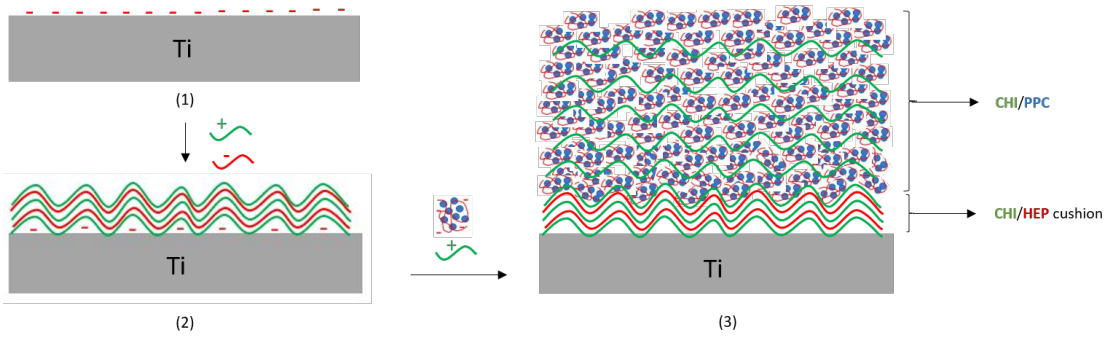

Figure 1: Schematic representation of the layer set-up. The green and red lines represent chitosan and heparin molecules respectively, while the blue dot is the LL-37 peptide.

This work is composed of two main parts. The first part aims at describing how the coating was formed and focusing on the surface characterisation of the obtained film. The purpose of this characterisation is twofold: firstly, to validate the method and obtain a better understanding of the layers architecture. Secondly, to investigate a causal relationship between the design of the multilayer and its antimicrobial activity. Indeed, the multilayer composition and organisation will certainly have an impact on its ability to prevent infections. The quantification of LL-37 in the multilayers through enzymatic tests was planned as well, but due to the sanitary conditions linked to the Covid-19 pandemic, this part of the work could unfortunately not be completed. A relative quantification was carried out instead by estimating the proportions of the peptide to the other components of the coating.
Several methods and devices were used to characterise the coating. Quartz crystal microbalance with dissipation (QCM-D) was used to monitor the growth of the layers in situ and determine the mass adsorbed and indirectly the thickness. Ellipsometry was used for this last purpose as well. X-Ray photoelectron spectroscopy (XPS) allowed the chemical composition of the layers to be determined.

Then, the second part of this work focuses on the role of LL-37 into the coating. The behaviour and antibacterial activity of the peptide in its complexed state on the one hand and of the free peptide in solution on the other hand will be compared. This will help to determine whether the complexed state of LL-37 and its configuration into the multilayers have an influence on the activity of the coating, and if a release in the environment of the peptide has to be considered to improve its bactericidal action. The effect of the coating on bacterial adhesion and biofilm formation will be measured as well.
Hence, the goal of this research is to provide a better insight on the presence, mechanism, activity and potential of LL-37 into the designed coating.

Part III
State of the art

1 Context

1.1 Total hip arthroplasty

Nowadays, ageing of the population in our western society leads us to face many new challenges in different domains. The medical sector is one of them, having to deal with increasing medical problems caused by malfunctions of the body related to ageing. Medical devices are constantly designed and implemented to improve the quality of life of these elderly patients. One of these devices is the prosthetic joint. This implant replaces the hip or knee joint of a patient and is implemented by a surgical procedure known as hip or knee arthroplasty. Severe arthritis pain or fractures can be treated using this procedure. In Belgium alone, 274 hip replacement surgeries were performed per 100 000 inhabitants in the year 2017, making it one the most common surgical procedures [2]. As can be extracted from the 2017 report of Orthopride, 79% of the primary hip replacement surgeries in Belgium were performed on people aged 60 or above. [3]
Over the last few years, an increasing incidence of arthroplastic surgeries was observed. Pabinger et al. found a 23% rise in the total number of hip arthroplasties performed between 2005 and 2011 in OECD countries, and this number has kept rising since then. [4]

Most of the time, arthritis is the reason for total hip arthroplasty (THA). The different forms of this disease, including osteoarthritis, rheumatoid arthritis or post-traumatical arthritis all involve damage of the cartilage cushioning the hip bones. Without this cushion, the bones start to rub against each other, which causes pain to the patient. Surgery known as total hip arthroplasty allows removal of the damaged bone and cartilage and replacement by prosthetic components. As shown on Figure 2, the implant is composed of different parts. The femoral stem is placed into the hollow center of the femur after removal of the damaged femoral head, which is replaced by a metal or ceramic ball.
The hip is a so-called 'ball-and-socket' joint. The cartilage surface of the socket is called the acetabulum, and is replaced with a metal socket. Screws or cement are sometimes used to hold the socket in place. To allow a smooth gliding surface, a plastic, ceramic, or metal spacer is inserted between the ball and the socket. [5]

The success rate of THA at ten years or longer exceeds 95% [6, 7]. However, several reasons can cause failure of the surgery. The Belgian Hip and Knee Arthroplasty Registry reports that the main causes for hip arthroplasty failure in 2017 were identified as aseptic loosening (34%), instability (15.9%) and prosthetic joint infection, also referred to as PJI (13.5%) [3]. These complications result in a second revision surgery, which is very heavy for the patient and often has a less favourable outcome than a primary total arthroplasty.

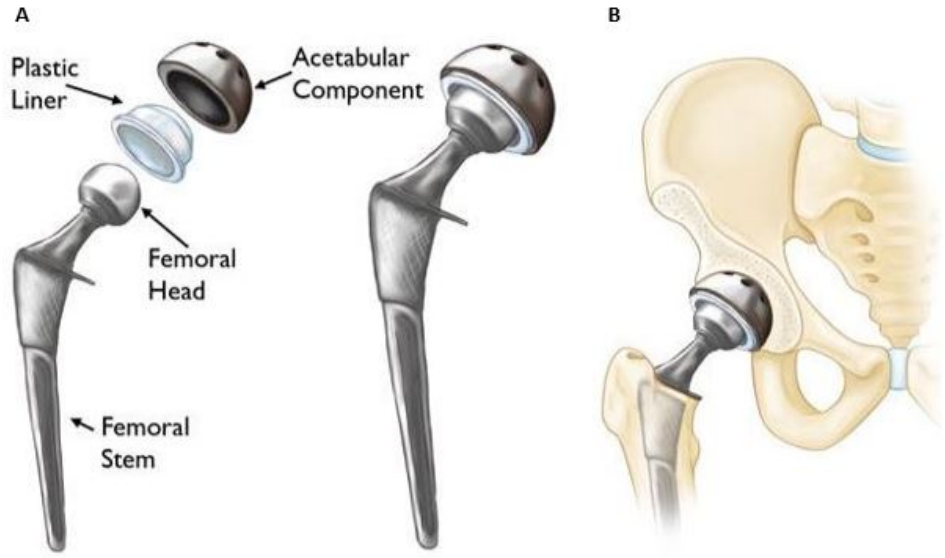

Figure 2: (A) The individual components of a hip replacement prosthesis. (B) The implant as it fits into the hip. Reproduced from the American Academy of Orthopaedic Surgeons [5].

The major cause of hip replacement failure is thus aseptic loosening. This occurs when the implant, that was once firmly attached to the bone, loosens. This can be due to failed osseointegration, in which case fibrous tissue is formed at the bone-implant interface. The bond between implant and bone is then weakened, resulting in a painful hip. The reasons for failed osseointegration are not always clear, but can involve the biocompatibility of the implant, its design, the bone quality, component malpositioning etc. Therefore, choosing biocompatible materials that promote osseointegration of the implant in the body, is of primary importance. [8]
Furthermore, wear debris, generated at the prosthetic joint surface, can cause a biological response known as osteolysis around the implant. Inflammation reactions and phagocytosis of the particles activate cellular pathways that result in destruction of periprosthetic bone tissue, which subsequently leads to loosening of the implant. Excessive motion and physical stress as well as poor initial implant fixation accelerate the erosion and the formation of wear debris. [9]

1.2 Prosthetic joint infection

Aside from aseptic loosening, prosthetic joint infection consists in another possible complication of hip replacement surgeries. According to a study conducted by Ong et al., the incidence of infection for patients that did undergo a total hip arthroplasty was 1.63% within 2 years and 0.5% between 2 and 10 years [10]. PJI is defined by Tande et al. as an "infection involving the joint prosthesis and adjacent tissue" [11]. Bacteria attach in and around the surface of the prosthesis, and form biofilms which are very difficult to eradicate.

Different medical and surgical strategies are possible to treat PJI, and the goal of the treatment is to eradicate the infection, relieve the pain for the patient and restore the function of the joint, while keeping

mortality rates as low as possible. Depending on the infecting microorganism, the symptoms and the patient, different strategies include debridement with prosthesis retention, removal of the prosthesis with or without reimplantation, amputation, or antimicrobial suppression without surgery. The reimplantation can occur at the same time as the removal or can be delayed by weeks to month. This two-stage revision surgery is the most frequent and involves removal of the implant, treatment of the patient for infection and a second surgery to implant a second device. A study on 929 patients confirmed that this treatment has a success rate of 89% [11]. Hence, the need for a second or even third surgery results in higher morbidity rates and a high cost for the health care system. Indeed, compared to other causes of revisions like aseptic loosening, patients who suffer PJI require more hospital visits and longer stays which results in greater hospital costs.

1.2.1 Infection mechanisms

There are different categories of infections, depending on the time since the surgery and the infection mode, that are summarised in Table 1. The most frequent cause of infection is perioperative and occurs when microorganisms are introduced in the body at the time of the surgery, during the implantation of the prosthesis. They colonise the surface and form biofilms that are very difficult to eradicate. A low inoculum is sufficient to cause an infection: it has been shown that $< 10^2$ CFU of *Staphylococcus aureus* will be able to attach to the device, proliferate and secrete biofilms. Symptoms of the infection can then be perceived directly after the surgery (early PJI) or after more than 3 months (delayed PJI), depending on the virulence of the inoculated mircroorganisms. Early PJI can more frequently be treated with debridement procedures where the implant is not removed [11].

Table 1: Classification schemes of PJI. Reproduced from Gemmel et al. [12]

Classification according to the route of infection	Pathogenesis	According to the onset of symptoms	Microorganisms
Perioperative	Inoculation of microorganisms into the surgical wound during implantation or immediately thereafter	Early PJI (<3 months): acute onset of symptoms with fever—systemic symptoms—wound secretion, typical for surgical site infection	$> \frac{3}{4}$ staphylococci; other gram-pos. species; gram-neg. bacilli
		Delayed PJI (3–24 months): prolonged indolent course with a subtle presentation, persistent joint pain, mimicker of aseptic condition	Low-virulence organisms such as coagulase-negative staphylococcus and *Propionibacterium acnes*
Contiguous	Wound contamination due to penetrating trauma (open fractures) or from an adjacent focus of infection (skin and soft tissue lesions)	Delayed PJI (3–24 months): subacute presentation with sometimes sinus tract formation, prolonged wound secretions	Low-virulence organisms such as coagulase-negative staphylococcus and *Propionibacterium acnes*; gram-neg. rods
Haematogenous	Microbial spread through blood or lymph from a distant focus of infection (e.g. skin, lung, dental & urinary tract)	Late PJI (> 24 months): acute onset of symptoms of infection in a previously well-functioning joint	> Staphylococci (*S. aureus* in 50%), *Escherichia coli*, polymicrobial and exotic organisms

Secondly, infection may spread from an infected site at an adjacent location to the prosthesis and is then called contiguous. This typically occurs from 3 months to 2 years after the surgery, which classifies the infection as a delayed PJI. Superficial surgical site infection can progress and reach the implant shortly after the surgery, or even disruption of the tissue by trauma, fractures or lesions can cause an infection to spread. Finally, bacteria can spread through the blood or lymph: this is called haematogeneous seeding. This infection pathway is more rare and often involves *S. aureus*.[11]

1.2.2 Microorganisms involved in PJI

In order to determine the best strategy to fight PJI, the microorganisms responsible for infection and their mechanisms of action should first be investigated. Several microbiological studies were conducted to determine the types of microorganisms involved and their frequency and time of occurrence. Table 2 shows the principal organisms responsible for PJI, for early infections and over all time periods.

Table 2: Microorganisms responsible for PJI, in % of patients with PJI. Modified from Tande et al. [11]

	Hip and knee	
	All time periods	Early infection
Staphylococcus aureus	27	38
Coagulase-negative *Staphylococcus*	27	22
Streptococcus species	8	4
Enterococcus species	3	10
Aerobic Gram-negative bacilli	9	24
Anaerobic bacteria	4	3
Culture negative	14	10
Polymicrobial	15	31
Other	3	

Gram-positive cocci are the most common bacteria type involved in PJI. This includes *S. aureus*, other coagulase negative *Staphylococci* species and some *Streptococci* species. Staphyloccoci alone are responsible for 50-60% of the infections.
Aerobic gram-negative bacilli are very present when the infection occurs in the 3 first months after surgery. Together with *S. aureus*, they account for 60% of the early infections, probably because their virulence leads to the appearance of symptoms within the first few months. The most commonly found gram-negative bacilli is *Escherichia coli*, although *Pseudomonas aeruginosa* was also well represented in some studies. [11]

As stated before, *S. aureus* is a leading pathogen in PJI. This bacteria is known to be present in hospitals and medical environments, triggering nosocomial infections or wound infections after surgery. Therefore, it is not surprising to find *S. aureus* as an important instigator of PJI. Besides, *S. aureus* is an opportunistic pathogen that can be carried by humans and become a cause of infection. Its ability to form biofilms and

the antibiotic resistance of certain strains make this bacteria difficult to fight using antibiotics only [11]. Moreover, *S. aureus* is found to be responsible for 50% of late-onset infections caused by haematogenous seeding [12].

Coagulase-negative staphylococci are less virulent bacteria and therefore, if they were inoculated at the time of surgery, the symptoms will only appear after 3 months (delayed PJI). These low-virulence organisms mainly include *S. epidermis*, but also other staphylococci like *S. stimulans, S. caprae* or *S. lugdunensis*.

1.2.3 Biofilm formation

Nevertheless, simple microorganisms are relatively harmless as they can be eliminated by the host immune system or with antibiotic treatment. Unfortunately, the presence of a medical device in the body encourages bacteria to produce biofilms, which are the real cause of prosthetic joint infection. A biofilm consists of communities of microorganisms embedded in a biologically-active extracellular matrix, attached to a substrate. The extracellular matrix secreted by the bacteria themselves is made of polysaccharides, proteins and/or extracellular DNA. It is an insoluble and slimy secretion, that encapsulates millions of cells in a well-structured matrix. This encapsulation has the ability to protect the microorganisms from antimicrobials and the host immune system. The microenvironment benefits the microorganisms and allows them to grow together and proliferate. [13, 11]

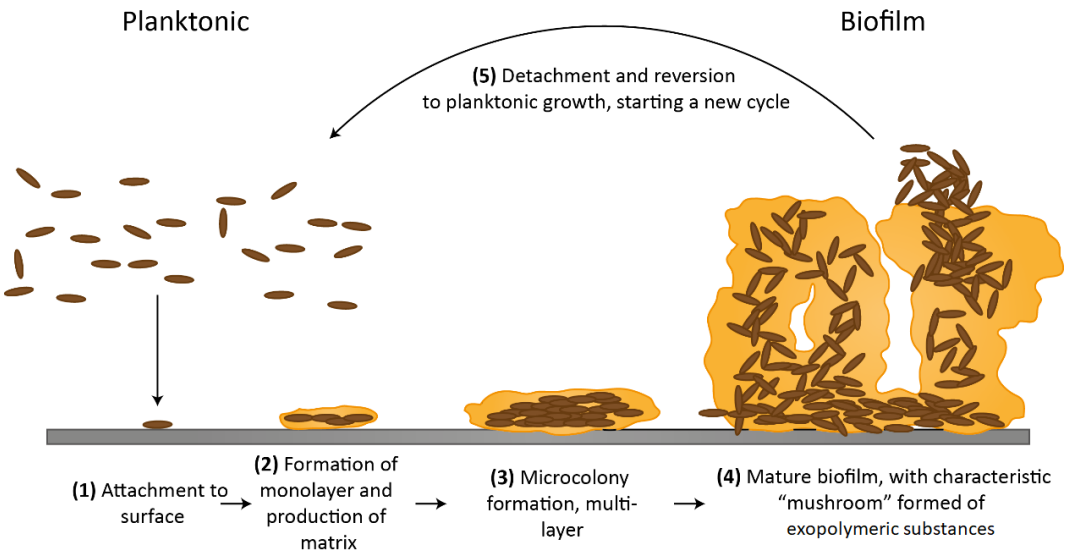

Figure 3: Mechanism for biofilm formation, reproduced from British Society for Immunology [14]

There are different steps in the mechanism of biofilm formation, represented on Figure 3. The first step involves the initial adhesion and attachment of the bacterial cells to the substrate, in our case the implant's surface. The attachment of bacteria to the surface is a two-stage process: the initial attachment is reversible and the secondary attachment is irreversible and specific. There are various interactions responsible for the primary attachment, including hydrophobic interactions, electrostatic interactions and

Van der Waals forces. Initial adhesion can also be facilitated by the use of flagella and type-IV pili, that function as adhesins.[15]

The secondary attachment however depends on protein interactions. Directly after incorporation in the body, the implant is coated with human extracellular matrix (ECM) proteins and immune protein components from physiological fluids. Bacterial adhesins can then specifically bind to matrix proteins such as collagen, fibronectin and fibrinogen. Adhesins are cell wall-anchored microbial surface components that recognize adhesive matrix molecules. [15, 16]

Then, the bacterial cells aggregate and form a stable microcolony on the surface of the foreign body. The cells proliferate and form several layers of cell clusters. Extra polymeric substances (EPS) are produced, encapsulating the bacterial cells in a matrix and attaching them irreversibly to the surface. EPS include exopolysaccharides, proteins, extracellular DNA and teichoic and lipoteichoid acids. Their function, aside from holding the bacterial cells together, is to trap nutrients, provide structural support, and shield against host immune responses and antimicrobial treatments. Protected by the matrix, the bacterial cells can communicate together by quorum sensing, that is proved to regulate cell attachment and detachment. By producing and responding to so-called 'autoinducers', bacterial population can adapt their gene expression to coordinate EPS production, monitor cell density, secretion of virulence factors, etc. This signaling system allows the adaptation of the bacterial community to changing environmental factors and the protection of the embedded bacteria [16].

Finally, some cells of the mature biofilm start to detach and are dispersed. They can then migrate and restart the whole biofilm formation process, including in another distant location. The consequences of those biofilm infections are various. They can induce tissue destruction, systemic dissemination of a pathogen through the body and dysfunction of the medical device.[11, 13, 14]

Unfortunately, antimicrobial agents alone or the immune system are almost ineffective against biofilms. Bacteria in biofilms have shown to be thousands of time more tolerant to antibiotics than planktonic cells [16, 17]. Antibiotics cannot penetrate through the extracellular matrix, resulting in a protected microenvironment for the biofilm bacteria development. Other resistance mechanisms to antibiotics include enhanced horizontal gene transfer between cells in the biofilm, a reduced growth rate making these cells difficult to target by conventional antibiotics and the upregulation of efflux pomp that allow bacteria to pump intracellular toxins out. Additionnally, biofilm formation acts as an immune evasion mechanism. The bacterial cells protected by the biofilm induce less inflammatory responses and therefore manage to partially escape host immunity [13, 15, 16].

Current strategies to treat bacterial biofilms involve prevention, dispersal and eradication of the biofilm. Dispersal agents have the ability to interfere with chemical pathways and processes such as quorum sensing, hereby disturbing the biofilm regulation mechanisms. Moreover, several studies have shown the promising action of biofilm eradication agents (BEAs), that can target and eradicate biofilm bacterial cells. BEAs include among others anti-microbial peptides, quaternary ammonium compounds, antimicrobial lipids.

However, BEAs are an emerging area of biofilm treatment research [17]. Up to now, biofilm inhibition by prevention of initial bacterial adhesion on surface is thus still considered to be the most efficient way to treat biofilms. The most common method to prevent bacterial adhesion is to modify the surface of the medical device. Different strategies to achieve this will be discussed in the next section.

2 Antibacterial strategies to prevent biofilm formation

Regarding the difficulties of treatment of prosthetic joint infection, there is a need for novel approaches to prevent bacterial adhesion on medical devices. Various treatments have been tested on implants to prevent the adhesion of microorganisms and thus the formation of biofilms.

2.1 Overview of different approaches

To face the upcoming challenge of implant infection, various approaches have been investigated and developed to fight biofilm formation and infection [18]. These approaches can be classified in two different strategies that can be combined in a multifunctional approach to obtain even better results.
The anti-adhesive approach consists in preventing the bacteria to adhere to the surface. This way, the bacteria remains in its planktonic, non-adhering state, and cannot manage to induce the formation of a biofilm. Moreover, they are more sensitive to antibiotics and the host immune system, which increases the probability of clearing them before they can initiate an infection. Surface coatings can also be based on bactericidal strategies, which consist in killing the bacteria before or after attachment to the implant surface.

Surface coatings preventing biofilm formation can release antimicrobials or present them as attached to the surface. Contact killing surfaces can be created by covalent binding of antibacterial compounds to the material surface. Alternatively, the progressive release of compounds has multiple benefits, but is often difficult to control. When the antimicrobial compounds are released, they can potentially kill pathogens in the surrounding area. But for many of these compounds, an initial massive burst in the release profile can be observed, followed by a longer period of diminishing release. During the latter period, the lower concentration of active compound may not be sufficient to kill the microorganisms, and could even induce resistance of the pathogen. [18]

A variety of approaches have proven to be effective. A non-exhaustive list of them can be found in Table 3. The use of **anti-adhesive polymers** aims at preventing the critical step of bacterial adhesion to the surface of the implant. This can be done by modifying the surface chemistry and structure, to create a sort of barrier that can prevent the adsorption of proteins and thus the adhesion of bacteria. This can be done for example by grafting long polymer chains to the surface. Polyethylene glycol (PEG) was one of the first polymers used to this end and demonstrated encouraging results. [19, 20]

Secondly, **super hydrophobic surfaces** also have anti-adhesive properties. They are resistant to bacterial adhesion and biofilm formation. However, host cell attachment may also be affected by such surface modifications and are a negative drawback for implants requiring cell ingrowth.[18]

Table 3: Anti-infectious strategies to treat orthopaedic implant surfaces, modified from Gallo et al. [19]

Strategy	**Examples**
Prevention in adhesion and adsorption	Anti-adhesive polymers (ex. PEG,...)
	Super hydrophobic surfaces
Bactericidal	Nanoparticles (Ag, Cu, ...)
	Antibiotics
	Antibacterial enzymes
	Antimicrobial peptides
	Chitosan derivatives
Combined	

Known for their antibacterial properties, some **nanoparticles** can also be incorporated in surface coatings. Although the toxicity mechanism of these nanoparticles is not fully unravelled yet, a suggested mechanism is that they attach to the bacterial cell wall by electrostatic interactions and disrupt the membrane. Besides, nanoparticles can generate reactive oxygen species that form free radicals and kill bacteria by inducing oxidative stress. Anti-bacterial nano-particles include silver ions, Cu or CuO. [18, 19]

Enzymes as well can be used as bactericidal agents in coatings. They are by nature biocompatible and serve as catalysts for various chemical reactions in the human body. Some enzymes are able to interfere with the adhesion mechanisms of bacteria and prevent their adhesion to a surface. Others will kill them by catalysing the hydrolysis of the peptidoglycane cell wall. Some enzymes such as DNase I or a glycoside hydrolase known as dispersin B have also shown efficiency against biofilms by attacking the extracellular polymeric substances components necessary for its formation. However, the challenge consists in retaining the enzymatic activity of the enzyme even when included in a coating. [18]

The use of naturally-derived components such as hyaluronic acid, collagen, alginate, dextran or chitosan for surface coatings is not new. However, **chitosan** has the advantage of presenting strong antibacterial activity against Gram-positive as well as Gram-negative bacteria, and is thus a material of choice in the design of antibacterial coatings. [18, 19] Furthermore, this polymer is easy to modify and is very biocompatible. Chitosan will be used in the design of our coating and its properties will thus be discussed in Section 3.5.1.

Despite their relative inefficiency against biofilm formation when administrated after infection, **antibiotics** can be promising when incorporated in a surface coating. They can be bound to the surface or released over time [18]. However, since the resistance of some bacterial strains is becoming a rising problem in the medical world, alternative antimicrobial therapeutics are gaining more interest. One of them is the use of antimicrobial peptides, which will be discussed extensively in the next section.

2.2 Antimicrobial peptides

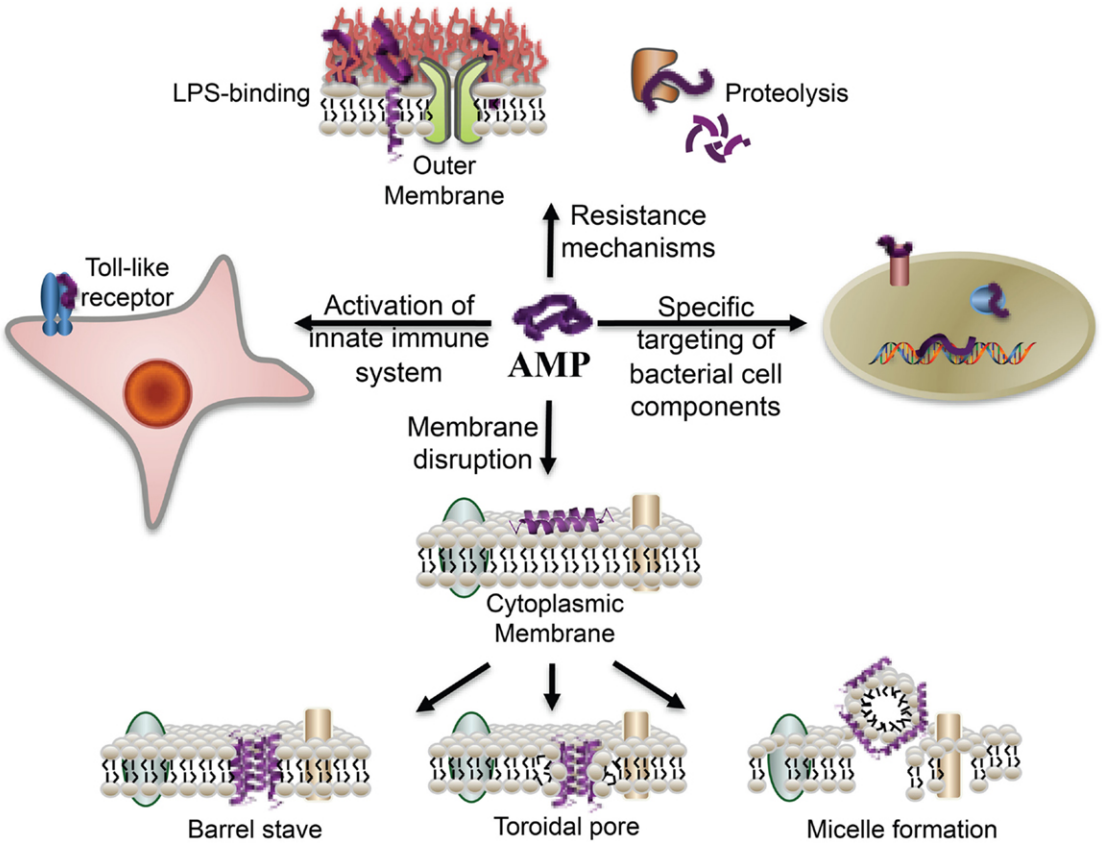

Figure 4: Cellular interactions associated with antimicrobial peptides, reproduced from Duplantier et al. [21]

Prevention of bacterial adhesion and therapy based on the use of antimicrobial peptides (AMPs) is a very promising alternative for antibiotics. These compounds have unique properties making them excellent coating agents for medical devices. They offer the advantage of being far less susceptible to pathogen resistance compared to conventional antibiotics and having a very broad antimicrobial spectrum, targeting both gram-negative and gram-positive bacteria. AMPs are components of the human innate immunity: they are part of the first line of defense of our body against pathogens. Biological roles of AMPs include direct antimicrobial killing and activation of the host immune system [22]. Some of them also proved to have antibiofilm action.

What makes AMPs different from conventional antibiotics is their mechanism of action. Antimicrobial peptides consist of between 10 and 50 amino acid residues with an overall positive charge and a high ratio of hydrophobic amino acids [23]. They are therefore cationic and can bind to the negatively charged bacterial cell wall. This leads to the formation of pores and the disruption of the membrane or the inhibition of intracellular functions leading to bacterial cell lysis. AMPs are able to target specific species selectively, thanks to their difference in membrane composition. They have also proved to be capable of binding and neutralising lipopolysaccharides, promoting angiogenesis and wound healing, and exerting anti-tumor

activity [21, 24].

Several models describe the mechanisms of action of AMPs [25, 22]. The first step is the electrostatic interaction of the cationic peptide with the negatively-charged bacterial membrane. The insertion into the membrane can occur by different mechanisms depicted on Figure 5. The toroidal model and the barrel-stave model involve the formation of channels by reorientation of the peptide molecules perpendicular to the membrane. In the barrel-stave model, peptides interact laterally with each other and use the lipid core region of the membrane to align their hydrophobic side to it. In the toroidal model, peptides affect the local curvature of the bilayer to form a pore, so that the core would become lined by the heads group of both the inserted peptides and the lipid monolayer [21, 26]. The carpet model suggests that peptides aggregate parallel to the lipid bilayer and are able to permeabilize the membrane. At high peptide concentration, this can result in a detergent-like activity and formation of micelles.

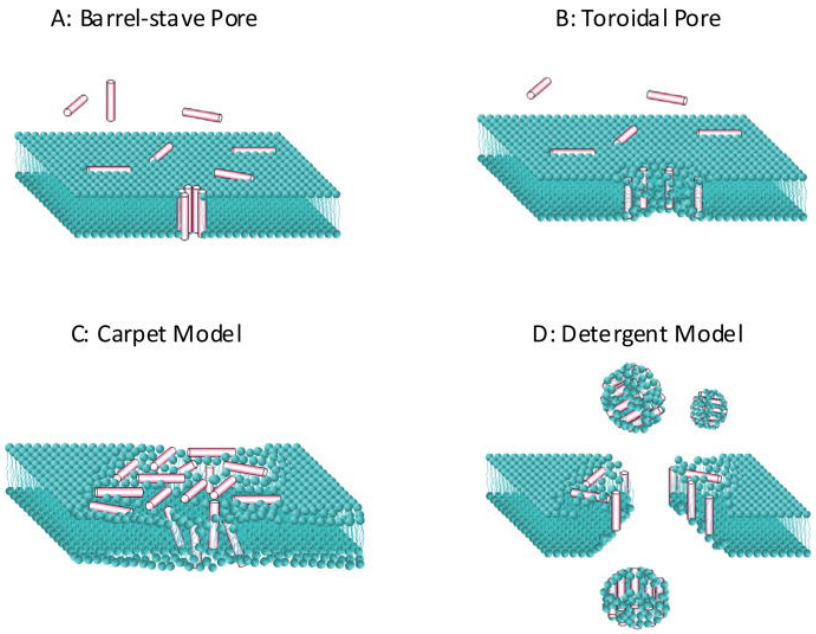

Figure 5: Models for AMP activity. Reproduced from Wimley et al. [26]

Once the peptide is inserted into the bacterial membrane, it can either disrupt the membrane physically and cause cell lysis, or translocate across the membrane and act on internal targets.

In order to exploit the bactericidal properties of AMPs on medical devices, they have to be easy to incorporate into surface coatings. Different immobilisation techniques exist, and AMPs can be immobilised either physically or chemically [27]. Layer-by-layer assembly of polymeric films containing AMPs is a well-known approach, consisting in trapping the peptide between two charged polymers. This method will be the one used in this master thesis and will thus be discussed later. Other approaches include covalent coupling of AMPs to a surface, via the self-assembly monolayer of reactive compounds or using functionalised polymer resins such as polyethylene glycol [27]. Although the immobilisation of peptides in

the multilayers is beneficial for a stable coating construction, it can also become a drawback by reducing its mobility and therefore activity. It is thus necessary to study whether the release of the peptide or its immobilisation is more efficient for the required application.

2.3 LL-37

The properties of AMPs and their potential in antimicrobial surface coatings have been discussed in the previous section. LL-37 is a single cahtelicidin AMP present in the human body, which has both antimicrobial and antibiofilm properties against multiple human pathogens. As a member of the cathelicidin family, LL-37 acts as a primary defense against bacteria and other pathogens at site of inflammation. Cathelicidins have also proved to be capable of stimulating the host defense system [24]. The combination of the antibiofilm, antibacterial and wound-healing effect of LL-37 make it thus a promising agent for antimicrobial surface coatings.

2.3.1 Structure

LL-37 is an amphipathic, cationic, linear α-helix peptide composed of 37 amino acids. The amphipathic nature of LL-37 is very important for its interaction with the bacterial cell wall. When looking at the secondary structure on Figure 6B, a hydrophobic side (top) and a positively-charged polar side (bottom) can be distinguished. The concave hydrophobic surface is formed by four aromatic phenylalanine side chains. At physiological pH, the peptide has a net positive charge of +6 [21].
Figure 6A represents its structure, which consists of a curved amphipathic helix-bend-helix motif (regions I and II: the arrow indicates the helical bend) followed by a C-terminal tail (region III). Studies and experiments on LL-37 showed that the C-terminal α-helix is responsible for the antimicrobial and antiviral effect [24].

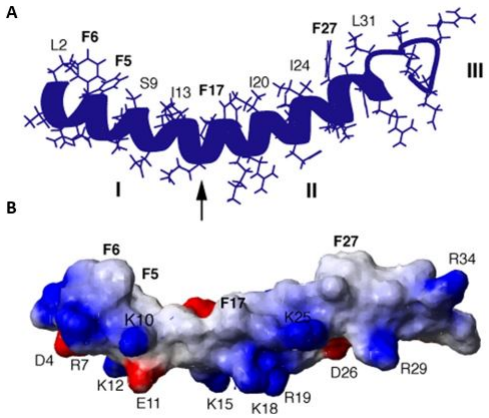

Figure 6: Structure of LL-37. (A) Ribbon representation of the LL-37 structure with hydrophobic side chains labeled. The helical bend is indicated by an arrow, and the three structural regions are labeled with Roman numerals I, II, and III. (B) Surface of LL-37 with the hydrophobic surface at the top and hydrophilic surface at the bottom. Color code: acidic residues in red, basic residues in blue, and hydrophobic residues in white. Modified from Wang et al. [28]

2.3.2 Mechanism and activity

Several groups have studied the mechanism of action of LL-37 specifically, and Vandamme et al. concluded that LL-37 uses a toroidal pore mechanism to form pores in the bacterial cell wall [24]. A detergent-like mechanism is rejected since no micelles were observed during the action of LL-37. The positively-charged amino acids of the peptide bind to the charged phospholipids of the bacterial membrane and cover it in a carpet-like fashion, parallel to the surface. When the threshold concentration is reached, the strain on the membrane becomes to large and this results in the formation of small toroidal pores and transport of the peptide to the inner part of the membrane. Subsequently, the membrane collapses or the peptide diffuses to intracellular targets, killing the bacteria [24].

LL-37 has the ability to distinguish bacterial from eukaryotic cells thanks to their membrane components. The membrane of both Gram - and Gram + bacteria contain negatively charged molecules, respectively lipopolysaccharides and teichoic acid. The eukaryotic membranes on the contrary are zwitterionic and will thus not bind with the cationic LL-37 [24].

Anti-biofilm activity was demonstrated for *S. aureus* by Dean et al. [29], but the mechanism by which this activity is carried out is not unraveled yet. However, Overhage et al [30] studied the effect of LL-37 on *P. aeruginosa* and suggested several mechanisms for anti-biofilm activity, including the down-regulation of key components of the quorum sensing systems Las and Rhl. Other mechanisms include reduction of the initial attachment of *P.aeruginosa* cells to the surface and promotion of the surface motility of the cells by stimulating the expression of genes related to type IV pilus biosynthesis and function [21].

Literature reports different values for the minimal inhibitory concentration (MIC) of LL-37, depending on the inhibited microorganism. The MIC is defined as the lowest concentration of a chemical or drug which prevents visible growth of a bacterium or bacteria. Table 4 gives an overview of the LL-37 activity for a number of Gram-positive and Gram-negative bacterial strains. According to Turner et al. [31], LL-37 displays antimicrobial activity against both Gram-positive and Gram-negative bacteria at a MIC in the $<$ 10 μg/ml range. However, other articles cite different values including 64 μg/mL [21, 30] and 144 μg/mL [32] for *S. aureus* for example. Furthermore, multiple studies have shown that LL-37 demonstrates reduced antimicrobial action in environments with high ionic strengths such as in physiologic salt concentration ($\sim$150 mM NaCl). [31, 32]

Regarding anti-biofilm activity, Dean et al. [29] demonstrated that $\sim$40% of formation of bacterial biofilms for *S. aureus* was inhibited at concentrations of 10 μg/mL. Moreover, the attachment of *S. aureus* to polystyrene wells was shown to significantly decrease in presence of LL-37, suggesting that the peptide may inhibit biofilm formation by interaction with bacterial adhesins [29].
Overhage et al. [30] conducted the same study on *P. aeruginosa* and found that LL-37 potently inhibited the formation of bacterial biofilms in vitro, at a concentration of 0.5 μg/mL. This very low concentration is far below the MIC, and this suggests that the mechanisms for biofilm inhibition and antibacterial activity may be completely different [30].

Table 4: MIC (μg/mL) of LL-37 in presence of a number of bacterial strains, in the absence of NaCl. Modified from Turner et al. [31]
* indicates different strains were tested.

Organism	**LL-37 activity: MIC (μg/mL)**
Gram-positive bacteria	
S. epidermis	7.6
*S. aureus**	2.9-12.5
MRSA ATCC 33591	3.4
Gram negative bacteria	
*E. coli**	0.1-1.9
*P. aeruginosa**	1.3-5.7

2.3.3 Challenges

Hence, the antimicrobial and antibiofilm properties of LL-37 explain its selection as an adequate AMP to use in the design of our coating. However, several challenges have to be faced for the optimal design of a coating containing LL-37.
The first challenge lies in defining the optimal efficient concentrations of the peptide to be incorporated in the coating. Literature shows different values for the MIC of LL-37, and an appropriate concentration must be selected in order to prevent bacterial adhesion and biofilm formation on the long term. Furthermore, the complexation state of LL-37 may have an influence on its activity and therefore on the MIC, and this influence requires a study as well.

Secondly, an efficient strategy must be found to incorporate the LL-37 peptide in the coating. The method selected here, and that will be discussed in more details in Section 3.3, was the immobilisation of LL-37 under the form of a protein-polyelectrolyte complex and its incorporation between charged polymeric layers in a LBL approach. However, this immobilisation must maintain the activity of LL-37 and allow the peptide to exert its antibacterial action. Therefore, the behaviour and activity of LL-37 in the constructed coating must be investigated as well, to determine the influence of its configuration into the multilayers on its activity. Indeed, the mechanism of action of the peptide involves direct contact with the target bacterial cells, and its complexed state as well as its position between the polyelectrolyte layers may hinder this contact. Consequently, a release and diffusion of LL-37 from the layers and into the bulk environment may be necessary, and this possibility must be explored as well.

Keeping those constraints in mind, different experiments will be conducted to assess and explain the activity of LL-37 in the multilayers.

3 Substrate and surface modification

In order to have efficient implants that minimise the risk of PJI, the interaction of the device with the physiological environment must be studied closely. The surface of the prosthesis, which will be in direct contact with the human body, is therefore a crucial element of the implant itself. Different treatments can be applied to the device to modify and adapt the surface structure, with the aim of influencing the host response to the implant and reducing the risk of infection.

Strategies to fight bacterial infections on medical devices have been discussed before and involve surface modifications and coating additions. However, body response to the implanted foreign device must also be controlled. Even if the material is biocompatible and does not induce an immunogenic reaction, inflammatory reactions such as the foreign body reaction remain possible. Close attention must therefore be payed to a good osseointegration of the implant. Parithimarkalaignan et al. define osseointegration as 'a direct structural and functional connection between ordered, living bone and the surface of a load-carrying implant.'[33] In short, it consists in the integration of bone tissue to/through the implant surface. Poor osseointegration of orthopedic implants is associated with loosening of the implant after implantation to the bone.

Hence, the substrate and the architecture of the implant surface must be chosen keeping the two aforementioned constraints in mind, that is good osseointegration and antibacterial properties.

3.1 Substrate

The material used for orthopaedic implants is important for the fixation process and must have a high mechanical strength, a Young modulus resembling that of a bone, be biocompatible and resist degradation by corrosion. Metal is often chosen because of its mechanical properties, but corrosion can remain a problem and must therefore be avoided. Corrosion of a metal in the body can result in rupture or degradation of the material and create toxic corrosion products. Titanium alloys, stainless steel, and cobalt-chromium-molybdenum alloys are widely used in the manufacturing of orthopaedic devices [34].

Accordingly, titanium is a material of choice, because of its biocompatibility, mechanical properties such as its Young modulus ($\sim$ 110 GPa) and good fatigue strength, and excellent resistance to corrosion [35, 34, 36]. A passive metal oxide film (TiO_2) of 3-7 nm forms spontaneously at the surface when the substrate comes in contact with air [36]. This layer protects titanium and enhances its resistance to corrosion. This makes titanium and its alloys a highly bioinert and biocompatible material, often employed in medical devices and especially for orthopaedic implants. However, surface modifications are necessary to improve the biocompatibility and osseointegration of the implant, and in our case, to prevent infections.

Up to 822.5 °C, titanium in its elemental form possesses an α hexagonal closely-packed crystal structure, and transforms to a β body-centered cubic structure above this temperature. According to their microstructure, titanium alloys can thus be classified as α, near-α, $\alpha + \beta$, metastable or stable β. An extensively used titanium alloy for biomedical devices and especially implants consists in Ti6Al4V (ELI),

which belongs to the category of the $\alpha + \beta$ alloys. This alloy contains 6% Al, which is an α-stabilizer and 4% V, which is a β-stabilizer. The combination of both results in a higher strength of the material [36].

3.2 Immobilisation of AMPs on biomaterial surfaces

AMPs carry unique bioactive properties and have a great potential for several biomedical applications. However, the difficulty to immobilise them on solid surfaces limits their current use and new immobilisation strategies are required to ensure their applicability for biomaterial coating. Current approaches for immobilisation include physical methods such as adsorption, self-assembled monolayers (SAMs), layer-by-layer self-assembly and chemical methods like selective and non-selective covalent binding. [37]

Physical immobilisation Molecular assemblies that adsorb spontaneously on the surface of certain substrates are called self-assembled monolayers. The molecules that form the SAM often possess a chemical head group that is able to bind to the underlying substrate, and an attached 'tail' with a terminal group that can chemically bind to other molecules (typically a carboxylate function).

The LBL self-assembly technique remains one of the most used strategies for immobilisation of AMPs and consists in alternate adsorption of cationic and anionic polyelectrolytes on the substrate surface. The created films are functionalised by incorporating AMPs between the layers. This method was selected for the construction of the coating in the present work and will be further detailed in the next section.

An advantage of those physical immobilisation methods is that they require no chemical changes of the functional peptide. However, the main drawback pointed out by Silva et al. is that the diffusion of AMPs is difficult to control [37]. Peptides adsorbed in the lower layers have a restricted contact with the surrounding bulk and their diffusion depends on the layer thickness and on the interactions between the polymer and the peptide. A fast peptide release from the film may not be beneficial either since the amount of anchored AMPs would decrease, and this would influence the minimal AMP concentration needed to inhibit the growth of microorganisms. AMP leaching in high concentrations can also result in toxicity for the patient and initiation of bacterial resistance, and must thus be avoided.

Covalent immobilisation These limitations of the physical anchoring methods resulted in development of chemical methods to immobilise the peptide onto the solid surface through formation of covalent bonds between the peptide and the surface or a linker molecule. The covalent bond provides stability to the AMP and prevents spontaneous peptide uncoupling. In addition, a favourable orientation of the biomolecule can be achieved through covalent binding, resulting in enhancement of its bioactivity. However, chemical modifications can alter the structure of the molecule of interest, restrict its mobility and interfere in the mechanism of action [37].

Hence, both methods have strengths and weaknesses and the choice of the most appropriate method depends on several factors such as the chosen substrate, the AMP characteristics and the experimental conditions.

Immobilisation of LL-37 The aforementioned approaches for AMP immobilisation can thus be applied on the LL-37 peptide. Several studies have already succeeded in its immobilisation on a surface. Gabriel et al. grafted the peptide covalently with the aid of functionalized poly(ethylene glycol) molecules on titanium surfaces and showed bactericidal activity against *E. coli* [38]. Another study by Qin et al. demonstrated bactericidal activity of LL-37 against *P. aeruginosa*. The peptide was adsorbed through electrostatic interactions on SAMs derived from HS-OH and HS-COOH presenting carboxylate anions [39]. A similar strategy was adopted by Cassin et al. who adsorbed LL-37 physically on polyelectrolyte multilayers made of collagen and hyaluronic acid [40].

3.3 Layer-by-layer approach

This approach consists in constructing multilayers of polyelectrolytes (PE) based on electrostatic interactions and is schematically represented in Figure 7. Two oppositely-charged polyelectrolytes are adsorbed one by one on a substrate, forming a succession of layers. The negatively-charged substrate is dipped in a solution of a cationic PE. Electrostatic interactions will allow the adsorption of the PE on the surface and a reversal of the surface charge. Rinsing is then performed to remove unbound PEs and prevent cross-contamination of the solution. After rinsing, the process is repeated with an oppositely-charged PE (anionic in this example). Doing so, a multilayer is constructed and this can be continued until the desired thickness is obtained. Apart from electrostatic interactions, the assembly and stability of the layer is influenced by hydrogen bonds, hydrophobic interactions and van der Waals forces [41, 42].

The strong electrostatic interactions between the different layers and between the substrate and the film result in a relatively stable coating [43]. Other advantages of this method include the simplicity of the process, its versatility and application to most substrates (even objects with irregular shapes and sizes), the availability of an abundance of charged macromolecules and colloids and the control over the multilayer thickness [42].

It has been demonstrated that proteins can be successfully integrated in these polyelectrolyte layers, keeping their conformation and protecting them from denaturation [44]. However, due to the polyampholyte nature of proteins and their heterogenous spatial charge distribution, the incorporation of proteins in multilayers can be challenging. vander Straeten et al. [45] showed that the creation of a protein-polyelectrolyte complex (PPC) as building block for LbL assembly simplifies the incorporation of the protein in the multilayers.

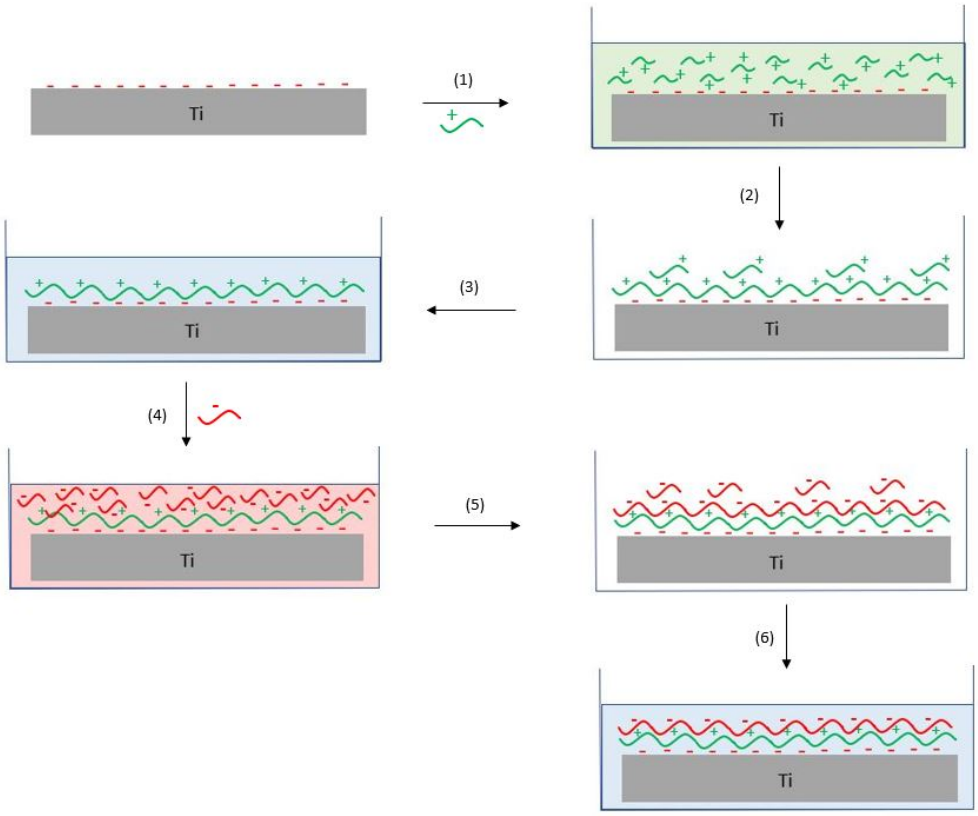

Figure 7: Description of the layer-by-layer method. The cleaned Ti sample has a negative surface charge. (1) The sample is immersed for 30 minutes in a polycationic solution. (2) The solution is removed and some polycations are weakly bound to the surface. (3) The sample is immersed 30 seconds in water, 3 times in a row. This allows the removal of the weakly bound polyelectrolytes. (4) The sample is immersed for 30 minutes in a polyanionic solution, (5) and again, some polyanions are weakly bound and (6) removed by washing with water. These steps can be repeated as many times as necessary depending on the desired layer set-up.

3.4 Protein-polyelectrolyte complex

The electrostatic complexation of the protein of interest, in our case LL-37, with a polyelectrolyte is shown in Figure 8. This method allows the standardisation of the protein surface charge and favours interactions with the counter polyelectrolyte. The multilayer construction is then based on PE-PE interactions only, and is independent of the charge state of the protein. A higher protein content is then immobilised in the layers and a higher hydration level compared to bare protein molecules is obtained [45].

3.4.1 Influence of pH and ionic strength on PPC formation

The influence of pH and ionic strength on the PPCs size and electrical composition was thoroughly investigated by vander Straeten et al [45]. He proved that PPCs with very different morphologies were obtained as function of pH and ionic strength (I). Experiments with lysozyme as a protein and poly(styrenesulfonate) (PSS) showed that low pH and low I are favourable for PPC formation. Indeed, at low pH, the protein is

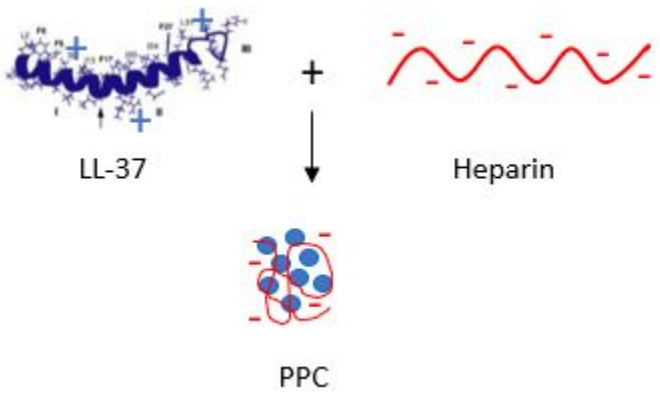

Figure 8: Protein-polyelectrolyte complex formation from heparin and LL-37.

highly charged, which results in a high coulombic attraction between the positively-charged protein and the negatively-charged polyelectrolyte. On the other hand, the increase of ionic strength causes a screening of the electrostatic charges and results in less effective electrostatic interactions between the protein and its counter PE.

3.4.2 PPC behaviour in layer-by-layer assembly

The incorporation of PPC at different pH values and ionic strengths in a self-assembled layer-by-layer film was investigated as well, using the same design of PPC described above and poly(allylamine hydrochloride) (PAH) as the counter cation. The results showed that a low amount of proteins was immobilised at high I (>200mM) due to a screening of the polyelectrolyte charges.
At I = 10 mM, the immobilised protein amount was found to be independent of the pH value. This proves that the LBL assembly is regulated by PE-PE interactions and that the pH-driven variation in charge density of the protein does not interfere with the LBL assembly.

When I $\approx$ 0 mM, two distinct evolutions are observed, dependent on the pH value. If the pH value is low (3.0), a low protein content combined with a high water content was observed in the obtained multilayer films. This can be explained by a high charge density of the counter polycation, that results in maximal electrostatic interactions between PSS and PAH that may displace the more weakly complexed protein and remove it from the layer. The result is a thick film with a high water content and a low immobilised protein amount [45].

If pH values up to 7.5 or 9.6 are reached, a very high protein content is trapped in the layers. This may be due to the lower ionisation degree of the counter polycation PAH, resulting in a more loopy conformation and thus a lower ability to displace proteins from the multilayer. High pH values would therefore increase PPC stability when integrated in multilayers [45].

3.5 Polyelectrolytes

In order to construct the LL-37-containing multilayer, appropriate polyelectrolytes must be chosen. As a reminder, a polyelectrolyte is defined as 'a polymer in which the monomeric units of its constituent macromolecules possess ionisable groups.' [46] Polyelectrolytes can dissociate in aqueous solutions and bear charges dependent on the pH value. They can thus be cationic, anionic or ampholytic dependent on the charge of its ionised groups. They have convenient properties for LBL assembly, including their ability to interact strongly with oppositely-charged surfaces or molecules and their ability to bind large amounts of water. Due to their nature, they are sensitive to pH and ionic strength [47].
Two polyelectrolytes were used in this thesis: chitosan and heparin.

3.5.1 Chitosan

Chitosan is a naturally-occurring polysaccharide. It is a linear polycation with a high charge density and reactive hydroxyl and amino groups. Chemically, chitosan is composed of two monomers (N-acetyl-D-glucosamine and D-glucosamine), linked together by β-(1-4) glycosidic bonds. Their relative amount can vary, resulting in molecules of different degrees of deacetylation, molar masses, pK_a, etc. These differences influence the physico-chemical properties of chitosan, including solubility in aqueous media or charge distribution. Pure chitosan has a pK_a of 6,3 [48]. It is biocompatible, biodegradable through natural enzymes and non toxic.

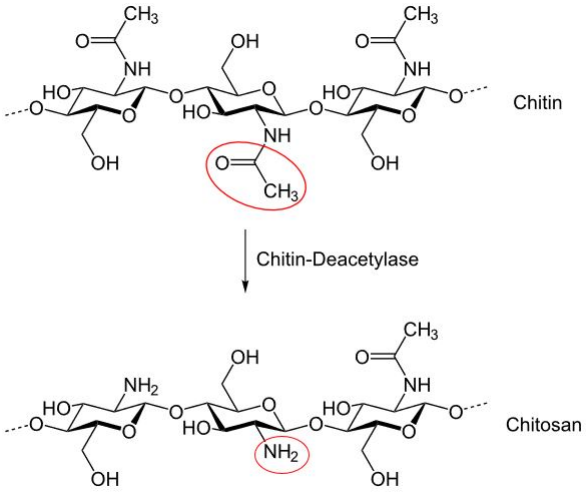

Figure 9: Chemical structure of chitosan and its production from chitin through deacetylation. The deacetylated function is circled in red on the figure.

This biopolymer is typically derived from chitin, which is the major component of the exoskeleton of insects and crustaceans. The production of chitosan from chitin occurs by deacetylation under alkaline conditions, as can be seen on Figure 9. The degree of deacetylation or DD is defined as the molar fraction of D-glucosamine, and can vary from 50% to 95% [48]. Under 50% of deacetylation, the polymer is called chitin.

Furthermore, chitosan is known to have antimicrobial properties towards a number of human pathogens as well as food-borne organisms [49]. However, its activity has proven to be better against Gram-positive than Gram-negative bacteria [48]. The antibacterial mechanism of chitosan is not fully unraveled yet, but its capacity to kill bacteria is supposedly due to an interaction between the positively-charged polysaccharide and the negative bacterial membrane, resulting in membrane permeability [50]. It is important to note that chitosan's antimicrobial activity depends on different factors. In that respect, the type of chitosan and its molar mass and degree of deacetylation influence its activity. Chitosan's antibacterial activity increases with its degree of deacetylation [50]. In fact, Younes et al. demonstrated that chitosan with a DD between 76 and 98% showed strong bactericidal effect, higher for Gram-negative than for Gram-positive bacteria. Chitosans with DD $<$ 59% possessed low or no antibacterial activity at all [51]. The environmental conditions like pH, ionic strength, etc. must be taken into account as well. Raafat et al. showed that a higher activity is observed at lower pH values, probably due to the protonation of the amino groups which makes the polyelectrolyte more cationic. The effect of ionic strength however is not completely understood yet [48].

Moreover, chitosan has demonstrated to have antibiofilm properties. Carlson et al. tested the activity of a chitosan-coated surface against biofilm formation and found a reduction in biofilm viable cell numbers ranging from 95% to 99,99% for a number of common Gram-negative and Gram-positive bacterial strains [52]. This combined with its antibacterial properties and its polycationic nature point chitosan as an ideal building block for LBL assembly of antibacterial coatings.
Finally, chitosan has the ability to facilitate osseointegration by promoting the expression of extracellular matrix proteins in osteoblasts and chondrocytes [41]. This is of interest for the good implementation of the hip prosthesis in the human body.

3.5.2 Heparin

The second polyelectrolyte that will be used to form coatings in the present work is heparin. Heparin is a naturally-occurring polysaccharide belonging to the family of glycosaminoglycans (GAG's). It consists of repeating disaccharide units as can be seen on Figure 10. The presence of 3 sulfonate groups (pKa 0,5-1,5) and one carboxyl group (pKa 2-4) that can be easily ionised explain its strong polyanionic nature. In fact, heparin is the strongest natural polyelectrolyte that can be found. It is always fully negatively charged, and is therefore very convenient for LBL constructions based on electrostatic interactions [53].

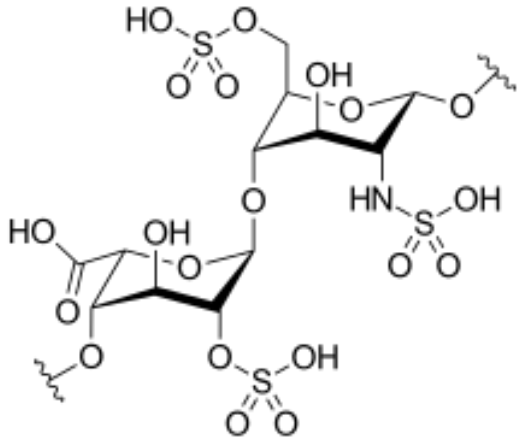

Figure 10: Chemical structure of heparin. Reproduced from Sigma-Aldrich [54]

Discovered in 1916 by Mclean, heparin is now the most used anticoagulant drug. Its action prevents the formation of clots in blood. Commonly, heparin was isolated from animal tissues (pig intestinal mucosa), where it can be found in cytoplasmic granules of mast cells. However, the animal origin of pharmaceutical heparin induces potential impurities and contamination issues. Novel approaches for heparin biosynthesis are therefore being investigated, including chemoenzymatic modifications, microbial production or mammalian cell production [55].

Although less studied than its anticoagulant properties, the potential use of heparin as an antimicrobial agent has also been investigated. Heparin could have an inhibitory effect on pathogen adhesion to cell surface and therefore be useful in the field of infectious diseases [55]. This anti-adhesive property of heparin is of interest for the construction of the antibacterial coating targeted in this study. Moreover, heparin can interact with different growth factors that promote osseointegration, such as transforming growth factor-β (TGF-β) and bone morphogenetic proteins (BMPs) [56].

3.6 Properties of chitosan/heparin multilayers

Different studies have already been conducted on multilayered surface coatings composed of heparin and chitosan [56, 57, 53]. Shu et al. demonstrated that the LBL self-assembly technique allows a successful construction of the chitosan-heparin multilayer on a titanium substrate, and that the presence of this coating improves the adhesion, proliferation and differentiation of osteoblasts [56].

The antibacterial and anti-adhesive properties of the same multilayer but deposited on poly(ethylene terephthalate) (PET) was investigated by Fu et al. They found that the adhesion of *Escherichia coli* on the CHI/HEP films was diminished dramatically compared to the control PET. Moreover, the CHI/HEP multilayer can kill the bacteria effectively. In addition, it is interesting to note that the assembly pH has a remarkable effect on the antibacterial property of the multilayer. A film constructed from a solution at pH 3.8 was more efficient in preventing bacterial adhesion and in killing adhered bacteria compared to a film deposited at pH 2.9 or 6. According to the authors, the reason is twofold. First of all, the surface

hydrophilicity has an important effect on bacterial adhesion. Due to the higher charge density of CHI at the defined pH, charge repulsion between the segments can be observed. This repulsion induces a flat structure of the chitosan chains, and the obtained film is thinner. Since heparin is fully charged at all tested pH values, its thickness remains constant. Consequently, the ratio of the thickness of the heparin layer to the chitosan layer is higher and chain segments from the underlying heparin layer will penetrate into the chitosan layer. This results in a more hydrophilic layer which will prevent the adsorption of bacteria on the surface [57].

Secondly, since the charge density of chitosan is lower for high pH values, more chitosan is needed to balance and overcompensate the oppositely charged heparin layer. This explains why the films grew better at pH 3.8 than 2.9. Both reasons explain why a pH value of 3.8 was found to be more efficient than a pH of 2.9 or 6 in preventing bacterial adhesion [57]. These interesting results will be taken into account for the selection of the optimal assembly pH of the multilayers used in this work.

Finally, Lundin et al. focused their research on the effect of solution pH and ionic strength on the LbL assembly of chitosan and heparin. They found that an increase of the ionic strength of the polymer solution at fixed pH and an increase of the pH at constant ionic strength both had the same effect, that is increasing the dry and wet mass of the multilayer. This is due to the decrease in charge density of chitosan with increasing pH, that results in a decreased repulsion between the charged segments. This favours a coiled-state conformation of the chains, leading to thicker and denser films. Furthermore, it was established that chitosan is the dominating species in the layer, and that the multilayer growth of CHI and HEP is exponential-like [53].

3.7 Layer disassembly

In the sections that follow, it will be seen that a disassembly of the multilayers may be useful for a better understanding of the LL-37 action in the coating. Different approaches for the deconstruction of polyelectrolyte multilayers are reported in literature [58, 59]. In this section, two commonly used methods will be briefly presented.

According to Hoogeveen et al., the stability of the multilayer depends on the charge density of the constitutive polyelectrolytes [60]. This charge density can be compensated by addition of the opposite polyelectrolyte, but at some point, when the charge density of one of the polyelectrolytes is too low, the adsorbed amount of the counter one will drop and the layer will be weakened. A minimum charge density of about 20% is required to form stable multilayers [60]. A sufficient number of polymer-polymer interactions must be broken to allow dissociation of the multilayer. The charge density can be altered in different ways, including changes in pH or salt concentration. Dubas et al. report that delamination of layer-by-layer assembly of oppositely charged polyelectrolytes can be driven by those changes [61]. A change in pH will modify the charge of weak polyelectrolytes, resulting in decreased electrostatic interactions which can cause dissociation of the multilayer. Similarly, when the salt concentration is increased, ionic strength will rise and charge screening will occur, resulting in weakening of the electrostatic charge between the polymer molecules.

A second approach to disassemble polyelectrolyte multilayers has been reported by different authors and consists in disrupting the internal molecular interactions via competitive binding [58, 62, 63]. This means that an ion-containing structure is destabilized through the addition of another charged species. Commonly, ionic surfactants are used, and they will complex preferentially with one of the two polyelectrolytes composing the multilayers, resulting in a removal of this component and dissolution of the multilayers.

Part IV
Materials and methods

1 Layer construction

In this chapter, the construction of the coating will be described. An overview of the assembly method and the chosen physico-chemical conditions is given.

1.1 Overview of the coating architecture

The first layers of the coating depicted on Figure 11 consist in a chitosan-heparin multilayer film on a titanium substrate. This cushion is important for the stability of the coating. To immobilise the LL-37 peptide in the coating, complexes were first created with heparin to allow a standardisation of the protein's surface charge. These protein-polyelectrolyte complexes (PPC) were then incorporated in the coating using the lLBL self-assembly approach described in Section 3.3 of State of the Art. Chitosan and the LL-37/HEP complex were adsorbed alternatively in a LBL fashion on the already grown CHI/HEP cushion. This approach allows the construction of up to 6 PPCs/chitosan layers and results in a stable coating. The different steps are detailed below.

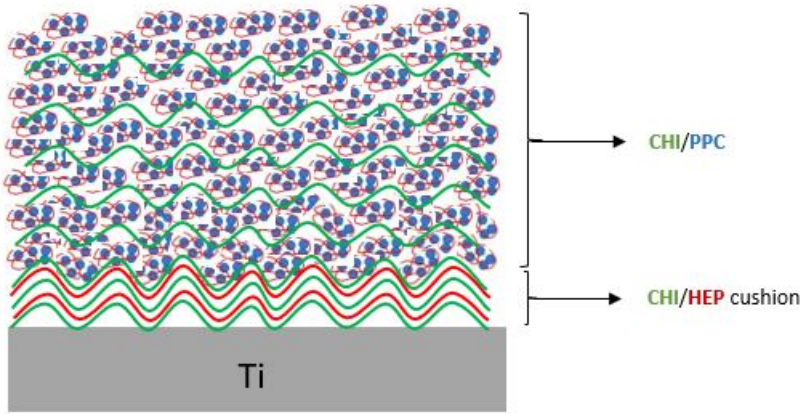

Figure 11: Schematic representation of the architecture of the developed coating. This representation is not on scale. The green lines represent the chitosan chains, the red lines are the heparin chains, and the blue dots are the LL-37 molecules.

1.2 Substrate preparation

As exposed previously, the properties of titanium make it a material of choice for orthopaedic devices. In this master thesis, we will work on coupons made of a Ti6Al4V titanium alloy, often used for orthopaedic implants (Grade 23; President Titanium, Massachusetts, United States). The coating was developed on small titanium alloy coupons, which were prepared, polished and washed following the protocol described below.

To facilitate the polishing step, three coupons at the time were embedded together in a thick polyfast resin layer by hot mounting (LaborPress-3, Struers). The resin was heated for 6 minutes at 180 °C and then cooled down for 3 minutes. This step resulted in a resin coating containing 3 coupons, as depicted in Figure 12.

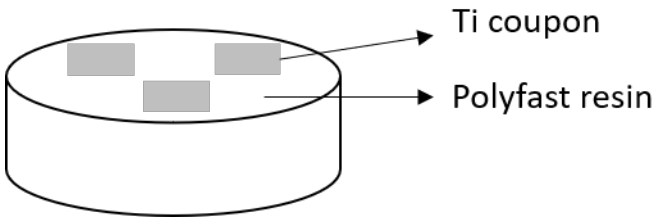

Figure 12: Schematic representation of 3 coupons embedded in the polyfast resin for polishing.

To obtain an uniform surface for all samples, the coupons were polished in two steps. The pre-polishing step or grinding step was carried out using a grinder (Buehler, Metaserv 2000 Grinder/Polisher 95-2829) and silicon carbid (SiC) paper with different grain sizes (320-800-1200) at 200-300 rotations per minute, until the samples were flat and smooth. Water was used as a lubricant. The polishing was then completed using the polishing machine (Struers, Pedemin DAP-7) with a Ti MD PLAN 9 µm Blue as abrasive, at a rotational speed of 125 rpm. A diamond spray was used (DP Spray-P 9 m, Struers).

After breaking the resin to recover the polished coupons, they were washed by hand using a tissue soaked in ethanol (Ethanol 99%, VWR Chemicals). Then, they were washed in an ultrasonic bath for 10 min, first in ethanol (2x) and then in acetone (2x) (Acetone 99.8 %, Merck, Darmstadt, Germany). They were then dried with gaseous nitrogen and put into the UV-O_3 cleaner (UVO Cleaner 42-220, Jelight Company, Irvine, United States) for 15 minutes. This last cleaning step is important to remove any contaminants on the substrate surface and to increase the surface energy by formation of high energy hydroxide groups [64].

1.3 Polyelectrolyte solution

In order to construct the layers, the solutions of chitosan, heparin and heparin/LL-37 complex must be prepared. The optimal pH and ionic strength must be chosen to ensure a good stability of the layers. The chitosan and heparin solutions were thus prepared at pH 3.5, an ionic strength of $\approx$ 0 mM and a concentration of 0.5 g/L.

The assembly pH of 3.5 was experimentally selected by Cédric Vranck by testing the construction of the multilayers at different pH values with the QCM-D, that allows visualisation of the adsorption of each layer. The same experiment performed at an assembly pH of 5.5 showed no absorption of the layers and the assembly pH of 3.5 was thus retained. Moreover, as explained in Section 3.6 of the State of the Art part, Fu et al. demonstrated that the assembly pH has an influence on the antibacterial activity of the multilayers. According to their study, an assembly pH of 3.8 shows the best bactericidal effect compared to pH values of 2.9 and 6, with a decrease of 68% of viable bacteria on the multilayer after 7 hours. [57]

The ionic force was kept as low as possible, this is, close to 0 mM. At low pH, the ionic strength of the solution has an important effect on the layer build-up. Indeed, the electrostatic charges on the polyelectrolytes are screened by the charges added by the salt. The effect is less pronounced at higher pH since the charge density of CHI is lower [53]. To avoid this screening effect that causes decreased attraction forces and consequently lower adsorption, the ionic strength of the CHI and HEP solutions is kept as low as possible.

It was found that a concentration in the range of the g/L was highly sufficient to reach the plateau of adsorption and saturate the surface to reverse charge polarity for each adsorbed layer [42, 65]. A slight excess ensures that there is no depletion of the solution when constructing several layers.

1.3.1 Chitosan solution

To obtain 50 mL of a 0.5 g/L chitosan solution, 25 mg of 95% deacetylated chitosan (Heppe Medical Chitosan Gmbh, Halle, Germany) was weighted and added to a 50 mL flask. Since chitosan is insoluble in water, an additional solubilisation step with HCl was performed. To maintain the ionic strength as low as possible, 30 µL of concentrated HCl 12M (Prolabo, VWR Chemicals, Leuven, Belgium) was added to the flask, together with 25 mL of ultrapure water. The solution was then heated at 60°C and mixed from time to time until complete solubilisation of chitosan occurred. After cooling down, 25 µL of NaOH 10 M (Sigma Aldrich, Steinheim, Germany) was added to neutralise the acid. Ultra-pure water was added to reach the 50 µL mark. In order to eliminate impurities, the solution was filtered twice: first using a cellulose filter 5 µm (Ahlstrom, Barenstein, Germany) and then with a polyether sulfonate 0,2 µm (VWR Chemicals, Leuven, Belgium). The pH of the solution was then measured with a pH-meter (inoLab® pH 7110, Xylem Analytics, Weilheim, Germany) and adjusted to 3.5 with concentrated HCl and NaOH to keep the ionic strength as low as possible. This solution was kept in the fridge at 4°C until further use.

1.3.2 Heparin solution

The 0.5 g/L heparin solution was prepared from a stock solution of sodium heparin (5000 I.E./mL ; B.Braun, Melsungen, Germany) which contains 200 IU/mg. Thus, the concentration of this stock solution is 25 mg/mL (5000/200), and 1 mL must be poured in a 50 mL flask to reach the desired concentration. A stock solution of ultra-pure water at pH 3.5 was prepared by adding a few drops of concentrated HCl 12M to ultra-pure water until the desired pH was reached. A pH indicator paper was used for control.
The flask containing heparin was then filled with this stock solution until the 50 mL mark was reached. Again, the solution was kept in the fridge at 4°C until further use.

1.4 PPCs solution: Heparin/LL-37 complexes

vander Straeten et al. demonstrated that LBL construction using PPCs is independent of the charge state of the protein, and only relies on interactions between the formed complex and the counter polyelectrolyte [45]. Consequently, only the global charge of the PPCs matters for the layer build-up, which can be controlled by adapting the HEP/LL-37 charge ratio. This ratio is obtained by adapting the amount of positive and negative species (in this case, HEP and LL-37) introduced in solution to form the complexes.

A negative-to-positive charge ratio of 1.5 for the PPC was found experimentally by Cédric Vranckx. Indeed, as of this charge ratio, the complexes are well formed for their integration in the multilayers.

The isoelectric point of LL-37 and its charge at pH 3.5 were calculated using the PDB2PQR server and the PROPKA tool for prediction of the pKa values of a protein [66]. It was found that LL-37 has 10.4 positive charges per peptide at pH 3.5.
Heparin is a strong polyanion and its degree of charge does not depend on pH. It has 4 negative charges per sodium heparin dimer. Since the molar mass of heparin dimer is 665 g/mol, the prepared stock solution (1.3.2) of 0.5 g/L has 0.003 mol (-)/L. This solution needs to be diluted 6 times to obtain a concentration of 0.5 mM (-).

The stock solution of LL-37 (Proteogenix, Schiltigheim, France) has a concentration of 450 µg/mL and LL-37 has 10.4 positive charges per peptide at pH 3.5 and a molar mass of 4493.26 g/mol. This results in a concentration of 1.0410 mM (+) in the stock solution. By diluting this solution 10.41 times, we obtain a concentration of 0.1 mM (+).

As explained previously, a (-)/(+) charge ratio of 1.5 is desired for PPC formation. To satisfy this ratio, we need 3 volumes of the (-) species (0.5 mmol (-)/L) and 10 volumes of the (+) species (0.1 mmol (+)/L). Water must be added with a volume equal to 1/10 of the volume of the (+) species in order to keep a constant concentration in (+) charges whilst changing the ratio's. For a total volume of 10.931 mL, Table 5 shows the composition of the solution.

Table 5: Composition of the PPCs solution (LL-37/HEP complex)

LL-37	750 µL	10.41 times diluted to obtain solution of 0.1 mmol (+)/L
Ultra-pure water (pH 3.5)	7058 µL	
Heparin 0.5 g/L	389 µL	6.01 times diluted to obtain solution of 0.5 mmol (-)/L
Ultra-pure water (pH 3.5)	1953 µL	
Ultra-pure water (pH 3.5)	781 µL	To keep a constant concentration in (+) charges
Total	**10.932 mL**	

The reagents are put together in a 15 mL tube, which is vortexed for 10 seconds and kept in the fridge at 4°C until further use.

1.5 Construction of the multilayers

Construction of the coating is performed on clean titanium substrates and using the solutions described in the previous section. This will be carried out using the aforementioned layer-by-layer approach. The construction of the layer set-up used in this work is depicted in Figure 13.

The cleaned, negatively charged titanium coupons are placed in a 24 well plate. 1 mL of the first polyelectrolyte solution, in this case CHI, is added to each well containing a coupon. The coupons remain immersed in the solution for 30 minutes to adsorb the first monolayer. Then, the solution is removed

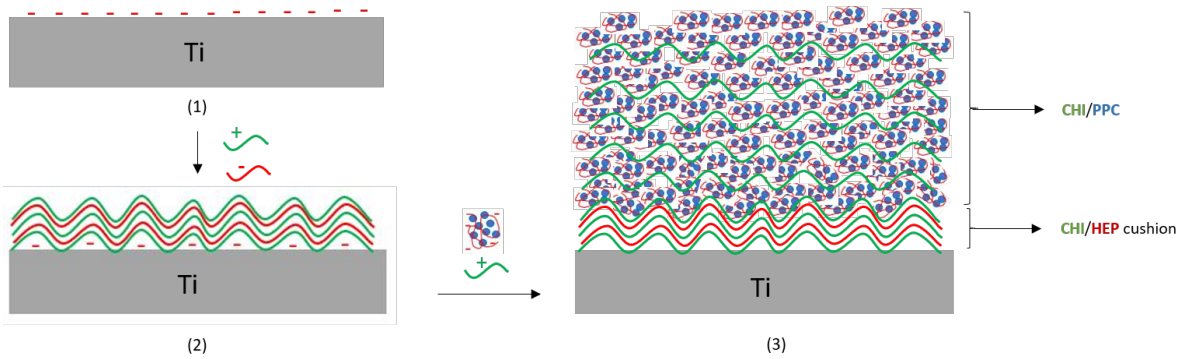

Figure 13: Construction of the layer set-up used in this work. CHI is represented in green, HEP in red and the LL-37 peptide as blue dots.

and 1 mL of ultra-pure water at pH 3.5 is added to the well. The plates are gently mixed during 30 seconds and the water is then removed. This cleaning step is repeated 3 times and allows the removal of unbound polyelectrolytes. After that, 1 mL of the oppositely-charged polyelectrolyte solution, here the HEP solution, is pipetted into the well and the adsorption takes place during 30 minutes. (Step (1) on Figure 13).

These adsorption steps are repeated until a $[Chi/Hep]_2$ cushion with 3 layers of CHI and 2 layers of HEP is formed (Step (2), Figure 13). The washing step is performed between each layer deposition. Then, the same pattern is repeated by alternating the adsorption of the PPCs solution and the HEP solution (Step (3) on Figure 13) until a $[CHI/HEP]_2/[CHI/PPCs]_6$ multilayer is obtained.
After the last layer has been deposited, the samples are washed 7 times during 30 seconds and put under a gaseous nitrogen flow to dry.

According to the desired layer set-up, the number of adsorption steps of each PE or PPCs solution can be adapted to vary the design of the film.

The multilayers can also be constructed in an hydrated environment using the Quartz Crystal Microbalance with dissipation. This will be further detailed in Section 2.1.

1.6 Layer disassembly

As described in section 3.7 of State of the Art, changes in the physico-chemical environment of the multilayers can induce their disassembly. Hence, a solution at high pH and high ionic force was prepared with the aim to disassemble the previously formed multilayer. 438 mg NaCl (Prolabo, VWR Chemicals, Leuven, Belgium) is dissolved in 50 mL water to obtain a solution of 150 mmol/L. The pH is then adjusted to 9 with concentrated NaOH.

A second approach consists in the addition of a surfactant to the multilayers. Therefore, another solution was prepared with the anionic surfactant sodium dodecyl sulfate (SDS) (Sigma Aldrich, Darmstadt,

Germany) at 1% volume. Its structure is represented in Figure 14.
Each solution is then added to the coated sample for layer disassembly.

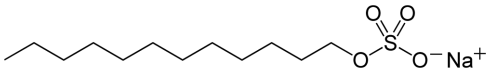

Figure 14: Structure of SDS.

2 Characterisation methods

Once the layers have been constructed, they need to be characterised to determine their physico-chemical properties. The methods described in this section allow retrieval of information on surface properties of the microfilm such as thickness, adsorbed mass and chemical composition. This section will present the principle of the used characterisation methods.

2.1 Quartz crystal microbalance with dissipation

Quartz crystal microbalance (QCM) is an extremely sensitive tool used for the study of soft and solvated interfaces between solid surfaces and bulk liquids. It provides information on the distribution of material at an interface, and can measure very small mass variations per unit area at the surface of a sample.

QCM relies on the principle of the inverse piezoelectric effect: application of a voltage to certain crystalline materials results in mechanical deformation of this material. This means that the application of an alternating voltage to the crystal will cause oscillations at a certain frequency. If the voltage frequency matches the resonance frequency of the crystal or one of its overtones, a standing wave is generated in the crystal.

Because of their stability and very low energy dissipation, quartz crystals are used as microbalances. The oscillation frequency of the quartz crystal is modified by addition or removal of a material. The deposited material increases the crystal thickness, creating a shift in the resonance frequency. The relationship between the adsorbed mass on the crystal and the frequency shift depends on the film type.

If the deposited film is considered to behave in the same way as the crystal, the Sauerbrey equation may be used to calculate the areal mass density of the adsorbed film. To satisfy this hypothesis, the adsorbed layer must be thin, homogeneously distributed and rigid. The energy dissipated by the film is then considered insignificant and the following linear relationship between the mass change and the change in resonator frequency can be derived.

$$\Delta f = -\frac{n}{C}\Delta m \tag{1}$$

where Δf is the frequency shift, Δm is the mass change per unit area, n is the overtone order and C is the mass sensitivity constant that depends on the material properties of the quartz crystal. [67]

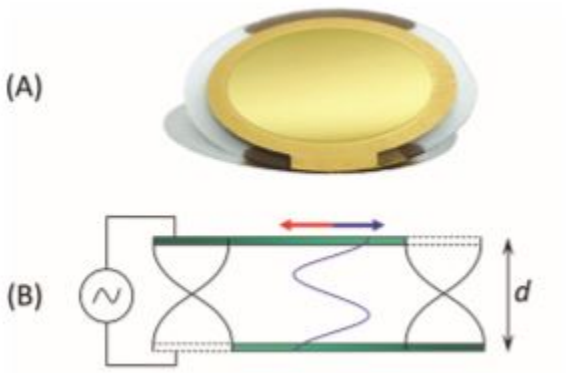

Figure 15: (A) Representation of a quartz crystal with gold electrodes. (B) Side view of the crystal. Application of voltage to the crystal results in an oscillatory motion, where the top and bottom surfaces move in an antiparallel fashion. Reproduced from Reviakine et al. [67]

However, the Sauerbrey equation is not valid for soft, viscoelastic films. Indeed, such viscoelastic films cause dissipation of oscillation energy due to mechanical losses in the softer mass, which dampens the crystal oscillation causing it to decay faster. This parameter is not taken into account in Sauerbrey's relationship. Therefore, measurements of both frequency and dissipation are necessary to calculate the adsorbed mass accurately. These parameters can be acquired using the quartz crystal microbalance with dissipation (QCM-D). [68]

In QCM-D, an external voltage is applied to excite the quartz crystal to its resonance frequency, and then turned off intermittently. The voltage decay as function of time is then monitored. The resonance frequency f and the energy dissipation D can be extracted from the decay curve, and the adsorbed mass and viscoelastic properties can then be calculated using the Voigt viscoelastic model.

QCM-D is thus very useful for the surface characterisation of the designed coating. It enables real-time data acquisition of the layer construction, and the analysis of the obtained parameters allows retrieval of the adsorbed mass per adsorption step.

To perform optimal QCM-D analysis, adsorption of the desired multilayers on titanium-coated quartz crystals is monitored in situ. The QCM used in this work is the Q-Sense E4 system (Biolin Scientific, Gothenburg, Sweden). The used crystals are AT-cut 5 MHz crystals coated with titanium from Q-Sense (QSensor QSX 310 Ti). Before use, they were washed following the suggested pre-cleaning protocol from QSense [69] (see Appendix A).

Using the experimental set-up described in Figure 16, 4 crystals were coated with 6 layers of PPCs to obtain a $[CHI/HEP]_2/[CHI/PPCs]_6$ coating. The module allows measurements on 4 crystals simultaneously. A pump running at a flow of 20 µL/min puts the first polyelectrolyte solution in circulation into the four QCM cells containing the crystals. The different layers are thus adsorbed successively on the titanium surface of the crystals, and the frequency shift and dissipation are monitored in real time. During each

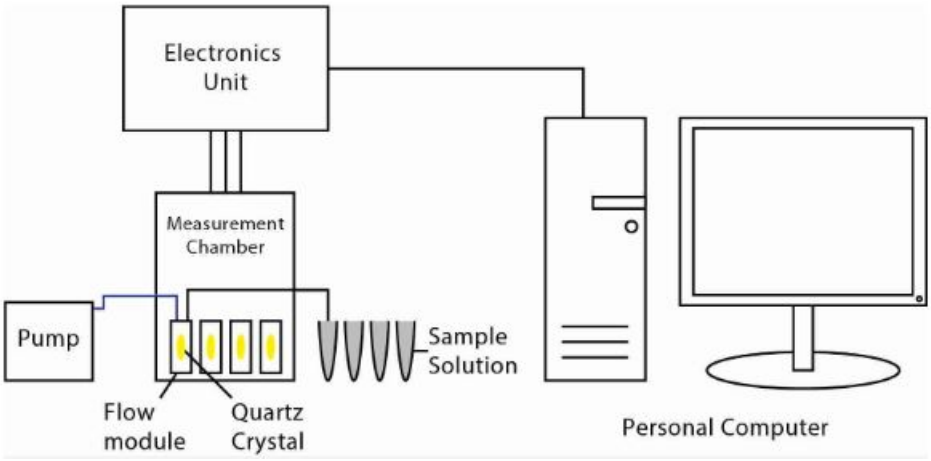

Figure 16: Experimental set-up of the layer construction using QCM-D. Image retrieved from Nanoscience Instruments [68].

layer adsorption, a frequency drop and a rise in dissipation energy can be observed. The adsorption goes on until the decrease stops and a stabilisation of the frequency can be observed.
Water is then pumped into the system for 10 minutes in order to rinse the sample. The adsorption of the next layer can then begin. Doing so, a $[CHI/HEP]_2/[CHI/PPCs]_6$ coating is constructed. The results were then treated and analysed using the Q-Stomize software.

With the aim to disassemble the multilayers and allow release of LL-37, three QCM crystals were coated in the same manner as the previous experiment. The NaCl solution at pH 9 and I $\approx$ 0 mM was flowed through the QCM, followed by a solution of SDS 1% until stabilisation of the frequency.

Moreover, the stability of the constructed multilayers upon bacterial tests was assessed by flowing the bacterial culture medium Mueller Hinton Broth (MHB) through the QCM and monitoring the change in adsorbed mass. The interaction of the layers with such medium, possibly occurring through complexation of LL-37 with one of its components, would diminish the antimicrobial activity of the peptide and needs thus to be avoided.

2.2 Ellipsometry

Ellipsometry is a very sensitive and non-destructive optical technique used to determine the thickness and optical parameters of thin layers. The principle relies in measuring the change of polarisation of a light beam after reflection on the sample surface. The samples properties (thickness, refraction index) determine the polarisation change. This change is quantified by two parameters: the amplitude ratio (ψ) and the phase difference (Δ). Light is an electromagnetic wave which can be described by its two orthogonal components: p-polarised and s-polarised light (respectively parallel and perpendicular to the plane of incidence). These waves are characterised by their amplitude and phase, and the resultant light is elliptically polarised. [70, 71]

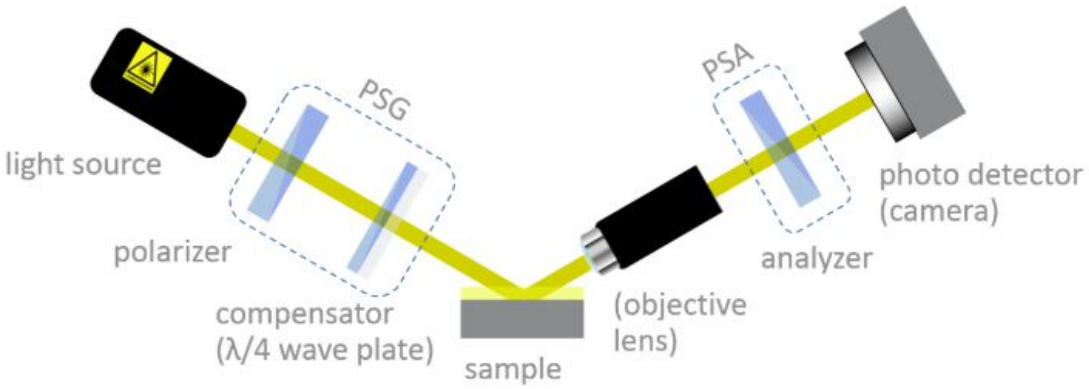

Figure 17: Schematic representation of the basic set-up of an ellipsometer.

Figure 17 shows the basic set-up of an ellipsometer. A light source emits a light beam, which is polarised through a polarizer (PSG) and falls on the sample surface at an angle ϕ. After reflection, the light passes through a polarisation state analyzer (PSA) and is then caught by the detector. The angle of incidence of the light beam can be varied, and the measurement is here performed at one single wavelength, that is 658 nm. The measured data is then fitted to a physical model of the analysed film.

In this master thesis, we used ellipsometry to measure the thickness of the deposited multilayers on a titanium substrate. The used ellipsometer was the Imaging Ellipsometer NanoFilm_ep4 (Accurion GmbH, Göttingen, Germany). Data were analysed using the Accurion NanoFilm_ep4 software.
Determination of the refractive index of the multilayer was quite difficult, since the layer is made of different components in unknown proportions. McMeekin et al. reported that the values for refractive indices of proteins are nearly constant and close to 1,60, and Lundin et al. measured a refractive index of 1,46 for the CHI/HEP multilayers. However, this value was found to be dependent of the solution's pH and the number of adsorbed layers [72, 53].
The $[CHI/HEP]_2/[CHI/PPCs]_6$ multilayers were thus considered as a single layer with a single refraction index evaluated between 1.45 and 1.6. Moreover, the deposited film is supposed to be homogeneous on the substrate surface. These simplifications must be kept in mind since they may have an impact on the interpretation of the obtained results.

Different measurements were performed with the ellipsometer, investigating different substrates that were all coated with a $[CHI/HEP]_2/[CHI/PPCs]_6$ film. Some measurements were performed on the QCM crystals, while the layers were constructed using QCM-D or in a multi-well plate. The drying method varied as well. The other measurements were performed on Si and Ti wafers. A naked, uncoated crystal was tested as well.

The coated samples were introduced in the ellipsometer and the measurements were performed at $\lambda =$ 658 nm and testing different incident angles. The obtained ψ and Δ values were fitted into an appropriate model. To design an optimal model taking the substrate and film properties into account, the expertise of Prof. Alain Jonas was requested. The results are discussed in section 1.2 of the Results part.

2.3 X-ray Photoelectron Spectroscopy

X-Ray photoelectron spectroscopy (XPS) is a surface analysis method which measures the elemental composition of a sample, as well as the chemical and electronical state of the elements. Its principle relies on the photoelectric effect. XPS spectra are obtained by irradiating a material with a beam of X-rays while simultaneously measuring the kinetic energy and number of electrons that escape from the sample surface. The atoms of the sample surface layer are excited by the X-ray photons, and electrons are expelled with a certain amount of kinetic energy. This kinetic energy is related to the binding energy of the electron to the atom by the following equation:

$$E_k = h\nu - E_b - \phi_{sp} - E_c \tag{2}$$

with E_k the kinetic energy, $h\nu$ the energy provided by the photon, E_b the binding energy, ϕ_{sp} the spectrometer work function and E_c the surface charge potential, equal to zero for conducting samples. The binding energy allows determination of the element and its chemical state. The number of emitted electrons is measured as well, and peak intensity can be related to surface elemental composition by means of sensitivity factors [73].

XPS probes a very thin layer of the sample surface, usually considered to have a thickness of 10 nm. Only these electrons that do not suffer energy losses while travelling through the material will contribute to the peaks. Atoms located deeper can also be ejected, but they will undergo inelastic collisions with other particles and lose energy. Some will have enough energy left to contribute to the background signal, while the deepest located electrons are not ejected from the sample.

XPS analyses are performed under ultra high vacuum, to avoid collisions between gas molecules and electrons which would make them lose their energy. Briefly, a typical XPS instrument as shown on Figure 18 consists of an X-ray source, a kinetic energy analyzer, an electron detector, and an ultra-high-vacuum system.
The analyses were performed on a SSX 100/206 photoelectron spectrometer from Surface Science Instruments (USA) equipped with a monochromatised and microfocused AlK_αX-ray beam (powered at 20 mA and 10kV). The pressure in the analysis chamber was around 10^{-9} Pa. The elemental composition of six different samples was analysed and will be discussed in section 1.5 of the Results part.
To treat the obtained data, CasaXPS was used (Casa Software LTD, UK) and the C-(C,H) component of the C1s peak of carbon was fixed at 284.8 eV to correct the binding energy scale.

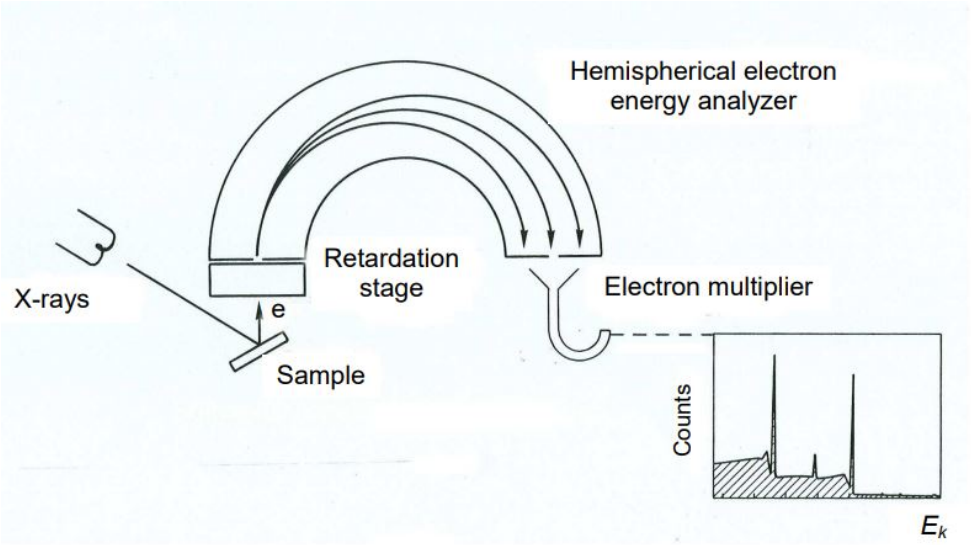

Figure 18: Schematic representation of an XPS system. Reproduced from Dupont et al. [73]

3 Antibacterial activity

Once the coating has been built and characterised, its antimicrobial activity should be assessed. In this section, the bacterial tests performed on the coating will be described, as well as the minimal inhibitory concentration (MIC) tests for LL-37. All tests involving bacteria were carried out at the Louvain Drug Research Institute in Woluwe (UCL), under the supervision of Prof. Françoise Van Bambeke and with the precious help of PhD candidate Dr. Hervé Poilvache.

3.1 Sterility

First of all, in order to measure antibacterial activity, the coating needs to be sterilised to avoid the growth of unwanted microorganisms and assess its effect on a particular bacterial strain. Sterilisation consists in killing or removing all microorganisms present in a defined environment [74]. Different sterilisation techniques exist, based on heat, filtration, radiation, or the use of gases or solvents. However, the sterilisation method must be selected carefully to maintain the integrity and bioactivity of the coating.

Sterilising the coating after its construction is very difficult without risking alteration of the structure or loss of its bioactivity. Autoclaving, radiation and solvent treatment of the final multilayers are therefore outruled. Instead, the choice was made to build the multilayers in a sterile environment. This sterile environment can be provided either by the use of a laminar flow hood or by working in the immediate environment of a flame.

Consequently, the assembly of the multilayers was carried out next to the flame of a bunsen burner. The chitosan and heparin solutions as well as the ultra pure water used for rinsing were filtered with a polyethersulfone filter with a pore diameter of 0.2 µm that is to small for microbes to pass through. The

titanium wafers were cleaned with ethanol and acetone as described in Section 1.2. They were then placed in sterile multiwell plates opened near the flame and rinsed once again with ethanol. The multilayers were then constructed as described in Section 1.5, until six layers of PPCs were adsorbed. Before starting with the antibacterial activity tests, the sterility was checked by 12 h incubation of the coated samples in Mueller Hinton Broth (MHB) (Sigma Aldrich, Darmstadt, Germany) culture medium at 37 °C. MHB is a nutrient broth composed of beef extract, casein hydrolysate, starch and water that allows microbiological growth.

3.2 Antibacterial activity test

The objective of the following test is to collect first data on the effect of the designed antibacterial coating on the adhesion of *S. aureus* and on the biofilm growth on the substrate. For this purpose, three different samples were tested in triplicate: a bare Ti wafer, a $[CHI/HEP]_2$ and a $[CHI/HEP]_2/[CHI/PPCs]_6$ sample. All manipulations were carried out in sterile conditions and under a laminar flow hood.

Bacterial suspension The bacterial strain ATCC 33591 of *S. aureus* was precultured on trypticase soy agar (TSA) from a stock frozen at -80 °C. The bacteria was left to grow overnight at 37 °C.
A bacterial suspension was prepared in sterile phosphate-buffered saline (PBS) and its turbidity was compared to that of a McFarland standard. A McFarland standard is a chemical solution of barium chloride and sulfuric acid, that has a turbidity comparable to that of a bacterial solution [75]. This method is useful to adjust the bacterial inoculum so that it would be in a defined range and standardised in all experiments. The goal is to obtain a concentration of 10^8 colony forming units (CFU)/mL, which is checked using the CECIL device at a wavelength of 620 nm and aiming for an optical density value of 0.5 +/- 0.02. CFU is a unit to estimate the number of viable bacteria in a sample. The bacterial suspension was then diluted 1:100 in TGN (Tryptic soy broth + 1% glucose + 2% NaCl) to reach a final concentration of 10^6 CFU/mL. This concentration used for inoculation is recommended for susceptibility testing [76] and was verified by Hervé Poilvache during his PhD thesis.

Multiwell plate Two 12-well plates were prepared by depositing three samples of each kind in the configuration depicted on Figure 19. Bacterial adhesion will be checked in the first plate while biofilm formation will be assessed in the second plate. A volume of 3 mL of bacterial suspension was then added to each well and the plates were incubated at 37 °C with an agitation of 50 rpm.

CFU count After 2 h of incubation, one of the two bacterial plates was retrieved in order to check bacterial adhesion on the coupons. The coupons were rinsed twice in PBS and vortexed for 30 seconds. They were then sonicated for 5 minutes in order to detach the bacteria and vortexed again for 30 seconds. The supernatant of each well was then diluted 10 times in PBS, 3 times in a row, to obtain solutions at 4 different dilution factors per sample: 10^0, 10^1, 10^2 and 10^3. 50 µL of each dilution was then spread on TSA medium in Petri dishes and incubated for 24 h at 37 °C to be counted. Since the bacterial concentration is unknown, several dilutions are required to find at least one concentration range where the CFUs would be easily countable on the Petri dishes.

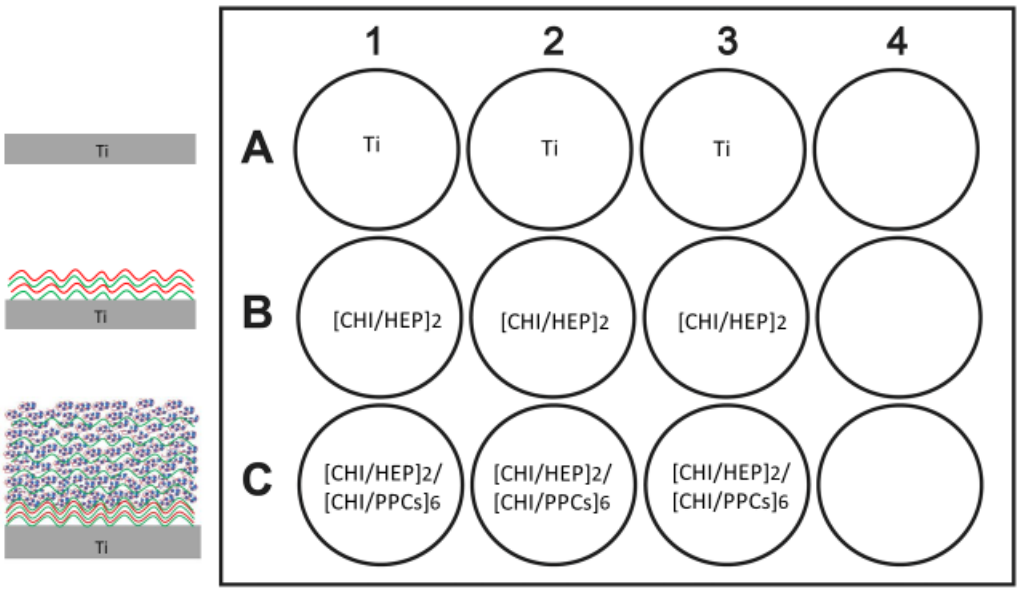

Figure 19: Schematic representation of the configuration of the multiwell plate for the antibacterial activity test. Two similar plates were prepared, to monitor bacterial adhesion and biofilm formation respectively.

The second plate was retrieved after 24 h to investigate the formation of biofilms. The same protocol was applied, with an extra dilution of the supernatant however to reach a dilution factor of 10^4. Indeed, more bacteria are expected to be found after 24 h incubation.

For each dilution of each sample, CFUs were counted using the Gel Doc XR+ machine.

3.3 Minimal inhibitory concentration determination

In order to characterise the bioactivity of the coating, the first step is to fully understand the action and activity of LL-37. Literature reports different values regarding its antibacterial and antibiofilm activity (see State of the Art 2.3.2), that are commonly measured by a minimal inhibitory concentration (MIC) test. The MIC is defined by Wiegand et al. as 'the lowest concentration of an antimicrobial agent that inhibits the visible growth of bacteria under defined test conditions' [76]. MIC test protocols involve broth or agar dilution methods, where a standardised amount of bacteria is put in presence of different concentrations of the tested antimicrobial agent (typically a twofold dilution series). After incubation, the activity of this agent can be deduced from the bacterial growth in the wells. The lowest concentration at which no visible bacterial growth is observed is the MIC. Guidelines for broth microdilution methods are given by the European Committee on Antimicrobial Susceptibility Testing (EUCAST) [77].

A first attempt to determine the MIC of LL-37 was made by Cédric Vranckx by testing concentrations of the peptide up to 2246 µg/mL against *S. aureus*. However, even this high peptide concentration showed no bacterial growth inhibition, which is very surprising considering the MIC values between 10 and 144 µg/mL found in literature [31, 32, 30, 21]. Hence, the followed protocol was considered non adapted to the MIC determination of LL-37 and needed some changes.

After bibliographic searches, an alternative protocol was found for cationic antimicrobial peptides. Steinberg et al. reported complexation of protegrin-1, a β-sheet antimicrobial peptide, with MHB culture medium compounds, and consequent diminution of its antimicrobial activity [78]. To overcome this problem, researchers prepared the peptide dilutions in a solution containing 0.01% of acetic acid and 0.2% of bovin serum albumin (BSA) as a carrier protein instead of MHB. Moreover, cationic peptides were found to adsorb on the negatively charged surface of glass and some plastics, particularly on the traditionally used polystyrene plates. This reduces their contacts with target bacteria, resulting in a decrease of activity. Polypropylene was thus used instead and proved to induce a higher antimicrobial activity of AMPs. Based on those two findings, a slightly adapted protocol for MIC tests on anti-microbial peptides was proposed by Wiegand et al. and adapted to use in this experiment [76]. Giacometti et al. compared this adapted protocol with the standard procedures outlined by the National Committee for Clinical Laboratory Standards (NCCLS) and found a fourfold reduction of the MIC values when using the adapted protocol. [79]

Bacterial suspension Two bacterial strains of *S. aureus* and *S. epidermis*, ATCC 33591 and ATCC 35984 respectively, were incubated overnight at 37 °C. A small number of colonies were diluted in 3 mL of PBS. The turbidity of the solution was compared with a 0.5 McFarland standard which corresponds to a bacterial density of $\pm$ 10^8 CFU/mL and diluted until the same turbidity was reached. The turbidity was also verified by measuring the absorbance of the solution spectrophotometrically. This solution was then diluted 100 $\times$ in MHB to reach an inoculum of 10^6 CFU/mL.

Preparation of solution of acetic acid and BSA A solution of 0.02% acetic acid (Sigma Aldrich, Darmstadt, Germany) and 0.4% BSA (Sigma Aldrich, Darmstadt, Germany) was prepared and filtered in a 0.2 nm filter to guarantee sterility. This solution (named solution A) was then diluted at a factor 1:2 to obtain solution B.

Peptide dilutions MIC tests for LL-37 alone and for a solution of PPCs (LL-37 + HEP) at a charge ratio of 1.5 were carried out, each in triplicate. Two 96-well polypropylene plates were prepared, for activity testing of *S. aureus* and *S. epidermis* respectively. The experimental design is schematically represented in Table 6. A two-fold dilution series was performed, starting at a concentration of 2250 µg/mL for LL-37 and 1125 µg/mL for the PPCs. Indeed, since the LL-37 stock solution was concentrated at 9000 µg/mL and LL-37 needed to be diluted with heparin to form PPCs, a concentration of 2250 µg/mL was not achievable.
To achieve this dilution series, 50 µL of the LL-37 sterile stock solution was added in the first well of the rows A,B and C. The same volume of the PPCs solution was added in the first well of rows D,E and F.

Table 6: Experimental design of the microtiter plate for MIC determination of LL-37, PPCs (LL-37 + HEP) and vancomycin as a control. G = growth control well and S = sterility control well.

	row/column	**1**	**2**	**3**	**4**	**5**	**6**	**7**	**8**	**9**	**10**	**11**	**12**
C_{LL-37} (µg/mL)		2250	1125	562	281	140	70	35	17	9	4	G	S
LL-37	**A**												
	B												
	C												
C_{LL-37} (µg/mL)		1125	562	281	140	70	35	17	9	4	2	G	S
PPCs (LL-37 + HEP)	**D**												
	E												
	F												
C_{Vanco} (µg/mL)		32	16	8	4	2	1	0.5	0.25	0.13	0.06	G	S
Vancomycine	**G**												
	H												

Then, 50 µL of solution A containing 0.02% acetic acid and 0.4% BSA was added to all wells of column 1. The solution was carefully mixed by pipetting up and down 6-8 times. 50 µL of solution B was then poured in the wells of column 2 to 12. 50 µL of the wells of the first column were then added to the wells of the second column to perform a dilution 1:2. The solution was carefully mixed by pipetting up and down several times and similar dilutions were continued from column to column until column 10. The last 50 µL were discarded. This results in a series of twofold dilutions ranging from 2250 to 4 µg/mL for LL-37 and from 1125 to 2 µg/mL for the PPCs, containing 0.01% acetic acid and 0.2% BSA in each well. Columns 11 and 12 are the growth (G) and sterility (S) controls respectively.

50 µL of the bacterial solution was then pipetted into the wells of column 1-11, to obtain a final volume of 100 µL in each well. The wells of column 11 contain only bacteria and culture medium, and the bacterial growth in absence of antimicrobial agent can thus be verified. The sterility of the procedure was controlled by adding 50 µL of MHB culture medium into the wells of column 12, but without inoculating bacteria. If these wells become trouble after incubation, this means that the plates were contaminated and the experiment must be repeated from the beginning.
Both multiwell plates were then incubated for 24 h at 37 °C to allow bacterial growth.

This experiment was repeated twice. The second time, all volumes were doubled to have a final volume of 200 µL in each well. Moreover, to verify that the susceptibility results were accurate, a commonly used antibiotic for which the MIC value is well defined in literature was included as a control. Vancomycine was thus tested twice at concentrations ranging from 32 µg/mL to 0.06 µg/mL, following the same protocol as described in the previous paragraph.

Reading of the MIC The MIC value can then be read with the bare eye, or with the help of a mirror, as the lowest concentration of antimicrobial agent that completely inhibits visible bacterial growth [77]. Viewing devices such as spectrophotometers can facilitate the reading and help to discern growth in

the wells, and several colorimetric methods based on the use of dye reagents exist for this purpose [80]. Consequently, two additional tests were performed to confirm the MIC endpoint. Firstly, the absorbance at 600 nm of the solutions in each well was measured with a spectrophotometer. Moreover, a metabolic activity assay was performed with resazurin. Resazurin is a non-fluorescent blue dye that is reduced by metabolic activity of living cells in a pink, highly fluorescent molecule called resorufin, as shown in Figure 20. The measured fluorescence is proportional to the number of viable cells in solution. The fluorescence is then read using a spectrophotometric microtiter well plate reader, with excitation at 560 nm and emission at 590 nm.

100 µL of a resazurin solution of concentration 20 µg/mL was added to each well, to reach a final concentration of 10 µg/mL. The microplate was then incubated for 30 minutes at room temperature and in the dark.

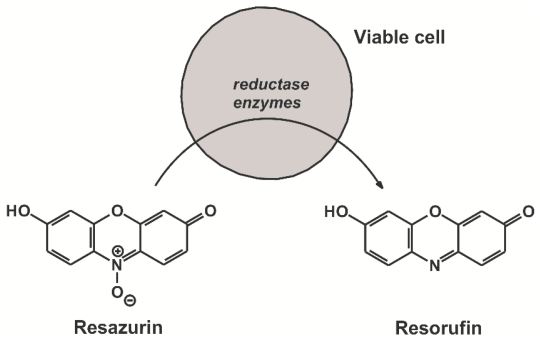

Figure 20: Mechanism of resazurin reduction, retrieved from Csepregi et al. [81]

Part V
Results and discussion

This results section is divided in two parts. The first part aims at describing the different characteristics of the adsorbed film. The first step has been to validate the build-up of the multilayers and prove the incorporation of the LL-37 peptide into the coating. By monitoring the mass adsorption layer after layer using QCM-D, the adsorbed amount of each chosen polyelectrolyte could be assessed, and the efficiency of LL-37 immobilisation through the use of PPCs was investigated. The thickness of the multilayer was then evaluated, based on the QCM results of adsorbed mass and density of the film on the one hand, and using ellipsometry on the other hand. Furthermore, the XPS results were interpreted to retrieve the elemental composition of the film. Using those results, an estimation of the ratios of LL-37 to HEP and CHI to HEP in the coating was made.

1 Layer construction and characterisation

1.1 Adsorbed mass and hydrated film thickness

A $[CHI/HEP]_2/[CHI/PPCs]_6$ film was constructed simultaneously on 4 titanium-coated quartz crystals following the conditions presented in Section 2.1 of Materials and Methods. As a reminder, the layers were constructed at pH 3.5, I $\approx$ 0 mM and with a HEP/LL-37 charge ratio of 1.5. The frequency shift and dissipation were monitored in real time for each crystal, resulting in 4 data sets. The reported values on the graphs are averaged from these 4 measurements. The results for the fifth overtone are presented here.

Validation of Sauerbrey's approach To calculate the adsorbed mass per area, the characteristics of the film must first be addressed. Since the measured dissipation is small, we assume that the film is laterally homogeneous. To control this hypothesis in a more quantitative way, the following ratio is considered for a 5MHz crystal [67]:

$$\Delta D_n/|-\Delta f_n/n| \ll 4 \times 10^{-7} Hz^{-1} \tag{3}$$

with ΔD_n the dissipation shift and Δf_n the frequency shift. Since this condition is satisfied, the film can be approximated as rigid and the Sauerbrey equation can be used to extract the areal mass density of the film. However, the film is solvated and the areal mass density thus also includes the mass of the solvent, in this case water.

Adsorbed mass Figure 21 (A) is an average of the obtained values for the 4 coated crystals. It represents the total hydrated mass deposited on the crystal in function of the adsorption step. Clearly, the multilayer grows at each adsorption step. This confirms that the formed PPCs are negatively charged and interact with the positively-charged chitosan. They are successfully integrated in the multilayer system and the

PPC approach to immobilise LL-37 in a LbL system can thus be validated. Moreover, almost no desorption occurs between the steps, which indicates that there is no significant loss of matter between each step.

On Figure 21 (B), the average adsorbed mass was computed at each step. Firstly, one can notice a much higher mass adsorption for the PPCs compared to the polyelectrolytes. This mass corresponds to the combined mass of heparin and LL-37 which are the two components of the PPCs, and at this point, we do not know their proportion to each other yet. However, the difference between the adsorbed mass of heparin alone and the PPCs mass is already an indicator of presence of LL-37.

Furthermore, the growth of the multilayers is not linear and tends to be exponential-like. This could be due to diffusion of at least one of the polyelectrolytes or the peptide within the film. Several studies have been conducted that reported the diffusion of polyelectrolytes within growing LBL films, leading to exponential growth [53, 82].

Thickness If we assume that film density is equal to 1 g/cm^3, a value that is reasonable for soft matter [67], the layer thickness can be computed from the adsorbed mass using the following equation:

$$h = \Delta m/\rho \tag{4}$$

where h is the film thickness, Δm is the adsorbed mass and ρ is the density. This gives us a film thickness of 152.1 $\pm$ 2.7 nm for the [CHI/HEP]$_2$/[CHI/PPCs]$_6$ system.

Dissipation The dissipation shifts measured during this experiment are inversely related to the frequency shifts (data not shown). A final dissipation of $2.07 \times 10^{-5} \pm 0.11 \times 10^{-5}$ was measured. This relatively high dissipation shift indicates a change in the softness of the adsorbed mass, suggesting that the layers become more viscoelastic and hydrated. The same observation was made by vander Straeten et al. with PAH - lysozyme/PSS complexes. He found a higher hydration level for these layers compared to layers assembled with free lysozyme molecules. [83]

The highest dissipation shifts are found at the PPCs adsorption steps, in line with the mass adsorption values. This higher dissipation value could possibly indicate the incorporation of more water molecules into the layer at this adsorption step. The highly hydrated nature of these films could help to retain the biological activity of LL-37.

The results obtained doing this QCM-D experiment trigger the need for additional analyses. The uncertainty on the hydration ratio of the multilayered film encourages the use of optical techniques to measure the dry mass, on a coated sample which should be dried prior to analysis. Doing so, the swelling ratio can be computed from the difference between dry and hydrated mass.

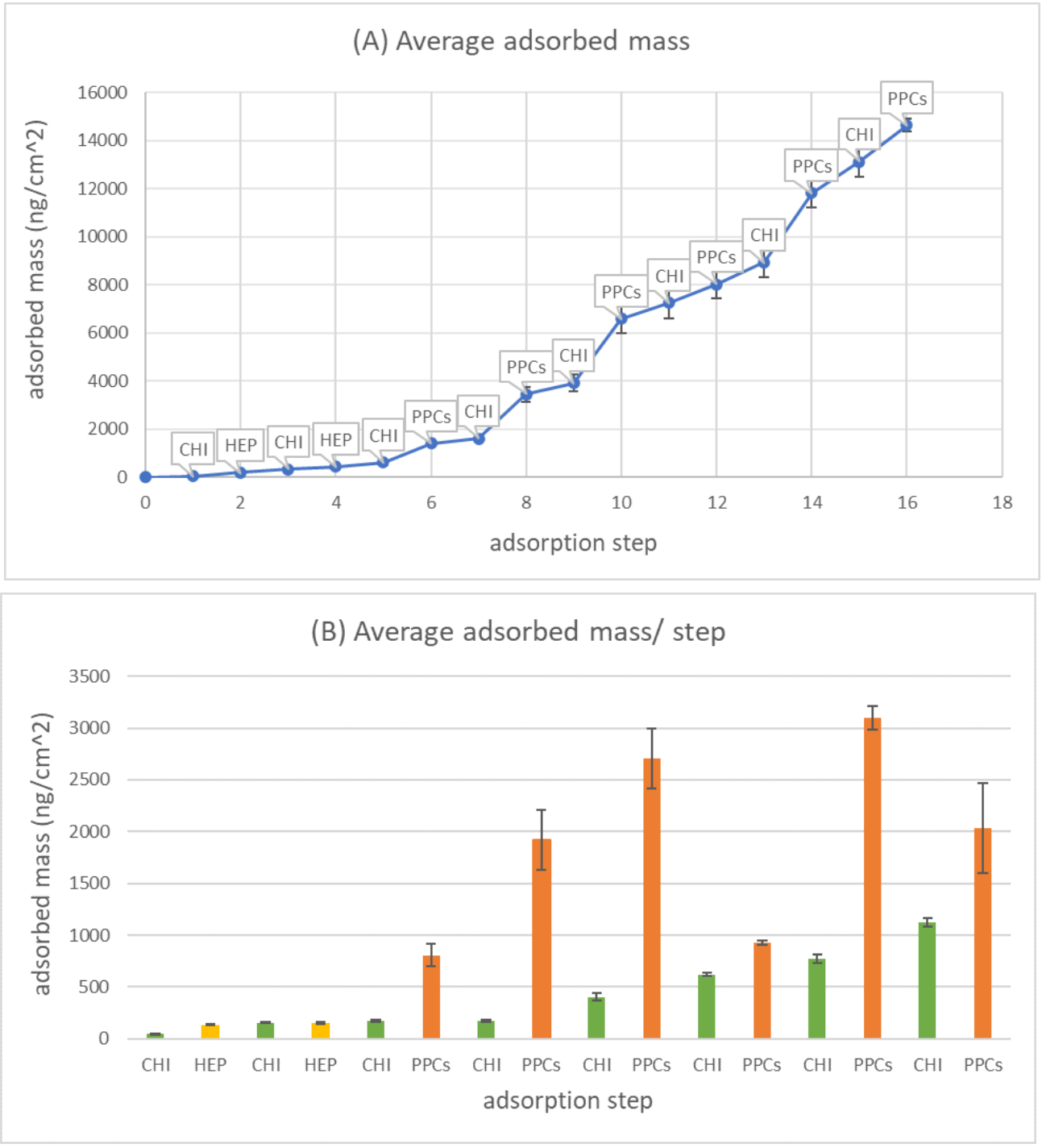

Figure 21: (A) Cumulative hydrated mass measured by QCM-D upon build-up of a $[CHI/HEP]_2/[CHI/PPCs]_6$ system. (B) Average adsorbed mass for each adsorption step. An average of the values for all 4 crystals was made, and the error bars show the standard deviation.

1.2 Dry film thickness

As mentioned before, the next step to gain further insight on the organisation and hydration level of the multilayer was to measure the dry thickness of the film. Ellipsometry was used for this purpose.

Table 7 summarises the experimental conditions of all performed measurements and the obtained results. First of all, the thickness of the coating was investigated using the titanium-coated quartz crystal used for QCM-D as a substrate. This was done because Hardy found in his master thesis that the Ti wafers were too rough to allow ellipsometry analysis. Indeed, AFM measurements on Ti wafers coated with CHI and HEP in different conditions showed a great initial roughness of the hand-polished Ti substrate. This surface roughness tends to decrease when the amount of layers increases. However, the roughness of the sample is still very high compared to the thickness of the formed layers and their visualisation by AFM is almost impossible. The measured height of features found on the Ti wafers can go up to 140 nm. [1]

In conclusion, the surface of the handpolished Ti wafers is really rough. Consequently, it is very difficult to measure the thickness using the ellipsometer, which supposes a smooth surface and a homogeneous film deposition. For this reason, it was decided to use the QCM crystals as a substrate, since they have a surface roughness of less than 1 nm according to the supplier (QSense, Biolin Scientific AB, Sweden), and should thus be easier to analyse using ellipsometry.

Table 7: Experimental conditions for different ellipsometry measurements.

Substrate	**Method**	**Ellipsometer parameter**	**Result**
Quartz crystal coated with gold and titanium	Multilayer constructed by QCM-D and dried in dessiccator	50° - 80° with 5° increment	No result
Quartz crystal coated with gold and titanium	Multilayer constructed in multi-well plate and dried with gaseous N_2	30° - 85° with 5° increment	No result
Si wafer	Multilayer constructed in multi-well plate and dried with gaseous N_2	30° - 85° with 5° increment	4,3-4,6 nm

The first measurement was thus performed on a QSense QCM crystal coated with gold and titanium. A $[CHI/HEP]_2/[CHI/PPC]_6$ coating was constructed and left to dry in the desiccator. The ellipsometry measurements were then applied following the experimental parameters listed in Table 7. However, no results were obtained because the coating appeared rough, not homogeneous, and formed small aggregates visible with the bare eye on the surface of the crystal (see Figure 22). This is believed to be due to the drying process: the multilayer is reorganised and modified upon water withdrawal, creating small aggregates responsible for the spatial heterogeneity and roughness of the surface. [84]

Therefore, the experiment was repeated but the multilayers were assembled in a multi well plate and dried with gaseous N_2 immediately after the last rinsing step, which allows a more homogeneous drying.

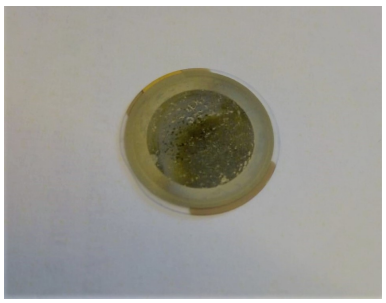

Figure 22: Small aggregates on the surface of the Ti-coated crystal.

No aggregates were visible anymore and the film appeared more homogeneous with the bare eye. A naked, uncoated crystal was analysed together as well.

The delta and psi values for this crystal were retrieved and fit to a model computed with the help of Prof. Alain Jonas in order to find the thickness of the film. This model is computed based on the substrate and film properties of the sample. However, due to lack of information on the quartz crystal composition, no correct model was found. Indeed, the supplier describes the QSense crystal as a quartz crystal with a gold coating and a top coating of Ti. No additional information is given though on the thickness of the gold or titanium layer. Moreover, a TiO_2 layer is supposed to form on the top of the crystal. Without further knowledge of the crystal composition, different simulations were performed, but none of them was satisfying enough to approximate the thickness of the multilayer.

Since the quartz crystals were not suitable to be analysed using ellipsometry, a last attempt involved the use of a silicon wafer. The silicon wafer has the advantage of being industrially polished, and is consequently far less rough compared to the Ti wafers that are used in the present work. Since the layer construction is supposed to behave similarly on Si, this substrate was used as an alternative to calculate the layer thickness. Moreover, Si wafers are often used in ellipsometry and are easy to model. A standard oxide layer thickness of 1.5 nm was determined and a proper fit was found for a thickness of 4.3 - 4.6 nm.

This result shows a surprisingly thin layer compared to the 150 nm obtained with QCM-D measurements. Assuming a dry film density of 1 g/cm^3, the dry mass would be only 430-460 ng/cm^2, which represents a $\approx$ 97% water content in the layers before drying. A possible explanation for this very high swelling ratio is given by vander Straeten et al., who observed a swelling ratio of 90% in PAH - lysozyme/PSS complexes. [45] He suggested that the high charge density of PAH at a low pH value would result in very strong electrostatic interactions between the PAH and PSS, resulting in displacement of the lysozyme of the layers. However, the 3D structure may be kept intact, resulting in a thick film with a high water content and almost no protein immobilised. In theory, this reasoning could be applied to our CHI/PPCs multilayers. However, no desorption of compounds is observed between the steps in the QCM experiment, and the XPS result confirm presence of LL-37 into the layers. It is therefore more likely that the obtained ellipsometer result is not correct.

Indeed, this result must be taken with caution, since it relies on different hypotheses and simplifications. First of all, the multilayers were considered as a single layer with a single refraction index evaluated between 1.45 and 1.6. The density was set to 1 g/cm^3. The multilayers were supposed to adsorb similarly on a silicon substrate compared to the Ti substrate. Lastly, the assumption was made that the deposited film is homogeneous and smooth enough to be measured using the ellipsometer. This should be verified using AFM, but due to lack of time this experiment could not be carried out.

1.3 Desorption of the polyelectrolyte multilayer

The protein-polyelectrolye complexes showed a good adsorption into the polyelectrolyte multilayers. However, although the immobilisation of LL-37 is necessary for a correct construction of the multilayer, its complexed state might also diminish its antimicrobial activity. An attempt at disassembling the obtained multilayers was thus made, as a first step to understand the release of the LL-37 molecules. The deconstruction of the layers was assessed using QCM-D and XPS. The QCM-D results are detailed in this section while the XPS results will be detailed in section 1.5. However, due to a problem with the size of the QCM file, data could not be extracted and are thus not shown.

As predicted in literature [60, 61], the change in pH and ionic strength resulted in mass loss attributed to desorption from the QCM crystal. This could indicate deconstruction of the polyelectrolyte layer, caused by the reduction of electrostatic interactions. Due to the pH above its pKa, chitosan loses its positive charge and desorption occurs. However, the mass loss observed in QCM-D finally reaches a plateau. This means that the desorption is not complete and that only parts of the film were removed.

Rahim et al. observed desorption of polyelectrolyte multilayers upon the addition of SDS, which was proven to be chemically adsorbed into the layers. [63] The same observation was made with the QCM-D, that shows a decrease in adsorbed mass and film thickness. The adsorption of SDS was later demonstrated by the XPS results (see section 1.5). Again, the mass loss reaches a plateau, proving that not all adsorbed mass was removed from the layers. However, since Rahim et al. demonstrated adsorption of SDS into the layers, this mass could be explained by association of SDS molecules with the remaining polyelectrolytes. Indeed, Rahim et al. noticed an increase in thickness of the multilayer after addition of SDS, although polyelectrolyte desorption was confirmed [63]. Hence, the QCM experiment alone does not tell to which extent the layers were disassembled, but shows that SDS had an effect on the multilayer architecture.

Moreover, the time of treatment may have been to short and more complete desorption could have been achieved through longer exposition to SDS or NaCl pH 9. Rahim et al. found that rapid desorption occurred during the first 30 min to 1 h of treatment, depending on the outermost layer. The desorption restarted after 8 h and continued for 8 days. In the experiment conducted here, the solutions were flowed through the QCM until stabilisation of the frequency, which occurred in about 2 hours.

1.4 Interaction with culture medium

To verify the influence of the bacterial culture medium on the multilayer, MHB was added to the film and its adsorption was monitored using QCM-D. No mass increase nor decrease was observed, suggesting that MHB compounds are not adsorbed on the multilayers and that their interaction with the species present in the coating is limited. This proves the stability of the multilayer in this medium.

1.5 Elemental and functional composition using X-ray Photoelectron Spectroscopy

In order to determine the elemental and functional composition of the $[CHI/HEP]_2/[CHI/PPC]_6$ multilayer, XPS analysis was performed on the samples. Six samples were analysed simultaneously, including one control sample, one sample coated only with the $[CHI/HEP]_2$ cushion and 4 samples coated with the whole multilayer ($[CHI/HEP]_2/[CHI/LL\text{-}37]_6$). Amongst these last four samples, one was analysed as such while the three others were treated with MHB, a NaCl solution at pH 9 and I $\approx$ 150 mM and SDS respectively with the aim to test the stability of the multilayers in bacterial medium and deconstruct the layers.

The objective of the XPS analysis is twofold. Firstly, retrieval of the elemental composition should allow identification of the molecules present in the multilayer. The data will be exploited at their maximum to obtain an estimation of the proportions of the different species in the multilayer, which should give us further insight on its composition and architecture. Secondly, the influence of MHB, NaCl solution (pH 9, I $\approx$ 150 mM) and SDS on the composition of the multilayer will be assessed, by comparison between those samples and the $[CHI/HEP]_2/[CHI/PPCs]_6$ sample.

Eight elements were identified by analysing the general spectrum. Ti, Al and V are constituent elements of the Ti wafer (Ti6Al4V). C, N and O are the building blocks of all organic molecules and are thus well represented in heparin, chitosan and LL-37. The S signal originates from the heparin molecules which possess a sulfonate group in their backbone. Finally, the very small Ca signal is a contaminant often due to skin contact.

1.5.1 Thickness of the probed layer

First of all, it is important to compute the thickness of the surface probed by XPS. The signal decreases exponentially in function of depth. 95% of this signal originates from a layer of thickness $3\lambda\cos\theta$, where θ represents the angle of the emitted electron with the normal to the surface of the solid and λ is the inelastic mean free path of the electrons, this is the average distance between inelastic collisions [73]. λ depends on different parameters, including the kinetic energy of the electrons, the molar mass of the species, the number of valence electrons, the band gap and the density of the film. These parameters were estimated for each species composing the multilayer.

The molecular mass and the number of valence electrons were easy to obtain for each species. Nevertheless, the band gap and the density are a little more tricky to calculate. The band gap is defined by Donev et al. as the minimum energy that is required to excite an electron up to a state in the conduction band

where it can participate in conduction [85]. No references were found for chitosan, heparin and LL-37 but a value of 7.5 eV was used after comparison with similar systems. Regarding the density of the film, literature reports values between 1 and 1.5 g/cm^3 with an average value at 1.33 g/cm^3 for LL-37. The density of chitosan and heparin in multilayers was assessed by Lundin et al. and found to be about 1.2 g/cm^3 [53]. Consequently, λ values were computed for each species at 1, 1.33 and 1.5 g/cm^3 and were found to be relatively close. The value at 1.33 g/cm^3 was retained.

Once these parameters were found, the electron mean free path was calculated for each species by means of an online simulator [86] based on an equation developed by Tanuma et al. [87]. The average of the obtained λs was then taken to compute the final thickness. For a θ angle of 55°, Table 8 shows the final depth of the investigated layer in function of the binding energy of different elements. This depth varies between 5.1 and 7.2 nm.

Table 8: Inelastic mean free path of the electrons and probed thickness in function of the binding energy for a θ angle of 55°.

Kinetic energy (eV)	S (1319)	C (1202)	N (1087)	O (856)
λ	4.16	3.87	3.57	2.97
$3\lambda\cos\theta$ (nm)	**7.2**	**6.7**	**6.1**	**5.1**

1.5.2 Elemental composition

The elemental composition of all samples is reported in Table 9. Firstly, one can notice the absence of signal for Ti when the whole multilayer is built. Al, V and Ca are only detected in the first bare Ti sample. The thickness of the probed layer was determined in the previous section and was found to be between 5 and 7 nm. Since the investigated coating is composed of several layers, it is thus not surprising that the underlying substrate is not detected when the number of adsorption steps increases. However, this is an interesting information since it confirms that the layers are thicker than 5-7 nm and that the ellipsometry results are consequently incorrect.
Nevertheless, titanium is still detected after deposition of the CHI/HEP cushion. This suggests that the cushion is very thin and measures less than 5-7 nm. The QCM results showed a hydrated thickness of 6 nm for the chitosan-heparin cushion but the dry thickness is indeed expected to be smaller. Moreover, film retraction upon drying may also lead to the exposure of the underlying substrate.

Furthermore, a clear increase in the carbon, nitrogen and sulfur fractions can be observed upon layer addition, while the fraction of oxygen decreases. Besides, the treatments applied to the fully-coated samples 4 and 5 seem to have a very limited effect on the surface elemental composition. The last sample treated with SDS however shows a higher fraction of carbon and sulfur and a decreased nitrogen and oxygen fraction compared to the other fully coated samples.

Table 9: Surface elemental composition of tested samples in % (excluding hydrogen). Bdl = below detection limit, / = no measurement.

	Ti	C	S	N	O	V	Al	Ca
(1) Ti wafer	11.4	42.0	/	0.9	43.5	0.3	1.7	0.2
(2) $[CHI/HEP]_2$	8.8	35.8	1.4	3.0	49.8	0.3	bdl	bdl
(3) $[CHI/HEP]_2/[CHI/PPCs]_6$	bdl	53.3	2.6	10.8	33.3	bdl	bdl	bdl
(4) $[CHI/HEP]_2/[CHI/PPCs]_6$ + MHB	bdl	55.8	2.0	10.8	31.5	bdl	bdl	bdl
(5) $[CHI/HEP]_2/[CHI/PPCs]_6$ + NaCl	bdl	55.4	2.1	11.4	31.1	bdl	bdl	bdl
(6) $[CHI/HEP]_2/[CHI/PPCs]_6$ + SDS	bdl	62.8	3.3	5.9	27.8	bdl	bdl	bdl

1.5.3 Titanium substrate

As mentioned before, the Ti substrate is visible only for the two first samples (bare Ti wafer and $[CHI/HEP]_2$). When analysing their Ti spectrum, 3 peaks can be distinguished as shown on Figure 23. The two main peaks at 458.8 and 464.5 eV correspond to Ti at an oxidation state of +IV. This is associated to the binding of Ti with two oxygen atoms to form TiO_2. The much smaller peak at 454.04 eV stands for the metallic titanium. The Ti^{+4} peak counts for 93% of the Ti signal, which proves that almost only the titanium oxide layer is present in the first 5-7 nm. This TiO_2 layer explains the higher oxygen fractions found in both samples compared to the others.

The high carbon and oxygen fractions observed on the bare Ti wafer are also due to surface contamination by organic compounds. This is very common in solids, particularly metals and oxides. The decrease in intensity of the TiO_2 peak from the first sample to the second sample until it becomes undetectable in the next samples shows clearly that the substrate is progressively covered by the growing layers.

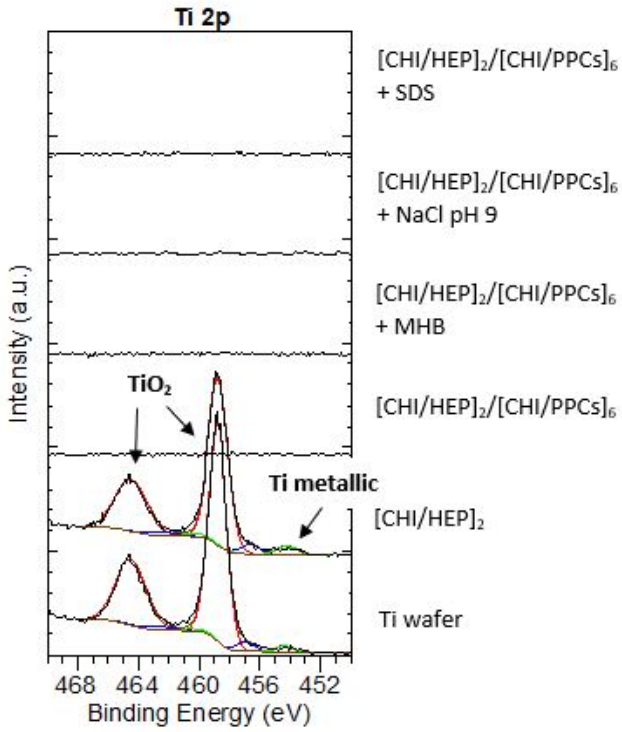

Figure 23: Ti spectra recorded by XPS on Ti substrates, as such, or covered by different multilayers. See text for details.

1.5.4 CHI/HEP ratio

The ratio of CHI unit to HEP unit in the cushion can be assessed by studying the second sample, coated with a $[CHI/HEP]_2$ multilayer. In this work, one unit of CHI is defined as a deacetylated monomer of the polyelectrolyte chain ($C_6H_{11}NO_4$), while one unit of HEP represents a dimer ($C_12H_19NO_20S_3$) (see Figure 24). In order to simplify the calculations, a degree of deacetylation of 100% was considered for CHI.
To distinguish the heparin signal from the chitosan signal, sulfur is used as a marker. Indeed, as can be seen on Figure 24, heparin is the only molecule that has sulfur in its formula. Therefore, the intensity of the S peak can serve as a marker for heparin. By using the molecular formula for one unit of HEP, the fraction of each element attributed to HEP can then be computed from the S fraction, as shown in Table 10. This allows determination of the fraction of heparin in the analysed layer. Assuming there was no contamination of the sample by nitrogen, the remaining N fraction can thus be attributed to CHI. Like for HEP, the fraction of the other elements in CHI is found by using the elemental ratios in the molecule, and the fraction of CHI in the analysed layer is thus obtained.

Table 10: Modelling of HEP and CHI composition for sample $[CHI/HEP]_2$. One unit is a dimer for HEP and a deacetylated monomer for CHI.

$[CHI/HEP]_2$	**Modelling HEP composition**						**Modelling CHI composition**				
	S	N	C	O	Total	Unit HEP	N	C	O	Total	Unit CHI
	1.42	0.47	5.7	9.49	17.09	0.47	2.49	14.91	9.94	27.34	2.49

Then, a ratio of chitosan monomer unit to heparin disaccharide unit is computed. This ratio equals 5.30 and indicates that chitosan is the dominant species in $[CHI/HEP]_2$ films. Since both species are considered to be fully charged at pH 3.5 (+0,9 and -4 for CHI and HEP respectively) [53], the higher charge density of HEP is compensated by the number of chitosan molecules. This results in a (+/-) charge ratio of approximately 1.19. These values have to be considered with caution since the outermost layer contributes more to the XPS signal than underlying layers, and the present analysis is made considering that the analysed volume is homogeneous, which may not be the case given the sequential deposition method.

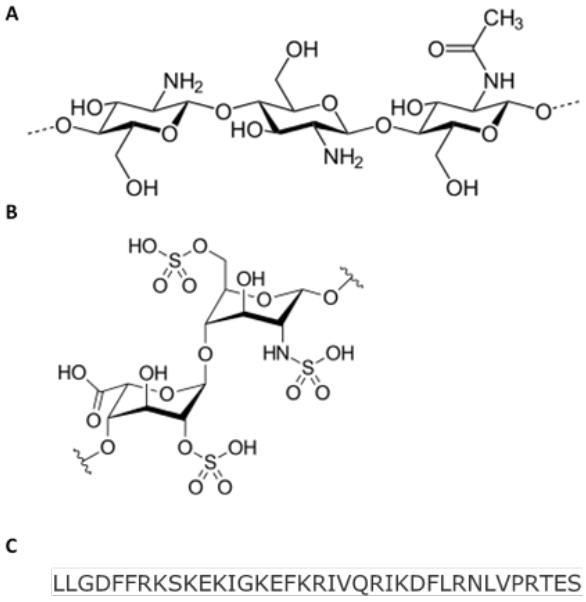

Figure 24: Molecular structure of (A) chitosan, (B) heparin and (C) amino acids sequence of LL-37.

1.5.5 HEP/LL-37 ratio

Unfortunately, the same approach is not possible for the 4 remaining samples. Indeed, the multilayers consist of chitosan and of heparin and LL-37 assembled in PPCs. Another marker atom or function is necessary to distinguish chitosan from LL-37 in order to assess their relative proportions. To do so, the molecular structure of all three molecules was thoroughly investigated and their respective chemical functions were computed.

First of all, the results confirm the presence of LL-37 in the multilayer. To demonstrate this, the hypothesis was set that no LL-37 is present in the layer. All the contributions to the N signal were thus attributed to chitosan and heparin exclusively, just like for the previous sample. Corresponding values were then computed for all other elements using the respective atomic ratio's from each molecule (see Table 11). Doing so, a total CHI fraction exceeding 100% was obtained, and the elemental fractions of C and O exceeded the measured values, which proves the used model is wrong. The initial assumption that only CHI and HEP can be found in the layers can thus be rejected.

Table 11: Modelling of HEP and CHI composition following the hypothesis that LL-37 is absent from layers. The obtained elemental fractions (in red) exceed the measured fractions, proving that this model is incorrect and that the initial assumption is wrong.

Sample	Modelling HEP composition					Modelling CHI composition				Total fraction from model		Total measured fraction	
[CHI/HEP]$_2$/[CHI/PPCs]$_6$	S	N	C	O	Total HEP	N	C	O	Total CHI	C	O	C	O
	2.6	0.9	10.3	17.2	31.0	10.0	59.9	39.9	109.8	70.2	57.2	53.3	33.3
[CHI/HEP]$_2$/[CHI/PPCs]$_6$	S	N	C	O	Total HEP	N	C	O	Total CHI	C	O	C	O
+ MHB	2.0	0.7	7.8	13.0	23.5	10.2	61.0	40.7	111.9	68.9	53.7	55.8	31.5
[CHI/HEP]$_2$/[CHI/PPCs]$_6$	S	N	C	O	Total HEP	N	C	O	Total CHI	C	O	C	O
+ NaCl	2.1	0.7	8.6	14.3	25.8	10.6	63.9	42.6	117.1	72.5	56.9	55.4	31.1
[CHI/HEP]$_2$/[CHI/PPCs]$_6$	S	N	C	O	Total HEP	N	C	O	Total CHI	C	O	C	O
+ SDS	3.3	1.1	13.1	21.9	1.09	4.8	28.9	19.3	53.1	42.1	41.2	62.8	27.8

Although this confirms the presence of LL-37 in the analysed samples, the next step is to try to evaluate the proportion of LL-37 compared to heparin and chitosan. Nevertheless, this is very difficult for two reasons. First of all, the exact dry thickness and architecture of the multilayer is not known. It is thus very difficult to know which layers correspond to the 5 to 7 nm probed by the XPS instrument. It could be only the last adsorbed layer (PPCs) or more. The QCM results indicate that the last adsorbed layer of PPCs has a thickness of 20 nm, which would mean that the underlying chitosan layer is not visible by XPS. However, this experiment was performed in a hydrated environment which is not the case in XPS. Additionally, it remains possible that underlying layers diffuse into the film, resulting in non-homogeneous layers.

Secondly, there is no obvious marker atom that would enable the differentiation between chitosan and LL-37. Hence, two different strategies were adopted to try to differentiate both molecules that are detailed below. The first one focused on the N shift of protonated and unprotonated amines and amides. A theoretical value for the fraction of protonated and unprotonated amin functions in both molecules was computed and fitted to the data. The second approach was to use the carbon shift and the different carbon functions of each molecule. Doing so, an estimated heparin to LL-37 ratio was obtained.

1st approach: analysis of the N peak Figure 25 depicts the nitrogen spectrum for each sample, which can be divided into two main peaks. The first one is located around 401.7 eV and corresponds to the NH_3^+ shift. A second peak occurs around 399.8 eV and can be attributed to three different functions of the nitrogen atom, that is NH_2, N-SO_3 and the amide function (C=O)-NH. A transition can be observed

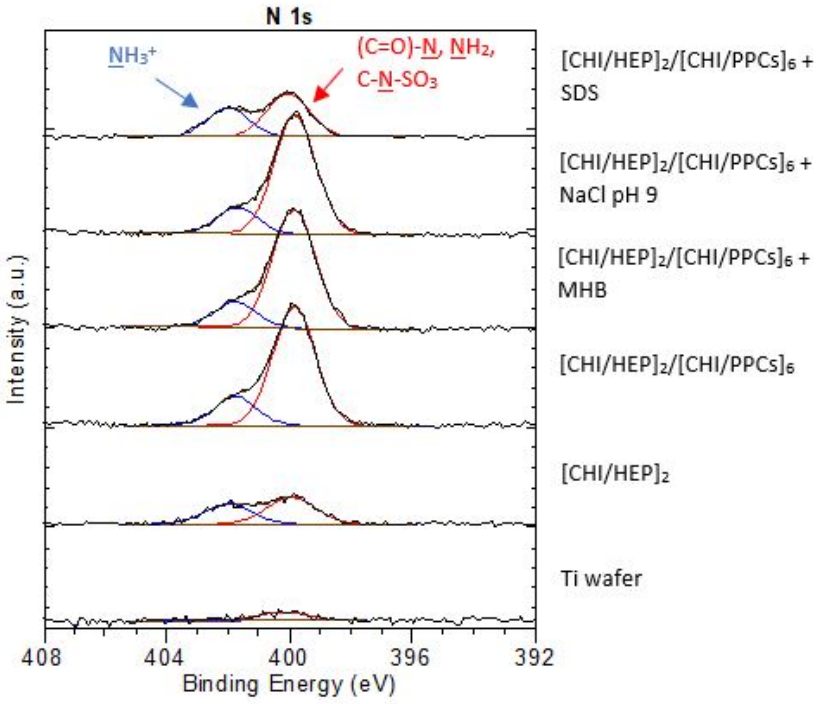

Figure 25: N spectra recorded by XPS on Ti substrates, as such, or covered by different multilayers.

from the second to the third samples, when the PPCs layers are adsorbed. The second peak at 399.8 eV (in red on Figure 25) becomes much more important and represents more than 80% of the signal compared to 60% before. This rise of the NH_2/NSO_3/amide peak is probably due to the addition of LL-37 to the layers. Indeed, this molecule is composed by 37 amino acids linked by a peptide bond represented on Figure 26, which is characterised by an amide function.

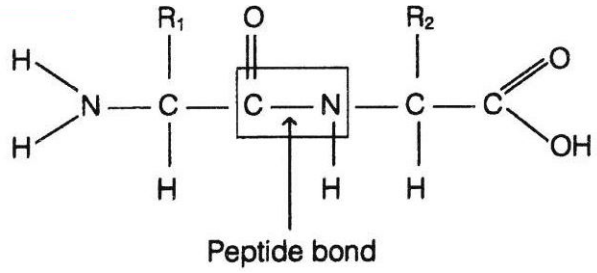

Figure 26: Peptide bond with its amide function

However, not only amide functions are to be found in LL-37. Protonated and unprotonated amines are present in some constituent amino acids. The calculation of the different functions of LL-37 and in particular of its nitrogen functions can be found in Appendix B.1, B.2 and B.3. A theoretical fraction of 80% of amide and NH_2 was found, leaving 20% of NH_3^+ in the peptide.

The chitosan used in this work is deacetylated at 95%. Hence, 5% of amide functions can be found in the molecule. Moreover, the 95% amino groups left can be either protonated or deprotonated. At pH 3.5, chitosan is expected to be almost fully charged and therefore almost totally protonated. [53, 88] Nevertheless, the distribution of the N signal of chitosan between both subpeaks was calculated from the previous sample ($[CHI/HEP]_2$), assuming that the protonation ratio of the amino group and the degree of deacetylation only depend on the pH and the purchased product, respectively. Consequently, this ratio should remain constant for each sample. For this $[CHI/HEP]_2$ sample, a protonation degree of 50% was found, which is lower than expected (see Appendix B.4). However, the drying step and the analysis under vacuum conditions may influence the charge distribution in the molecule. Hence, the obtained protonation degree remains an estimation which must be taken into account when interpreting the results.

The heparin contribution to the nitrogen peaks was easily quantified thanks to the S marker. The N-SO_3 function of the heparin molecule has a binding energy close to 400 eV and is therefore assimilated to the peak at 399,8 eV.
By assembling the contribution of each species to both peaks, the following relationship is obtained:

$$N^{399.8} = 0.8\ N_{LL37} + 0.5\ N_{CHI} + N_{HEP} \tag{5}$$

$$N^{401,7} = 0.2\ N_{LL37} + 0.5\ N_{CHI} \tag{6}$$

with $N^{399,8}$ being the fraction corresponding to the peak at 399.8 eV, $N^{401,7}$ the fraction corresponding to the peak at 401.7 eV, and N_{LL-37} and N_{CHI} being respectively the contributions to N 1s of both molecules. The contribution to N 1s of HEP is known and both equations can be solved together. Once the contribution of LL-37 and chitosan to the N 1s peak are found, the amount of both species is obtained and a ratio between the different species can be computed, which is shown on Table 12. A value of about 2 is found for the (-/+) HEP/LL-37 ratio of the whole multilayered system, which then decreases with further treatment of the multilayer. More detailed calculations can be found in Appendix B.5. Again, this result must be taken with caution because it relies on different hypotheses and simplifications which will be discussed below.

2nd approach: analysis of the C1s peak A similar approach was made but using the carbon spectrum this time. As can be seen on Figure 27, the carbon spectrum can be splitted into 4 different peaks attributed to different functions of C. The theoretical fractions of each function for heparin, chitosan, LL-37 and SDS were computed based on the molecular structure of the molecules and fitted to the peaks with the help of XPS engineer Pierre Eloy. Due to the high number of constituents and the possible presence of contamination and/or degradation, different fits are possible. The different fits were thus verified by comparing the corresponding outcome of N and S to the measured values until a good match was found (see Appendix B.6 for detailed calculation). A ratio of $\frac{deducedN}{detectedN}$ was computed and found to vary between 0.94 and 1.01 for all PPC coated samples, which implies an error of less than 5%. The same observation was made for the $\frac{deducedS}{detectedS}$ ratio that varies between 0.99 and 1.07.

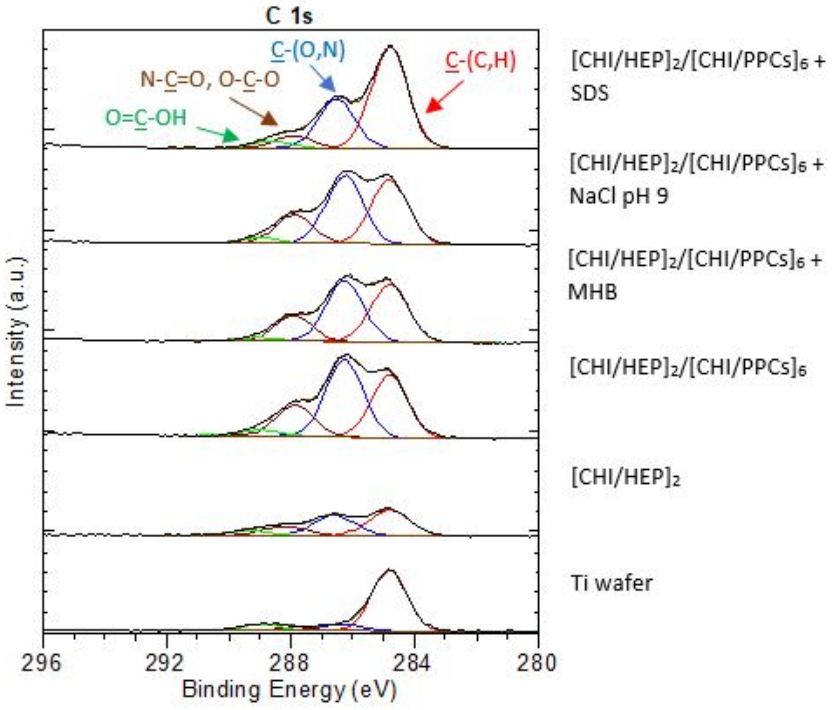

Figure 27: Carbon spectra recorded by XPS on Ti substrates, as such, or covered by different multilayers.

Figure 28 and 29 represent the selected fits for the decomposition of the carbon spectrum for each sample. This decomposition is based on the stoechiometry of the theoretical carbon functions that can be found in each molecule. It can be clearly seen that the LL-37 component represents an important fraction of the total signal when PPCs layers are added (sample 3,4,5,6). However, this share is reduced when SDS is added, which is not surprising considering the long hydrocarbon tail of the molecule. The absence of chitosan signal when PPCs layers are added could be due to the fact that the outermost layer containing PPCs is to thick to allow detection of the underlying CHI layer. The electrons of CHI are then buried to deep in the layers and cannot escape, which explains why CHI is not detected.

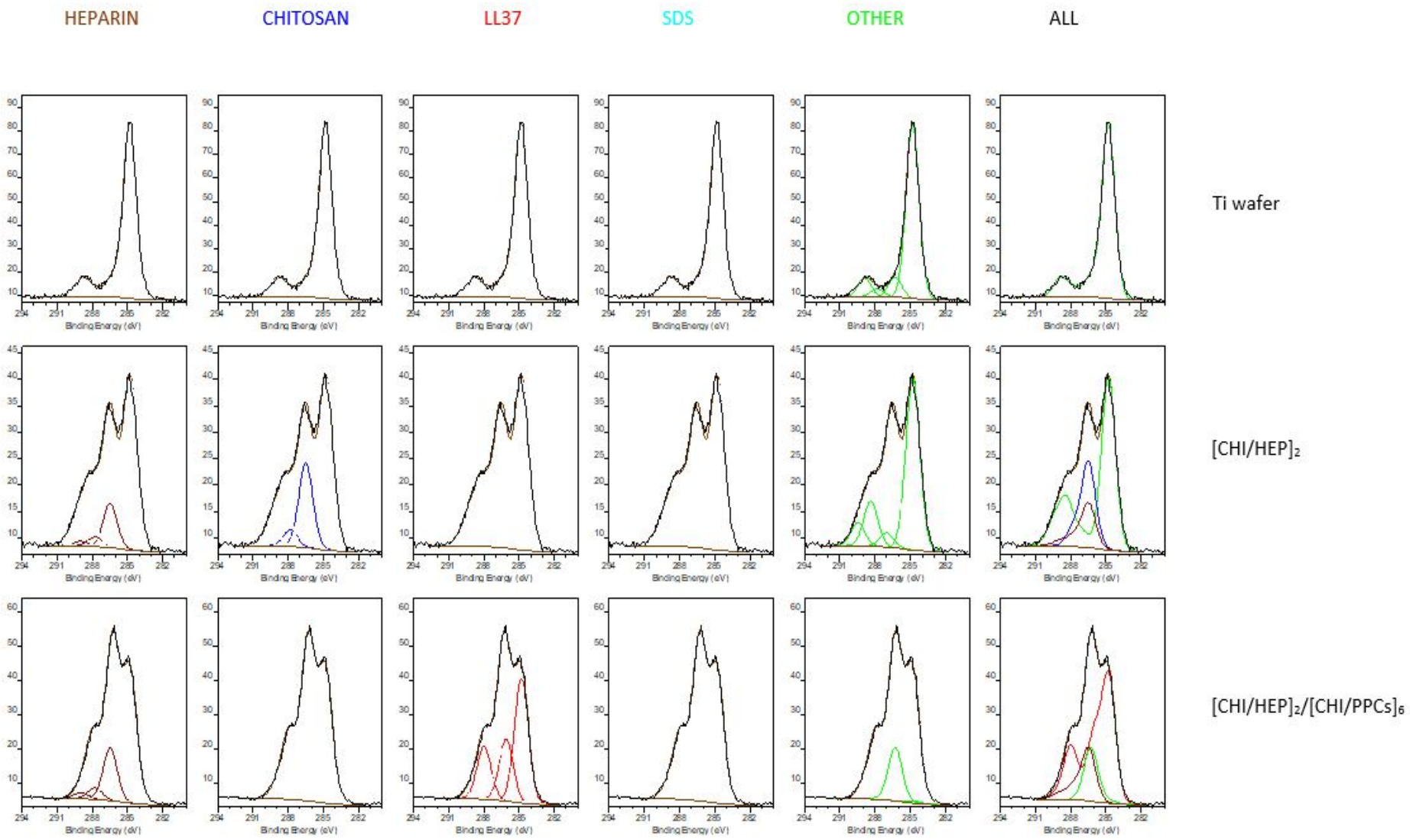

Figure 28: Decomposed carbon spectrum per sample and per molecule

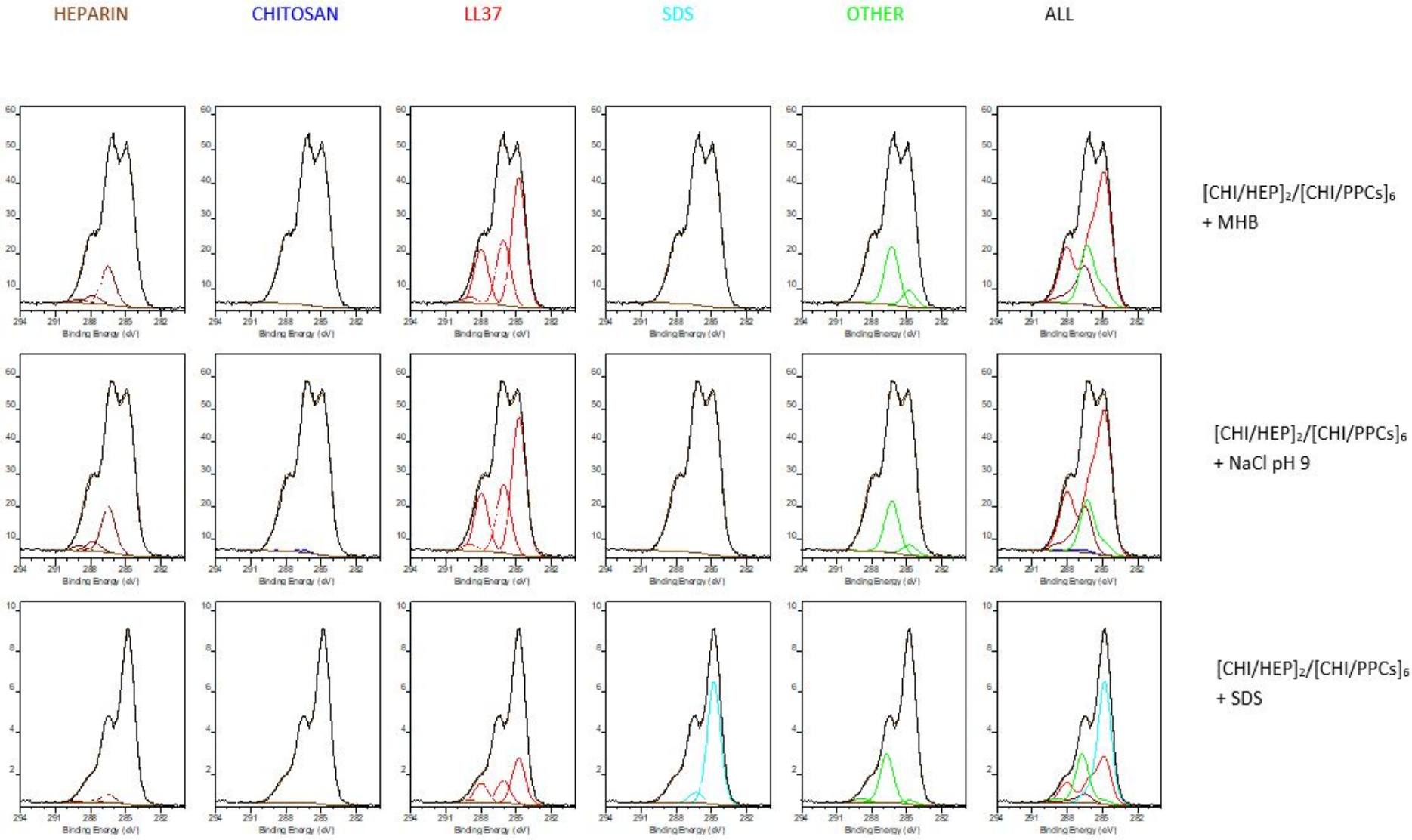

Figure 29: Decomposed carbon spectrum per sample and per molecule

1.5.6 Discussion

Once the relative amount of each species in the probed layer is found, either using the nitrogen peak or the carbon peak approach, a ratio can be computed between the different molecules. This ratio is computed per unit of each molecule, with this unit being a deacetylated monomer for chitosan, a dimer for heparin and one peptide for LL-37.

Table 12: Obtained proportions (in units) of heparin, chitosan, LL-37 and the HEP/LL-37 ratio for the whole multilayer. The results are given using both approaches (N peak and C peak).

Sample		**CHI**	**HEP**	**LL-37**	**HEP/LL-37 (unit)**	**HEP/LL-37 (-/+)**
(3) [CHI/HEP]$_2$/[CHI/PPCs]$_6$	N peak	0.4	0.86	0.16	5.39	2.07
	C peak	0	0.85	0.17	4.94	1.9
(4) [CHI/HEP]$_2$/[CHI/PPCs]$_6$ + MHB	N peak	0	0.65	0.17	3.85	1.48
	C peak	0.01	0.63	0.18	3.48	1.34
(5) [CHI/HEP]$_2$/[CHI/PPCs]$_6$ + NaCl pH 9	N peak	0	0.72	0.18	4.03	/
	C peak	0.09	0.71	0.18	3.85	/
(6) [CHI/HEP]$_2$/[CHI/PPCs]$_6$ + SDS	N peak	/	/	/	/	/
	C peak	0	0.22	0.09	2.35	0.90

Results of both approaches are presented in Table 12 and are found to be very similar, differing of less than 6% for heparin and LL-37. The amount of chitosan in the probed layer is very small or close to zero. An explanation for this absence of chitosan signal could be the thickness of the prospected layer. It was demonstrated in Section 1.5.1 that 95% of the XPS signal originates from a layer of 5 to 7 nm. The outermost layer of the analysed coating is composed of PPCs, this is LL-37 complexed with heparin, and has an unknown dry thickness. If this thickness exceeds 7 nm, the underlying layer which consists of chitosan in this case will not be seen by XPS (see Figure 30). Moreover, the previously realised QCM experiment indicates a hydrated thickness of 20 nm for the last PPCs layer. Although the dry thickness is expected to be inferior to the hydrated thickness, this observation confirms that the outermost layer could be thick enough to occult the signal coming from the underlying chitosan molecules. In order to verify this influence of the outermost layer, a second experiment was planned where a sample with CHI as the outermost layer would be analysed. Unfortunately, due to the sanitary crisis, this experiment could not be conducted.

When comparing the respective amount of species per sample, all samples present relatively similar results, except the last one to which the ionic detergent SDS was added. In section 1.4, the QCM-D experiment showed no adsorption of MHB onto the multilayers. The XPS results confirm this observation by showing almost no difference in elemental composition with or without addition of MHB. The NaCl solution (pH 9, I $\approx$ 150 mM) had an effect on the layer by occasioning a partial deconstruction, but the present results show again that the desorption did not reach the CHI/HEP cushion. Moreover, the layers seem to keep almost the same elemental proportions.

Figure 30 is a schematic representation of the estimated layer set-up of each sample, and the layer prospected by the XPS measurement. The figure is not on scale and the unknown degree of layer deconstruction is random on the picture.

Regarding the SDS sample, a decrease of the HEP/LL-37 ratio is noticeable. Overall, a decrease in the signal of each component was observed after SDS treatment, except for the S 2p and C 1s peak, indicating desorption of the polyelectrolytes from the film. Rahim et al. confirmed this in a similar experiment and found that SDS was chemically adsorbed within the layers, causing restructuration of the polyelectrolyte multifilms [63]. In the present experiment, the decomposition of the carbon peak on Figure 29 shows a great contribution of the SDS hydrocarbon tails to the C-(C,H) signal, which could indicate adsorption of SDS into the multilayer by competitive binding with the polyelectrolytes.

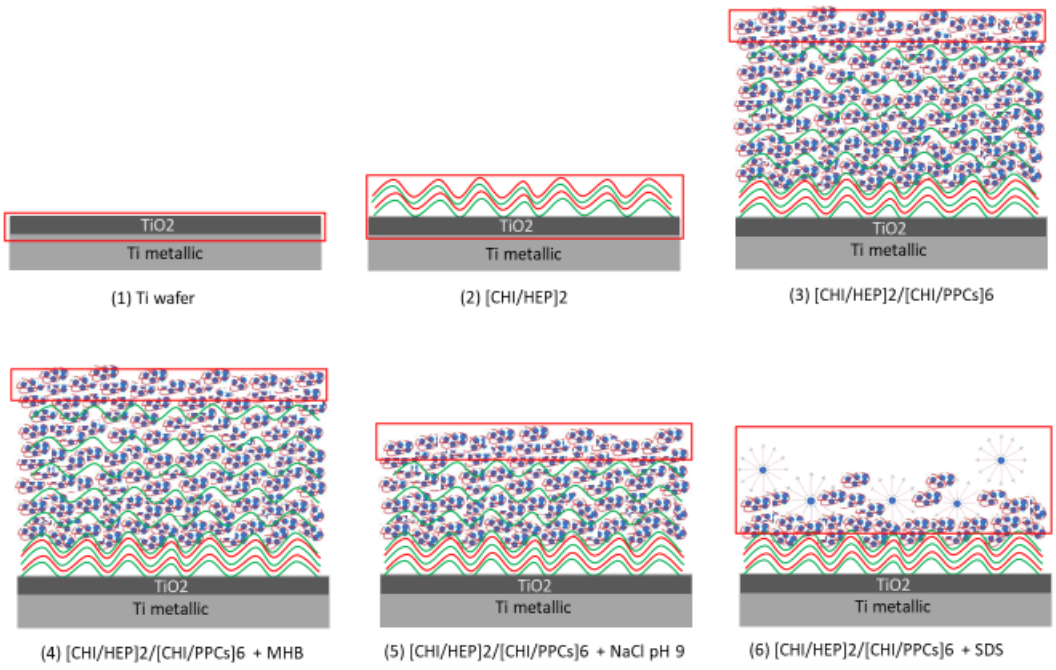

Figure 30: Schematic representation of an estimation of the layers probed by XPS for each sample (red box). This figure is not on scale.

Considering the unit ratio, the same calculation was applied as in section 1.5.4 to obtain the -/+ charge ratio. With a charge of -4 and +10.4 for heparin dimer and LL-37 peptide respectively, the unit ratios of samples 3 and 4 were multiplied by 0.38 to obtain the charge ratio. Ratios between 1.34 and 2.07 are obtained. This is close to the targeted experimental optimal charge ratio for PPCs incorporation in multilayers of 1.5. Nevertheless, this calculation is not applicable for sample 5, since the pH was changed to 9 and the I to 150 mM, leading to a peptide charge inferior to +10.4. A higher (-/+) charge ratio can thus be expected for this sample.

1.5.7 Limitations

It is crucial to understand the limitations of the above-mentioned approaches and calculations in order to interpret the results correctly. Different simplifications and hypotheses were made that need to be taken into account.

First of all, molecules may be subject to degradation during the analysis. Some molecules are more sensitive to degradation than others and this may result in underestimation of chemical functions. To check the degradation of the material, a record of the C1s peak was made at the beginning and at the end of the analysis. No significant differences were observed when comparing both. However, this does not exclude possible degradation of other functions.

Secondly, an exponential decrease of the signal with the depth is observed. This could induce overrepresentation of the surface layer, and since we are here in a multilayer configuration, some molecules may be overestimated.

Regarding the decomposition of the N peak, different objections can be made. The theoretical fractions of each function per molecule was computed. The protonation degree was obtained experimentally from the $[CHI/HEP]_2$ sample and supposed to remain constant throughout the experiment. However, as stated previously, the analysis under vacuum and the use of the flood gun may alter the charge distribution, but it is difficult to know to which extent. Consequently, the obtained protonation degree may be biased, which would have an influence on the theoretical distribution of the fractions and thus on the final results.

The C peak decomposition was obtained after different trials and the best fit was retained. However, the fact that the model fits the data does not necessarily mean that the model represents the reality. The shifts corresponding to the different functions are relatively close to each other, and different functions are attributed to the same peak. Hence, if the area under the peak or the position of the peak are not very accurate, this may have a strong impact on the final result. Moreover, the presence of carbon of contamination/degradation can be adapted to 'correct' the fits. Therefore, the results were controlled by looking at the N and S ratios to try to have the most reliable fit. Nevertheless, errors are still possible.

The behaviour of the multilayer in presence of MHB, NaCl pH 9 and SDS was investigated in Sections 1.3 and 1.4. Some informations were retrieved, however, the detailed interactions between those molecules and the layers are still relatively unknown and rely on assumptions. This is a major factor though that could influence the architecture and composition of the layers, and the interpretation of the results. The uncertainty about the multilayer thickness and the presence or not of diffusion of certain molecules into the layers adds to the fragility of the model.

Finally, to have statistical significance, each sample should have been analysed at least in triplicate. Unfortunately, this was made impossible by lack of time and the coronavirus situation.

To conclude, the results presented in this section are estimations and must be taken with caution. Additional analyses are necessary to confirm the obtained ratio's and to have a better insight into the multilayer structure and its behaviour.

1.5.8 Conclusion of the XPS experiment

Despite the aforementioned limitations of the technique, the interpretation of the surface elemental and functional composition provided new insights on the chemical architecture of the multilayer on the one hand, and on the effect of different treatments on the other hand.

First of all, the presence of LL-37 in the surface layers of the $[CHI/HEP]_2/[CHI/LL\text{-}37]_6$ system was demonstrated. The ratio of HEP dimer to LL-37 peptide was found to be equal to 5.17, which results in a (-/+) charge ratio of ≈ 1.99. This value ties in with the optimal ratios for PPCs formation found previously by C. Vranckx.

Regarding the $[CHI/HEP]_2$ cushion, CHI was found to be the dominant species in the film. Moreover, the measurement of a Ti signal for this sample demonstrates that the cushion does not cover the substrate in a continuous layer of more than 5 to 7 nm. The formed layers are either thin and homogeneous (less than 5 to 7 nm), either discontinuous.

On the contrary, the absence of Ti signal observed upon analysis of the whole multilayer indicates that their dry thickness exceeds 5-7 nm, which confirms that the ellipsometry result is incorrect. Moreover, the outermost layer composed of PPCs seems to be thick enough to occult the signal of the underlying CHI layer, resulting in a weak amount of CHI computed for the $[CHI/HEP]_2/[CHI/LL\text{-}37]_6$ system.

Finally, the effect of sample treatment with a solution of NaCl (pH = 9, I $\approx$ 0) and MHB culture medium on the surface elemental composition was relatively limited. The addition of SDS however modified the multilayer composition, suggesting a partial adsorption of the SDS molecules on the surface of the sample.

2 Antibacterial activity

In this second result section, the focus lies on the antibacterial properties of the constructed coating. The objective is to quantify the activity of LL-37 in solution and compare it with the complexed state in which it is found in the coating. With a better insight of the action and potency of the peptide, novel approaches can be explored to improve its activity into the coating, in order to have the desired antibacterial and anti-biofilm effect.

2.1 Sterility

To assess antibacterial activity, sterility of the sample is of paramount importance. Before any experiment was carried out, the capacity to obtain a totally sterile coating ready for analysis was thus verified. Samples obtained after construction of the multilayers in the immediate environment of a flame showed no bacterial growth after 24 h incubation, as can be seen on Figure 31. This result validates the sterile construction of the coupons, and allows the following experiments to be conducted properly.

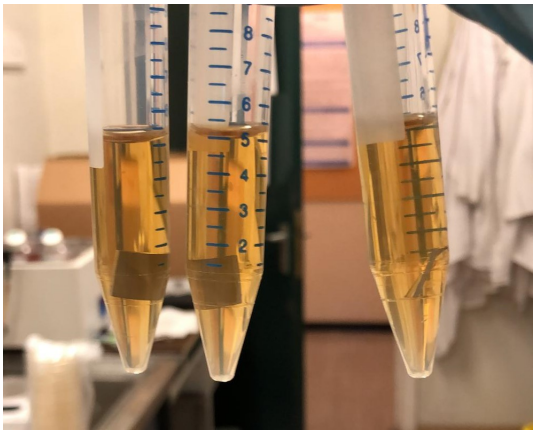

Figure 31: Sterility of the coating demonstrated after 24 h incubation in culture medium.

2.2 Measurement of the antibacterial activity of the coating

In a first time, a bacterial test was performed to assess the effect of the built multilayers on bacterial adhesion and biofilm formation of *S. aureus*. The goal is to have a better insight into the activity of LL-37 in the coating and the effect of complexation with heparin and PPCs formation.

As a reminder, the activity of 9 coupons was measured in this experiment. A comparison was made between uncoated Ti wafers, a $[CHI/HEP]_2$ coated wafer and a fully coated $[CHI/HEP]_2/[CHI/PPCs]_6$ wafer, each in triplicate. The amount of bacteria that adhered to the surface of the coupon was measured after 2 h incubation, and the biofilm formation after 24 h incubation.

Multiple dilutions were made for each sample and spread on culture medium, to guarantee an acceptable count of CFUs on the Petri dishes. Only the counts between 20 and 400 CFUs/dish were retained, higher or lower values are considered too variable. The amount of CFU/coupon was calculated with the following

formula:

$$N = \frac{C \times D \times 2}{0.05} \tag{7}$$

with N the number of CFU/coupon, C the number of colonies counted and D the dilution. This is multiplied 2 times to take into account the dilution in PBS and divided by 0.05 because 50 µL were spread on the TSA medium. The base-10 logarithm of this value was then taken. Despite the small number of measurements for each sample, the obtained logarithmic values were then averaged for the three samples of the same kind, and the standard deviation was computed as shown in Table 13. The choice to compute the mean after calculating its logarithm relies on the observation made by Robertson that a geometric mean, which corresponds to the means of the logarithms of the bacterial counts, is more correct than an arithmetic mean in the case of bacterial counts [89]. The retained values after 2 h and 24 h are presented in Table 13.

Table 13: Log (CFU/coupon) for a Ti sample, a $[CHI/HEP]_2$ sample and a $[CHI/HEP]_2/[CHI/PPCs]_6$ sample following exposure to *S. aureus* during 2 h and 24 h.

	2 h			24 h		
	Bare Ti	**$[CHI/HEP]_2$**	**$[CHI/HEP]_2/[CHI/PPCs]_6$**	**Bare Ti**	**$[CHI/HEP]_2$**	**$[CHI/HEP]_2/[CHI/PPCs]_6$**
Coupon 1	4.03	3.92	3.08	7.64	7.37	7.67
Coupon 2	4.25	4.03	3.44	7.80	7.79	7.58
Coupon 2	3.61	4.07	3.77	7.61	7.55	7.66
mean value	**3.96 ± 0.27**	**4.01 ± 0.06**	**3.43 ± 0.28**	**7.68 ± 0.08**	**7.57 ± 0.17**	**7.64 ± 0.04**

After 2h, all samples show a log CFU around 3.5-4, while after 24h, the values increase around 7.5-7.7. The means of the different samples after 2 h and 24 h were then compared two by two with a Student t-test to determine whether they can be considered as equal to each other or not. At a confidence level of 95%, no means were found to be significantly different from each other, confirming that the coating does not affect the bacterial adhesion or biofilm formation at this stage.

To be more reliable, this experiment could have been carried out with more samples in order to have more statistical significance. The choice of three samples per coating condition was made because of the high price of the LL-37 peptide, and because the experiment was intended as a first test of activity and was meant to be repeated later on.

Hence, the $[CHI/HEP]_2$ cushion shows no effect on bacterial adhesion, which is surprising considering the significant results obtained by Fu et al. at a similar pH on PET films with *E. coli* [57]. Moreover, the obtained results prove that the activity of the PPCs coating, that contains the antibacterial peptide LL-37, is not sufficient to avoid bacterial adhesion and biofilm formation. To justify the lack of activity of LL-37 in the layers, several hypotheses were made that will be described below.

Loss of availability of LL-37 through complexation First of all, the bactericidal mechanism of LL-37 described in Section 2.3.2 of the State of the Art involves direct contact of the peptide with the bacterial membrane. This implies that LL-37 must be available and sufficiently free to be able to enter in contact with the bacteria colonising the implant surface. Hence, the complexation of LL-37 with heparin to

form a protein-polyelectrolyte complex may 'emprison' the peptide, preventing it from reaching bacteria. Literature reports different immobilisation strategies for LL-37 on surfaces which allowed bacterial killing (see section 3.2 State of the Art), but none of them involve the formation of a complex adsorbed in a layer-by-layer fashion. Therefore, the drawbacks of this new method are not identified yet, and the formation of a PPC ,that could on the one hand favour assembly and protect LL-37 against denaturation, could on the other hand result in a loss of availability of LL-37.

Additionally, LL-37 may not be able to diffuse from the underlying layers to the surface because of its immobilisation within PPCs and the strong electrostatic interactions that result. In this case of figure, only the outermost layer of PPCs would be operational. This effect of the outermost PPCs-containing layer was observed by vander Straeten et al. for the lysozyme-PSS complex as well [83].

To verify the influence of the outermost layer and the lack of diffusion of the peptide throughout the multilayers to the surface, a comparison should be made between a chitosan-terminated multilayer and a PPCs-terminated multilayer. Unfortunately, this experiment was not carried out because of the lockdown caused by the Covid-19 pandemic.
Moreover, the effect of complexation of LL-37 with heparin on antibacterial activity must be assessed, to verify if LL-37 keeps its antibacterial activity even when complexed with the polyelectrolyte. To do so, MIC tests will be carried out on LL-37 alone and LL-37 + HEP to compare their activity. This will be further detailed in the next section.

If the peptide is effectively trapped in the multilayers and not able to diffuse through it to enter in contact with bacteria, a method must be found to disassemble the layers. A first attempt at layer disassembly is described in Sections 1.3 of Materials and methods and 3.7 of Results.

Release of LL-37 into the environment Secondly, another explanation for the lack of activity can be given, which is totally different of the one described above. There is a possibility that LL-37 is rejected and released from the layers, either complexed as a PPC or under its peptide form. The low pH value of 3.5 at which the multilayer was constructed could result in very strong electrostatic interactions between heparin and chitosan, displacing the more weakly complexed LL-37 and explaining its release. This theory has already been raised when discussing the layer thickness and dissipation values obtained by QCM-D, and is suggested by vander Straeten et al. in his study of lysozyme incorporation as a PPC into polyelectrolyte multilayers [45]. However, the XPS experiment proved the presence of LL-37 into the layers in the expected proportions, making this hypothesis relatively unlikely.

Consequently, a better insight into the amount of LL-37 present in the layers over time is necessary to understand its behaviour. A quantification test could give us valuable information about the exact amount present in the layers on the one hand, and released in the environment on the other hand. The release kinetics of LL-37 are thus important for a better understanding of the layer dynamics. This planned experiment was unfortunately not conducted because of the Covid-19 lockdown, and will be detailed in the section about future prospects.

Interaction with MHB culture medium Furthermore, the precipitation of AMPs in bacterial culture medium such as MHB resulting in a decrease of the MIC is described in several studies [78, 76]. This suggests that interactions between MHB compounds and LL-37 could possibly reduce its bioactivity and explain the lack of activity of the full coating. However, the stability of the coating in MHB medium was tested using QCM-D and XPS, and as described in Section 1.4 and 1.5.6 of the Results part, no adsorption of MHB was observed onto the layers, suggesting that its interaction with the coating is limited. Hence, this hypothesis can be rejected.

Immobilised LL-37 below required MIC Finally, since the real amount of the peptide immobilised into the multilayers is not known, its concentration may be too low to inhibit biofilm formation and bacterial adhesion. To verify this, the exact MIC must be determined and the amount of LL-37 present in the multilayers should be quantified.

2.3 Minimal inhibitory concentration (MIC) of LL-37

The previous experiments triggered the need for a better quantification of LL-37 activity. MIC tests provide a threshold concentration of the peptide at which bacterial growth is inhibited. This is a first step to our final goal, this is quantifying the amount of peptide needed in the multilayer to prevent biofilm formation.

Furthermore, the influence of complexation of LL-37 with heparin is investigated by comparing MIC values for both situations. A better comprehension of LL-37 behaviour and activity under the PPC form will help us to draw conclusions on the results of the activity test described in section 2.2.

Hence, the bacterial growth of two bacterial strains, *S. aureus* and *S. epidermis*, was measured after incubation in suspension with LL-37 and PPCs (LL-37 + HEP) respectively. The antibiotic vancomycine was tested in parallel, to control the validity of the method. Two experiments were carried out, the first one only testing *S. aureus* against LL-37 and PPCs while the second time, *S. epidermis* was tested as well. Moreover, the bacterial growth in presence of vancomycine was tested too, and additional activity and spectrophotometric tests were also performed.

2.3.1 Visual reading of MIC endpoint

Conventionally, and according to the EUCAST and NCCLS guidelines [77], the MIC is read with the unaided eye as the first well in which the broth appears clear and free of turbidity or cell deposition.

Figure 32 is a photography of the microtiter plates after 24 h incubation in the second experiment. Although the quality is not very good, the transition between troubled and clear wells can be noticed quite easily. For microtiter plate A, tested against *S. aureus*, rows A,B and C corresponding to the MIC of LL-37 alone show a transition between the 5th and the 6th well. The broth is clearer in well 5, although some colonies can still be observed at the bottom of the well. In the next wells, the broth is also clearer but never becomes as clear as the control well. According to the EUCAST norms, this is not enough to

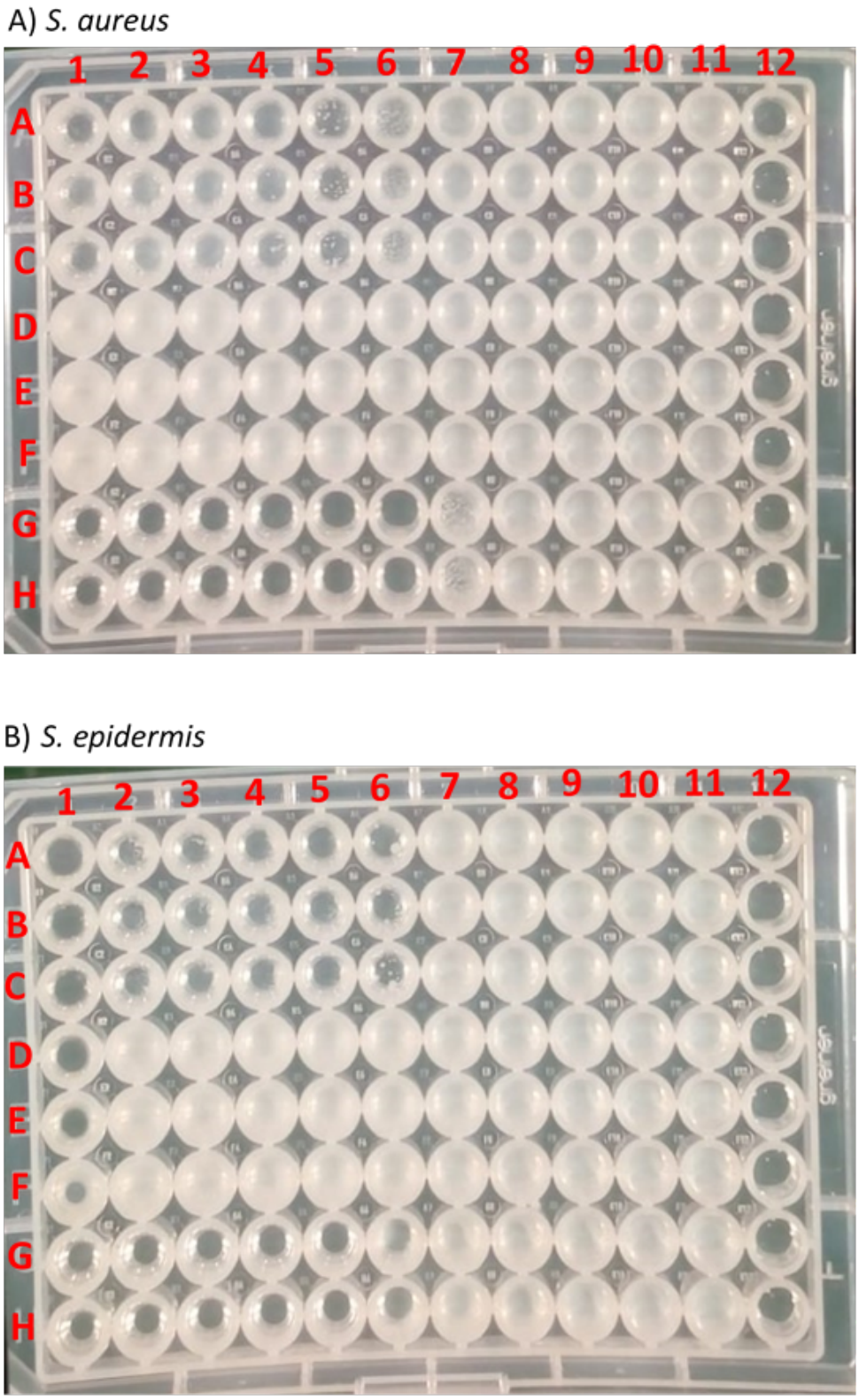

Figure 32: Visual MIC results for (A) *S. aureus* and (B) *S. epidermis*. Rows A,B,C correspond to LL-37, rows D,E,F to PPCs (LL-37+HEP) and rows G and H to vancomycine. Columns 1 to 10 are twofold dilutions starting at a concentration of 2250 µg/mL for LL-37, 1125 µg/mL for PPCs and 32 µg/mL for vancomycine. Columns 11 and 12 are the growth and sterility control wells respectively.

be determined as the MIC. Nevertheless, an important decrease of bacterial growth can be observed from well 5, which corresponds to a concentration of 140.4 µg/mL, which will be confirmed by the additional spetrophotometric and activity tests described below. The first experiment showed a transition at well 6, corresponding to a concentration of 70.20 µg/mL.

Regarding rows A,B and C of microplate B corresponding to testing against *S. epidermis*, a clear broth appears from the 6th well, which has a LL-37 concentration of 70.20 µg/mL. Again, small colonies can be noticed at the bottom of the well. Nevertheless, the transition between well 7 and 6 is quite clear.

One can see that the first column of microplate B is totally empty. In fact, the volume in the microwells evaporated during incubation and this column should thus not be read.

As can be seen on Figure 32 A and B, both bacteria could grow in the presence of the PPCs (rows D,E and F), independently of the concentration of LL-37 in the well. This means that the MIC was not reached and that the complexation of LL-37 with heparin effectively inhibits the bactericidal action of the peptide.

The growth of bacteria in presence of vancomycin is inhibited at 1 µg/mL (well 6), a concentration that matches with values found in the literature [90, 91, 92]. This demonstrates the validity of the protocol.

The visual interpretation of the result is thus not easy. Although a decrease in turbidity can clearly be observed, especially with *S. epidermis*, the broth is not clear enough to consider that the MIC was reached. The EUCAST and NCCLS guidelines specify that the presence of small colonies at the bottom of the well and the weak turbidity imply a form of bacterial growth [77]. The lack of conclusive results using this classical reading method led to the use of other, more objective and quantitative methods to read the MIC endpoint, including turbidimetry and resazurin metabolic activity assay discussed below.

2.3.2 Spectrophotometry measurements

Following the assumption that the turbidity of the wells increases with the bacterial concentration, the turbidity of the solutions in each well was measured at 600 and 620 nm with a spectrophotometer (Spectramax). Column 12 contains only culture medium and its value is therefore subtracted from all other values, as a blank. The growth control in column 11 where bacteria were allowed to grow without antimicrobial agent is then considered as 100% of the signal, and the other values are expressed as percentages of this signal. It is not surprising to find values above 100%, that are due to variability in the bacterial concentration when the MIC was not reached. Figure 33 depicts the % of positive control in function of the concentration of LL-37, LL-37 in PPCs or vancomycin. The means and the error bars for each concentration are computed.

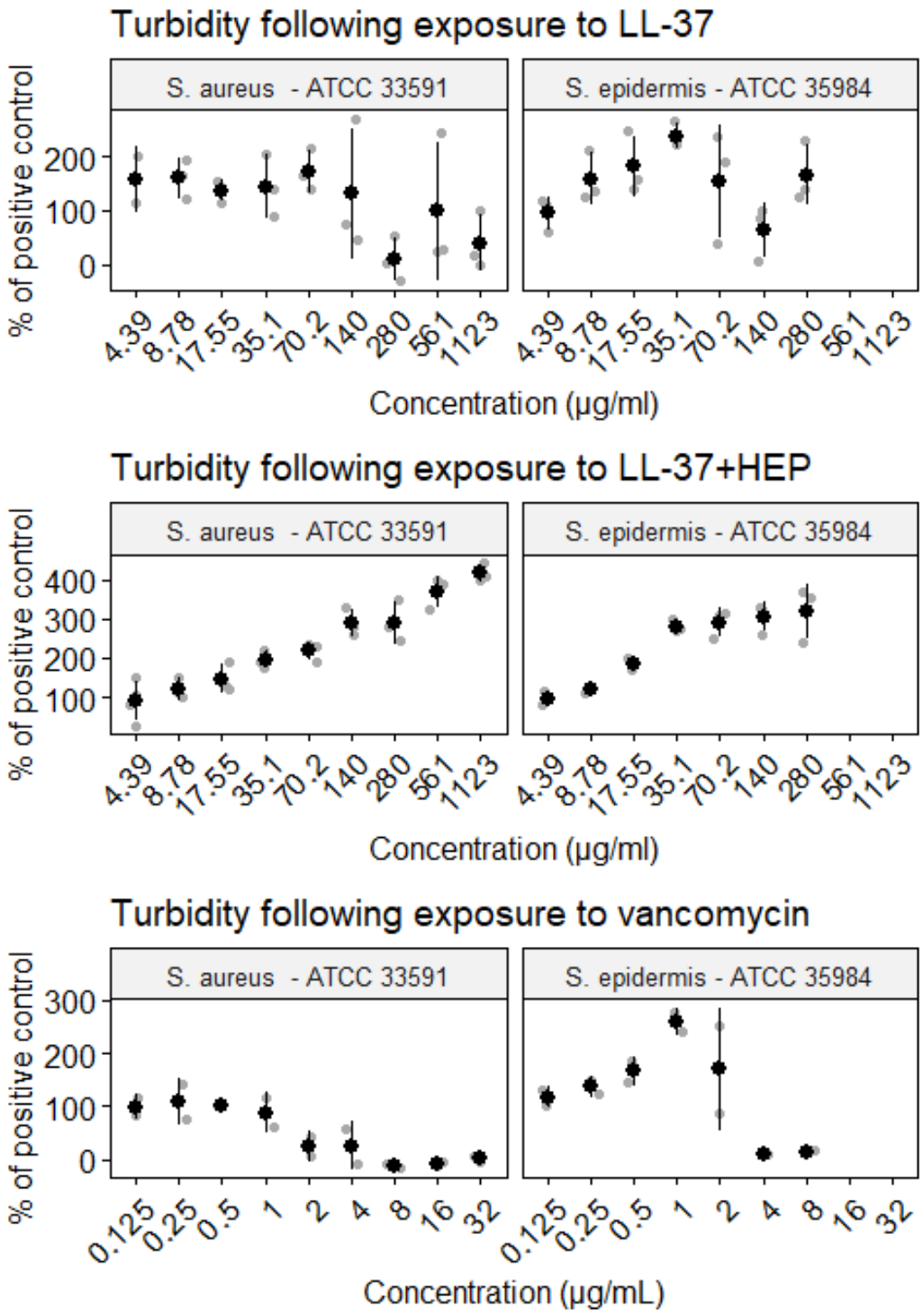

Figure 33: Turbidity following exposure of *S. aureus* and *S. epidermis* to LL-37, PPCs and vancomycin.

S. aureus Overall, a big disparity between the absorbances of the 3 replicates can be noticed for the LL-37 series. The absorbance is close to zero at a concentration of 280 µg/mL, but rises again for higher concentrations. This matches the visual observations and the absence of a total clear broth even at high

concentrations is confirmed. For the PPCs (LL-37 + HEP) series, the absorbance signal exceeds 100% of the positive control for all concentrations, confirming the turbidity observed with the bare eye. However, there could be an effect of the PPC itself on the turbidity, that showed absorbance at 600 nm in previous experiments by C. Vranckx. This would explain the rise of turbidity with PPCs concentration and the values much higher than 100%.
The vancomycine control however shows a dramatic reduction of the absorbance signal starting at 1 µg/mL to reach 0%, in line with the values found in literature.

S. epidermis Regarding the microplate tested against *S. epidermis*, the absorbance of the PPCs series does not decrease with the concentration, confirming that the MIC was probably not reached. For LL-37, a small drop of the absorbance can be noticed at 140 µg/mL, but it rises again above 100% of the positive control for higher concentrations.

2.3.3 Metabolic activity test

Fluorescence of the solutions after incubation with resazurin was measured and expressed in percentage of the positive control, after removal of the signal attributed to the culture medium. Again, variability in bacterial concentration when the MIC was not reached explains the values above 100%. Living cells metabolise resazurin in resofurin, which is highly fluorescent. Hence, a high fluorescence implies an active cell metabolism and living cells. On the contrary, if the fluorescence is close to zero, this means that all cells are dead and that bacteria were killed by the antimicrobial agent.

Given the results of the previous tests, the activity of both bacterial strains against PPCs was not measured. The test was focused on the effect of LL-37 alone and vancomycin as a control.

S. aureus Looking at Figure 34, a drop in the fluorescence can be observed at a concentration of 140 µg/mL. For higher concentrations, the fluorescence reaches zero, meaning that no bacterial activity was measured above this concentration.

S. epidermis Again, a drop beneath the 100% of positive control occurs at a concentration of 70.2 µg/mL. For higher concentrations, these values drop to zero, implying no bacterial activity at all.
Once again, for both strains, the expected MIC values for vancomycin are obtained.

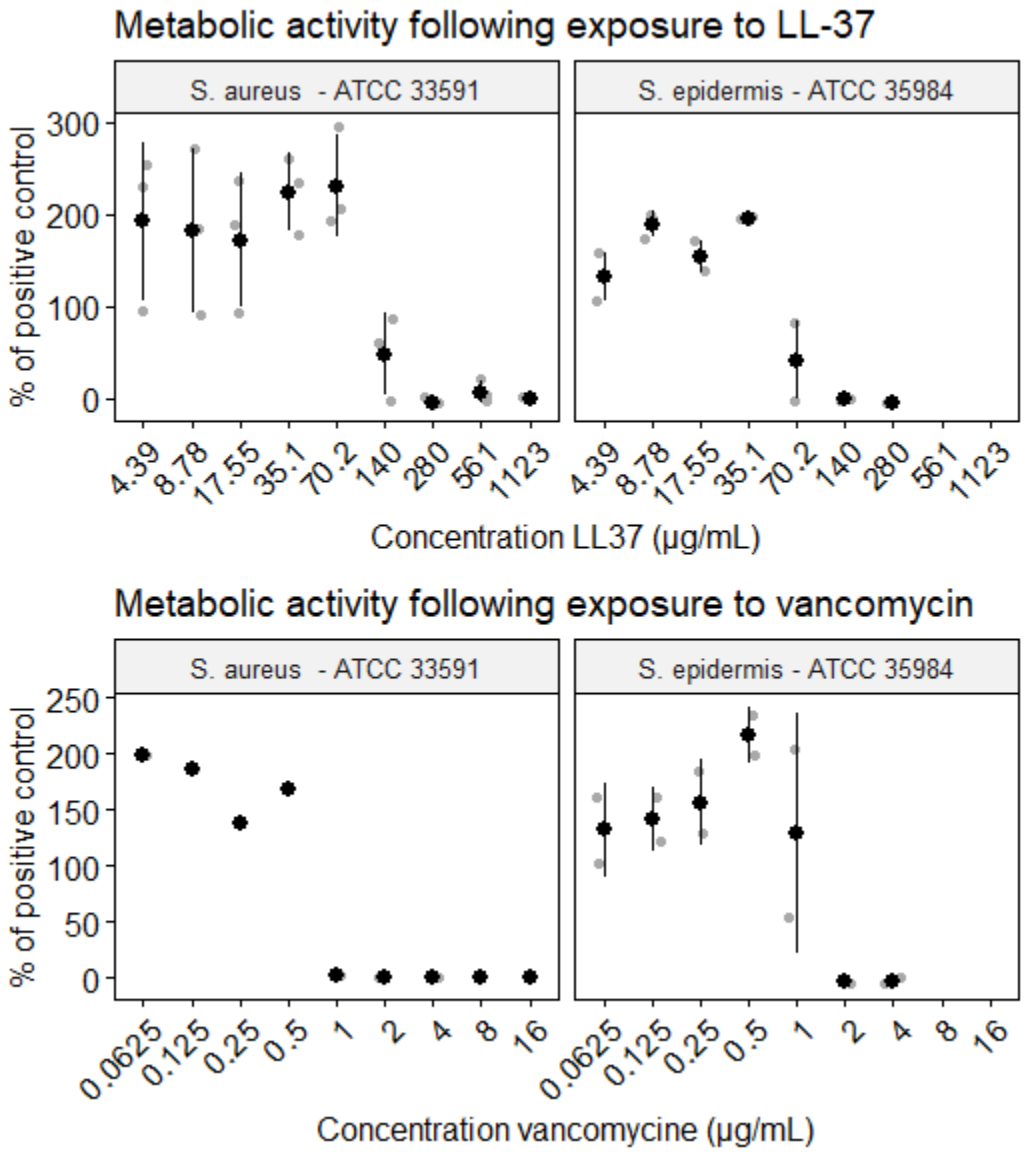

Figure 34: Metabolic activity following exposure of *S. aureus* and *S. epidermis* to LL-37 and vancomycin.

2.3.4 Discussion

Hence, the spectrophotometric results confirmed the turbidity of the broth observed even at high concentrations in the wells of *S. aureus* tested against LL-37. However, the resazurin assay provides a threshold concentration from where bacterial activity is close to zero. This threshold concentration is the same as the concentration at which a drop in turbidity is observed. These contrasting results suggest that LL-37 partially inhibited the growth of *S. aureus* and *S. epidermis* starting at concentrations of 140 and 70.2 µg/mL respectively. No bacterial activity was measured above this value, implying that all cells are dead and that the bactericidal activity of the peptide was complete. However, the uncertain visual read of the MIC endpoint triggers the need for additional experiments, in order to confirm the results obtained with the resazurin assay. Therefore, it was planned to repeat the experiment several times to have more robust

results, but due to the sanitary crisis and lockdown of the laboratories, these series of experiment could not be completed.

Regarding the MIC of the PPCs, the visual and spectrophotometric reads are consistent and seem to demonstrate no bacterial inhibition. However, PPCs were found to absorb light on their own at 450 nm, and this could contribute to the turbidity of the solution and result in biased values. The experiment should thus be repeated while adding a blank containing only PPCs and measuring its absorbance at 600 nm, to determine to which extent the complex itself influences the turbidity.

2.3.5 Limitations

One must keep in mind that the acquisition of the MIC value *in vitro* is hardly comparable to its effect inside the body. Other factors must be taken into account, such as host defense mechanisms, pharmacokinetic and pharmacodynamic properties of the AMP, etc. [76] AMPs *in vivo* are localised and probably act cooperatively to enhance the antimicrobial activity, resulting in lower levels needed than *in vitro* [39]. Despite this limitation, MIC values remain a good estimation of the minimal concentration range of LL-37 wanted to be immobilised into the multilayers.

Part VI
General discussion

The surface analysis and characterisation of the multilayers allowed retrieval of useful data, that is necessary to have a better understanding of the multilayers composition and the way they are organised and their compounds interact with each other. This knowledge of the coatings architecture is necessary to interpret and understand the second part of this work, which consists in evaluating the action of LL-37 and testing its antibacterial activity in the coating.

Using QCM-D, the construction of the film was validated. The cumulated adsorbed mass was found to increase in an exponential-like fashion at each adsorption step. The PPCs adsorption yielded the highest mass increase and dissipation values compared to adsorption of CHI and HEP. A final hydrated thickness of 6 nm for the $[CHI/HEP]_2$ cushion and of 152 nm after 6 PPCs adsorption steps was reached. The increasing dissipation values suggest a high hydration of the layers.

Following these findings, an attempt was made to measure the dry thickness of the multilayers using the ellipsometry technique. However, the roughness of the Ti wafer made this experiment very difficult and the final result showed a much smaller thickness than expected or found by QCM-D. Several hypotheses were explored to justify this, but in the light of the XPS and QCM-D experiments, the ellipsometry results were finally rejected.

XPS confirmed the presence of LL-37 on the surface of the samples. The elemental composition obtained with this technique provided useful information on the chemical architecture of the coating. First of all, the absence of Ti signal proved that the thickness of the $[CHI/HEP]_2/[CHI/PPCs]_6$ exceeds 5 to 7 nm, allowing the rejection of the ellipsometry results. Given the very low CHI amount found in the probed layer, one can suggest that the depth of analysis did not outreach the outermost layer coated with PPCs. This implies that the non-hydrated outermost layer is thicker than 5 to 7 nm. The weakness of the CHI signal also suggests that its diffusion to the top of the outermost layer is limited.

Finally, a ratio of CHI monomer to HEP dimer was estimated and found to be equal to 5.30, indicating that CHI is the dominant species in the $[CHI/HEP]_2$ films as predicted in literature [53]. This is not surprising considering the higher charge density of the HEP dimer, resulting in a +/- ratio of 1.19. The ratio of HEP dimer to LL-37 peptide was estimated for the $[CHI/HEP]_2/[CHI/PPCs]_6$ coated sample as well and an average value of 5.17 was found, which translates in a (-/+) ratio of 1.99. This matches the optimal ratio for PPCs formation found previously by C. Vranckx.

As the presence of LL-37 was proved, the antibacterial activity of the coating as constructed was measured. Unfortunately, bacterial tests in the presence of *S. aureus* showed no significant effect of the PPCs coating or the $[CHI/HEP]_2$ cushion at this stage. Several explanations were proposed to explain the lack of activity of the LL-37 peptide in the layers. Firstly, it was suggested that the PPC configuration in

which the peptide is trapped could hinder its contact with bacteria and therefore its activity. Moreover, as described in Section 3.2 of the State of the Art, the multilayer configuration could also restrict the contact of the peptide with the bacteria. Given the thickness of the layers and the strength of the peptide-polyelectrolyte interactions, the diffusion of LL-37 in the layers may be difficult. This would restrict the activity of the coating to the PPCs adsorbed in the outermost layer only.

In order to verify the effect of LL-37 complexation with HEP on the antibacterial activity, a comparison was made between the MICs of PPCs and LL-37 tested in suspension against *S. aureus* and *S. epidermis*. Lecture of the MIC endpoint after exposure to LL-37 with the bare eye gave uncertain results, hence a metabolic activity test with resazurin was performed. This revealed an inhibition of the growth of bacterial cells exposed to LL-37 at concentrations of 140 µg/mL and 70.2 µg/mL for *S. aureus* and *S. epidermis* respectively. These values are hard to compare with the literature since several authors reported different MIC values (see section 2.3.2 of State of the Art). In contrast with the results for LL-37, the MIC of the PPCs (LL-37 + HEP) was never reached. Even at a concentration of 1125 µg/mL, bacterial growth could still be observed.

Hence, this result made it clear that LL-37 suffers activity loss when complexed with HEP in a PPC. Its antibacterial mechanism involves direct contact with the bacteria, mediated by the electrostatic interaction of the cationic peptide with the bacterial membrane. As suggested before, the complexation state of the peptide may reduce its availability and prevent the initial contact and interaction with the bacteria.

Following these findings, the question of the optimal configuration of LL-37 into the coating must be raised. Should the peptide be released from its complex and from the multilayers in the environment to allow its bactericidal action or be presented as attached to the surface anyway? In the first case, the release of the peptide should be controlled over time to avoid an initial 'burst', followed by a decrease of the peptide concentration that could not be sufficient anymore to kill the microorganisms.

Hence, to explore the possibility of release of LL-37 into the environment, its release kinetics must be studied. To allow its release from the layers, their disassembly was initiated by changing the solution pH to 9 and ionic strength to 150 mM or adding a detergent to the film. Both methods resulted in mass desorption of the multilayers that was monitored using the QCM-D. Surface analysis by XPS showed very little difference in surface elemental composition when the pH and ionic strength were changed, suggesting that the initial architecture of the layers was maintained even after partial disassembly, or that uppermost layers were removed, leaving underlying layers of the same kind exposed to the surface. The addition of SDS on the contrary showed an important change in the elemental composition, suggesting that the detergent was partially adsorbed in the multilayers. Hence, if the coating is applied on an implant into the body, the first method seems to be the most appropriate, since the physiological pH and salinity could be sufficient to induce release of LL-37.

Following layer disassembly, the next step was to investigate the induced release of LL-37 over time. Unfortunately, this experiment could not be carried out and will be detailed in the future prospects.

Part VII

Future prospects

The second part of this master thesis was carried out in a particular context of sanitary crisis due to the outbreak of the Covid-19 pandemic. This unusual situation resulted in the closing of all university facilities, including laboratories. Consequently, the research activities planned for the second semester were suspended prematurely and certain experiments could not be completed. In this section, the intended experiments which would normally have been conducted in a normal situation are described.

1 LL-37 quantification

The quantification of the amount of LL-37 adsorbed in the multilayers is a crucial step in the characterisation of the coating. This would have been done by means of a quantitative LL-37 ELISA test. This sandwich-type enzyme-linked immunosorbent assay allows detection of LL-37 with a sensitivity in the range of 0.2-1 ng/mL, depending on the supplier. Its principle relies on the interaction between a LL-37-specific antibody that binds to the peptide. An enzyme-labeled antibody then binds to the captured LL-37, and the activity of the enzyme is measured spectrophotometrically. The absorbance is proportional to the amount of LL-37 and its concentration in the sample can then be obtained by using a standard curve.

However, given the complexed state of LL-37, it is not known whether it will be able to interact with the antibody coating of the ELISA test. Therefore, the test should be carried out first on a well-known quantity of LL-37 in PPC. If the peptide in the PPCs is not detected by ELISA, it will probably not be detected in the multilayers either and its release through layer disassembly will be necessary.

2 LL-37 release kinetics

As mentioned in the general discussion, the controlled release of LL-37 from the multilayers may be necessary to allow its bactericidal action. To achieve this, layer disassembly was initiated by a rise in pH and I. Previous experiments proved that desorption of compounds occurred from the film, however this desorbed mass was neither identified nor quantified. The above-mentioned ELISA test has the ability to measure the concentration of LL-37, and would allow quantification of its release over different time periods. Since the pH rise induces a decrease of the charge of LL-37 and consequently a weakening of the peptide-PE bond, the peptide has a better chance to interact with the antibody of the ELISA.
If the measured concentration is above the MIC determined in Section 2.3 of Results, the experiment may be repeated in presence of bacteria to see if the release of LL-37 has more effect than the previously tested coating.

3 Influence of the outermost layer

Regarding the characterisation experiments, a comparison of the bacterial activity of a CHI-terminated sample and a PPCs-terminated sample could provide information on the influence of the outermost layer. The diffusion capacity of the peptide into the layers could also be investigated by conducting XPS analysis on a CHI-terminated sample and comparing the obtained elemental composition with the PPC-terminated sample.

Part VIII
Conclusion

Throughout this master thesis, the use of the LL-37 peptide as a component of an antibacterial coating designed to prevent bacterial adhesion and biofilm formation on hip implants was studied. To facilitate its adsorption into the coating, this peptide was complexed with heparin to form a PPC. The difficulty of the selected approach has been to find a good compromise between the stable immobilisation of LL-37 and the preservation of an antibacterial activity of the peptide in the coating.

The coating was thus constructed by successive adsorption of oppositely-charged polyelectrolytes and PPCs, to obtain [CHI/HEP]2/$[CHI/PPCs]_6$ multilayers. This construction was monitored by QCM-D, and the adsorbed mass for each adsorption step could be calculated. This LBL construction strategy yielded a highly hydrated film with a final thickness of 152 nm. The surface composition was assessed using XPS, that confirmed the incorporation of LL-37 in the multilayers. Further analysis of the elemental composition obtained with this technique showed a HEP to LL-37 ratio of 5.17 in the surface layer that ties in with the expected values. Chitosan was proved to be the dominant species in the $[CHI/HEP]_2$ cushion. Finally, XPS and QCM experiments proved that rising the pH to 9 and I to 150 mM is an effective method to partially deconstruct the layers without altering their relative composition.

Secondly, a bacterial test with *S. aureus* proved that neither the cushion nor the full coating demonstrated a significant antibacterial or antibiofilm effect. The reduction of LL-37s activity due to its complexed state and its position in the multilayers was proposed as an explanation. To verify this, a MIC test was carried out on LL-37 and PPCs, in order to study the effect of complexation on the peptide's activity. Inhibition of the growth of bacterial cells exposed to LL-37 was observed at concentrations of 140 µg/mL for *S. aureus* and 70.2 µg/mL for *S. epidermis*. LL-37 complexed in PPCs however showed no inhibition at all, even at relatively high concentrations. This confirms the loss of activity of the peptide upon complexation.

Hence, these findings bring some elements of the response to the initial research question formulated at the beginning of this work. It is now clear that the incorporation of LL-37 into the coating as a PPC is an advantage for the build-up and stability of the multilayers. However, its loss of activity is a major drawback and requires implementation of new strategies to free the peptide and allow its diffusion in the environment.

In conclusion, the present work highlights the potential of the PPC method to immobilise AMPs in multilayers and form a stable coating. However, the impact of the complexation on the activity of the immobilised AMP was also demonstrated. Further research is thus necessary to unravel the way the PPCs configuration influences the activity of the AMP. Furthermore, a way must be found to recover the activity of the immobilised peptide, with the aim to create an effective antibacterial coating that would be used to prevent biofilm formation on the surface of hip implants. Although we are not there yet, this would be a

first step towards reduction of the infection rate of implants after hip arthroplasty, and the improvement of patients life quality.

References

[1] Romain Hardy. Titanium implant coatings composed of chitosan and heparin to promote osseointegration. Master's thesis, Université Catholique de Louvain, 2019.

[2] Eurostat. Surgical operations and procedures statistics. Technical report, European Union, 2017.

[3] Orthopride. Belgian hip and knee arthroplasty registry annual report 2017 orthopride. Technical report, Inami, 2017.

[4] C. Pabinger and A. Geissler. Utilization rates of hip arthroplasty in oecd countries. *Osteoarthritis and Cartilage*, 22(6):734 – 741, 2014.

[5] American Academy of Orthopaedic Surgeons Jared R. H. Foran. Total hip replacement. `https://orthoinfo.aaos.org/en/treatment/total-hip-replacement`, August 2015. Accessed on 2020-31-03.

[6] R. Pivec, A. J. Johnson, S. C. Mears, and M. A. Mont. Hip arthroplasty. *The Lancet*, 380(9855):1768–1777, 2012. Cited By :222.

[7] S. D. Ulrich, T. M. Seyler, D. Bennett, R. E. Delanois, K. J. Saleh, I. Thongtrangan, M. Kuskowski, E. Y. Cheng, P. F. Sharkey, J. Parvizi, J. B. Stiehl, and M. A. Mont. Total hip arthroplasties: What are the reasons for revision? *International orthopaedics*, 32(5):597–604, 2008. Cited By :185.

[8] Dragos Apostu, Ondine Lucaciu, Cristian Berce, Dan Lucaciu, and Dan Cosma. Current methods of preventing aseptic loosening and improving osseointegration of titanium implants in cementless total hip arthroplasty: a review. *Journal of International Medical Research*, 46(6):2104–2119, 2018.

[9] Yousef Abu-Amer, Isra Darwech, and John C Clohisy. Aseptic loosening of total joint replacements: mechanisms underlying osteolysis and potential therapies. *Arthritis research & therapy*, 9(S1):S6, 2007.

[10] K. L. Ong, S. M. Kurtz, E. Lau, K. J. Bozic, D. J. Berry, and J. Parvizi. Prosthetic joint infection risk after total hip arthroplasty in the medicare population. *Journal of Arthroplasty*, 24(6 SUPPL.):105–109, 2009. Cited By :278.

[11] Aaron J. Tande and Robin Patel. Prosthetic joint infection. *Clinical Microbiology Reviews*, 27(2):302–345, 2014.

[12] F. Gemmel, H. Van Den Wyngaert, C. Love, M. M. Welling, P. Gemmel, and C. J. Palestro. Prosthetic joint infections: Radionuclide state-of-the-art imaging. *European Journal of Nuclear Medicine and Molecular Imaging*, 39(5):892–909, 2012.

[13] S. Veerachamy, T. Yarlagadda, G. Manivasagam, and P. K. Yarlagadda. Bacterial adherence and biofilm formation on medical implants: A review. *Proceedings of the Institution of Mechanical Engineers, Part H: Journal of Engineering in Medicine*, 228(10):1083–1099, 2014.

[14] B. Hollmann, M. Perkins, and D. Walsh. Biofilms and their role in pathogenesis. `https://www.immunology.org/public-information/bitesized-immunology/pathogens-and-disease/biofilms-and-their-role-in`, 2020. Accessed on 2020-18-04.

[15] Carla Renata Arciola, Davide Campoccia, and Lucio Montanaro. Implant infections: adhesion, biofilm formation and immune evasion. *Nature Reviews Microbiology*, 16(7):397, 2018.

[16] Nira Rabin, Yue Zheng, Clement Opoku-Temeng, Yixuan Du, Eric Bonsu, and Herman O Sintim. Biofilm formation mechanisms and targets for developing antibiofilm agents. *Future medicinal chemistry*, 7(4):493–512, 2015.

[17] Anthony Daniel Verderosa, Makrina Totsika, and Kathryn E Fairfull-Smith. Bacterial biofilm eradication agents: a current review. *Frontiers in Chemistry*, 7:824, 2019.

[18] J. J. T. M. Swartjes, P. K. Sharma, T. G. VanKooten, H. C. Van DerMei, M. Mahmoudi, H. J. Busscher, and E. T. J. Rochford. Current developments in antimicrobial surface coatings for biomedical applications. *Current medicinal chemistry*, 22(18):2116–2129, 2015.

[19] J. Gallo, M. Holinka, and C. S. Moucha. Antibacterial surface treatment for orthopaedic implants. *International Journal of Molecular Sciences*, 15(8):13849–13880, 2014.

[20] M. R. Nejadnik, H. C. van der Mei, W. Norde, and H. J. Busscher. Bacterial adhesion and growth on a polymer brush-coating. *Biomaterials*, 29(30):4117–4121, 2008. Cited By :141.

[21] A. J. Duplantier and M. L. van Hoek. The human cathelicidin antimicrobial peptide ll-37 as a potential treatment for polymicrobial infected wounds. *Frontiers in Immunology*, 4(JUL), 2013. Cited By :76.

[22] R. E. W. Hancock and H. . Sahl. Antimicrobial and host-defense peptides as new anti-infective therapeutic strategies. *Nature biotechnology*, 24(12):1551–1557, 2006. Cited By :2323.

[23] L. . Zhang and R. L. Gallo. Antimicrobial peptides. *Current Biology*, 26(1):R14–R19, 2016. Cited By :166.

[24] D. Vandamme, B. Landuyt, W. Luyten, and L. Schoofs. A comprehensive summary of ll-37, the factoctum human cathelicidin peptide. *Cellular immunology*, 280(1):22–35, 2012. Cited By :267.

[25] H. Jenssen, P. Hamill, and R. E. W. Hancock. Peptide antimicrobial agents. *Clinical microbiology reviews*, 19(3):491–511, 2006. Cited By :1427.

[26] W. C. Wimley. Describing the mechanism of antimicrobial peptide action with the interfacial activity model. *ACS Chemical Biology*, 5(10):905–917, 2010. Cited By :469.

[27] S. A. Onaizi and S. S. J. Leong. Tethering antimicrobial peptides: Current status and potential challenges. *Biotechnology Advances*, 29(1):67–74, 2011. Cited By :176.

[28] G. Wang. Structures of human host defense cathelicidin ll-37 and its smallest antimicrobial peptide kr-12 in lipid micelles. *Journal of Biological Chemistry*, 283(47):32637–32643, 2008. Cited By :201.

[29] S. N. Dean, B. M. Bishop, and M. L. van Hoek. Natural and synthetic cathelicidin peptides with anti-microbial and anti-biofilm activity against staphylococcus aureus. *BMC microbiology*, 11:114, 2011. Cited By :127.

[30] J. Overhage, A. Campisano, M. Bains, E. C. W. Torfs, B. H. A. Rehm, and R. E. W. Hancock. Human host defense peptide ll-37 prevents bacterial biofilm formation. *Infection and immunity*, 76(9):4176–4182, 2008. Cited By :327.

[31] J. Turner, Y. Cho, N. . Dinh, A. J. Waring, and R. I. Lehrer. Activities of ll-37, a cathelin-associated antimicrobial peptide of human neutrophils. *Antimicrobial Agents and Chemotherapy*, 42(9):2206–2214, 1998. Cited By :558.

[32] U. H. N. Dürr, U. S. Sudheendra, and A. Ramamoorthy. Ll-37, the only human member of the cathelicidin family of antimicrobial peptides. *Biochimica et Biophysica Acta - Biomembranes*, 1758(9):1408–1425, 2006. Cited By :549.

[33] S. Parithimarkalaignan and Thallam Padmanabhan. Osseointegration: An update. *The Journal of Indian Prosthodontic Society*, 13, 03 2013.

[34] C. Y. Hu and T. . Yoon. Recent updates for biomaterials used in total hip arthroplasty. *Biomaterials Research*, 22(1), 2018. Cited By :2.

[35] A. Durán, A. Conde, A. Gómez Coedo, T. Dorado, C. García, and S. Ceré. Sol-gel coatings for protection and bioactivation of metals used in orthopaedic devices. *Journal of Materials Chemistry*, 14(14):2282–2290, 2004. Cited By :77.

[36] X. Liu, P. K. Chu, and C. Ding. Surface modification of titanium, titanium alloys, and related materials for biomedical applications. *Materials Science and Engineering R: Reports*, 47(3-4):49–121, 2004. Cited By :2202.

[37] Rafael R Silva, KYPS Avelino, Kalline L Ribeiro, Octavio L Franco, Maria DL Oliveira, and Cesar AS Andrade. Chemical immobilization of antimicrobial peptides on biomaterial surfaces. *Front Biosci (Schol Ed)*, 8:129–142, 2016.

[38] Matthias Gabriel, Kamran Nazmi, Enno C Veerman, Arie V Nieuw Amerongen, and Andrej Zentner. Preparation of ll-37-grafted titanium surfaces with bactericidal activity. *Bioconjugate chemistry*, 17(2):548—550, 2006.

[39] G. T. Qin, A. Lopez, C. Santos, A. M. McDermott, and C. Z. Cai. Antimicrobial peptide ll-37 on surfaces presenting carboxylate anions. *Biomaterials Science*, 3:771–778, 2015.

[40] Margaret E. Cassin, Andrew J. Ford, Sophia M. Orbach, Scott E. Saverot, and Padmavathy Rajagopalan. The design of antimicrobial ll37-modified collagen-hyaluronic acid detachable multilayers. *Acta Biomaterialia*, 40:119 – 129, 2016.

[41] B. Abinaya, T. P. Prasith, B. Ashwin, S. Viji Chandran, and N. Selvamurugan. Chitosan in surface modification for bone tissue engineering applications. *Biotechnology Journal*, 14(12), 2019.

[42] M. M. De Villiers, D. P. Otto, S. J. Strydom, and Y. M. Lvov. Introduction to nanocoatings produced by layer-by-layer (lbl) self-assembly. *Advanced Drug Delivery Reviews*, 63(9):701–715, 2011. Cited By :228.

[43] Kaiyong Cai, Annett Rechtenbach, Jianyuan Hao, Jörg Bossert, and Klaus D. Jandt. Polysaccharide-protein surface modification of titanium via a layer-by-layer technique: Characterization and cell behaviour aspects. *Biomaterials*, 26(30):5960 – 5971, 2005.

[44] R. A. Silva, M. D. Urzúa, D. F. S. Petri, and P. L. Dubin. Protein adsorption onto polyelectrolyte layers: Effects of protein hydrophobicity and charge anisotropy. *Langmuir*, 26(17):14032–14038, 2010. Cited By :73.

[45] A. Vander Straeten, A. Bratek-Skicki, A. M. Jonas, C. . Fustin, and C. Dupont-Gillain. Integrating proteins in layer-by-layer assemblies independently of their electrical charge. *ACS Nano*, 12(8):8372–8381, 2018. Cited By :6.

[46] D. W. Van Krevelen and K. Te Nijenhuis. Chapter 9 - limiting viscosity number (intrinsic viscosity) and related properties of very dilute solutions. In D. W. Van Krevelen and K. Te Nijenhuis, editors, *Properties of Polymers (Fourth Edition)*, pages 245 – 284. Elsevier, fourth edition edition.

[47] Martien Cohen Stuart, Renko de Vries, and Hans Lyklema. Chapter 2 - polyelectrolytes. In J. Lyklema, editor, *Soft Colloids*, volume 5 of *Fundamentals of Interface and Colloid Science*, pages 2.1 – 2.84. Academic Press.

[48] D. Raafat and H. . Sahl. Chitosan and its antimicrobial potential - a critical literature survey. *Microbial Biotechnology*, 2(2 SPEC. ISS.):186–201, 2009. Cited By :285.

[49] E. I. Rabea, M. E. . Badawy, C. V. Stevens, G. Smagghe, and W. Steurbaut. Chitosan as antimicrobial agent: Applications and mode of action. *Biomacromolecules*, 4(6):1457–1465, 2003. Cited By :1672.

[50] I. Younes and M. Rinaudo. Chitin and chitosan preparation from marine sources. structure, properties and applications. *Marine Drugs*, 13(3):1133–1174, 2015. Cited By :526.

[51] I. Younes, S. Sellimi, M. Rinaudo, K. Jellouli, and M. Nasri. Influence of acetylation degree and molecular weight of homogeneous chitosans on antibacterial and antifungal activities. *International journal of food microbiology*, 185:57–63, 2014. Cited By :122.

[52] R. P. Carlson, R. Taffs, W. M. Davison, and P. S. Stewart. Anti-biofilm properties of chitosan-coated surfaces. *Journal of Biomaterials Science, Polymer Edition*, 19(8):1035–1046, 2008. Cited By :128.

[53] M. Lundin, F. Solaqa, E. Thormann, L. MacAkova, and E. Blomberg. Layer-by-layer assemblies of chitosan and heparin: Effect of solution ionic strength and ph. *Langmuir*, 27(12):7537–7548, 2011. Cited By :62.

[54] Sigma Aldrich. What is heparin? `https://www.sigmaaldrich.com/technical-documents/articles/biology/what-is-heparin.html`, April 2020. Accessed on 2020-02-04.

[55] E. I. Oduah, R. J. Linhardt, and S. T. Sharfstein. Heparin: Past, present, and future. *Pharmaceuticals*, 9(3), 2016. Cited By :39.

[56] Y. Shu, G. Ou, L. Wang, J. Zou, and Q. Li. Surface modification of titanium with heparin-chitosan multilayers via layer-by-layer self-assembly technique. *Journal of Nanomaterials*, 2011, 2011. Cited By :20.

[57] J. Fu, J. Ji, W. Yuan, and J. Shen. Construction of anti-adhesive and antibacterial multilayer films via layer-by-layer assembly of heparin and chitosan. *Biomaterials*, 26(33):6684–6692, 2005. Cited By :368.

[58] Nicolas Schonbeck, Knut Kvale, Thomas Demarcy, Joanna Giermanska, J-P Chapel, and J.-F. Berret. Surfactant-triggered disassembly of electrostatic complexes probed at optical and quartz crystal microbalance length scales. *Langmuir : the ACS journal of surfaces and colloids*, 30 19:5620–7, 2014.

[59] Khalil Abdelkebir, Fabien Gaudière, Sandrine Morin-Grognet, Gérard Coquerel, Hassan Atmani, Béatrice Labat, and Guy Ladam. Protein-triggered instant disassembly of biomimetic layer-by-layer films. *Langmuir : the ACS journal of surfaces and colloids*, 27 23:14370–9, 2011.

[60] N.G. Hoogeveen, M.A. Cohen Stuart, G.J. Fleer, and M.R. Böhmer. Formation and stability of multilayers of polyelectrolytes. *Langmuir*, 12:3675–3681, 1996.

[61] Stephan T. Dubas, Tarek R. Farhat, and Joseph B. Schlenoff. Multiple membranes from "true" polyelectrolyte multilayers. *Journal of the American Chemical Society*, 123(22):5368–5369, 2001.

[62] Jing Kang and Lars Dähne. Strong response of multilayer polyelectrolyte films to cationic surfactants. *Langmuir : the ACS journal of surfaces and colloids*, 27(8):4627–4634, 2011.

[63] Md Arifur Rahim, Won San Choi, Ha-Jin Lee, and Il Cheol Jeon. Ionic surfactant-triggered renewal of the structures and properties of polyelectrolyte multilayer films. *Langmuir : the ACS journal of surfaces and colloids*, 26(7):4680—4686, April 2010.

[64] Ossila. Uv ozone cleaner: overview. `https://www.ossila.com/products/uv-ozone-cleaner?variant=1200242961`, March 2020. Accessed on 2020-19-03.

[65] G. Decher. Fuzzy nanoassemblies: Toward layered polymeric multicomposites. *Science*, 277(5330):1232–1237, 1997. Cited By :8799.

[66] Todd J. Dolinsky, Jens E. Nielsen, J. Andrew McCammon, and Nathan A. Baker. PDB2PQR: an automated pipeline for the setup of Poisson–Boltzmann electrostatics calculations. *Nucleic Acids Research*, $32(\text{suppl}_2) : W665 - -W667, 072004$.

[67] I. Reviakine, D. Johannsmann, and R. P. Richter. Hearing what you cannot see and visualizing what you hear: Interpreting quartz crystal microbalance data from solvated interfaces. *Analytical Chemistry*, 83(23):8838–8848, 2011. Cited By :376.

[68] Nanoscience Instruments. Quartz crystal microbalance (qcm). https://www.nanoscience.com/techniques/quartz-crystal-microbalance/, March 2020. Accessed on 2020-27-03.

[69] Biolin Scientific. Qsensor qsx 310 ti product information. Technical report, Biolin Scientific AB.

[70] Huaiyu Wang and Paul K. Chu. Chapter 4 - surface characterization of biomaterials. In Amit Bandyopadhyay and Susmita Bose, editors, *Characterization of Biomaterials*, pages 105 – 174. Academic Press, Oxford, 2013.

[71] J.A. Woollam. What is ellipsometry? https://www.jawoollam.com/resources/ellipsometry-tutorial/ellipsometry-data-analysis, March 2020. Accessed on 2020-28-03.

[72] MERTON L. THOMAS L. McMEEKIN and GROVESNORBERT J. HIPP. Chapter 4 - refractive indices of amino acids, proteins, and related substances. In Jacob A. Stekol, editor, *Amino Acids and Serum Proteins*, pages 54–66. ACS Publications, Washington D.C., 1964.

[73] Dupont-Gillain Christine C. Rouxhet Paul Genet, Michel. Chapter 5 - xps analysis of biosystems and biomaterials. In Egon Matijevic, editor, *Medical Applications of Colloids*, pages 177–307. Springer, New York, 2008.

[74] Warren Levinson. Chapter 13 - sterilization and disinfection. In Brian Kearns. Michael Weitz, editor, *Review of medical microbiology and immunology*. McGraw-Hill Education, 2016.

[75] Joseph McFarland. The nephelometer: an instrument for estimating the number of bacteria in suspensions used for calculating the opsonic index and for vaccines. *Journal of the American Medical Association*, XLIX(14):1176–1178, 10 1907.

[76] Irith Wiegand, Kai Hilpert, and Robert Hancock. Agar and broth dilution methods to determine the minimal inhibitory concentration (mic) of antimicrobial substances. *Nature Protocols*, 3(2):163–175, 2 2008.

[77] EUCAST. Eucast reading guide for broth microdilution. Technical report, European Committee on Antimicrobial Susceptibility Testing, 2020.

[78] D A Steinberg, M A Hurst, C A Fujii, A H Kung, J F Ho, F C Cheng, D J Loury, and J C Fiddes. Protegrin-1: a broad-spectrum, rapidly microbicidal peptide with in vivo activity. *Antimicrobial Agents and Chemotherapy*, 41(8):1738–1742, 1997.

[79] A. Giacometti, O. Cirioni, F. Barchiesi, M. S. Del Prete, M. Fortuna, F. Caselli, and G. Scalise. In vitro susceptibility tests for cationic peptides: Comparison of broth microdilution methods for bacteria that grow aerobically. *Antimicrobial Agents and Chemotherapy*, 44(6):1694–1696, 2000.

[80] Mounyr Balouiri, Moulay Sadiki, and Saad Koraichi Ibnsouda. Methods for in vitro evaluating antimicrobial activity: A review. *Journal of Pharmaceutical Analysis*, 6(2):71 – 79, 2016.

[81] Rita Csepregi, Beáta Lemli, Sándor Kunsági-Máté, Lajos Szente, Tamás Kőszegi, Balázs Németi, and Miklós Poór. Complex formation of resorufin and resazurin with -cyclodextrins: Can cyclodextrins interfere with a resazurin cell viability assay? *Molecules (Basel, Switzerland)*, 23(2), February 2018.

[82] L. Richert, P. Lavalle, E. Payan, X. Z. Shu, G. D. Prestwich, J. . Stoltz, P. Schaaf, J. . Voegel, and C. Picart. Layer by layer buildup of polysaccharide films: Physical chemistry and cellular adhesion aspects. *Langmuir*, 20(2):448–458, 2004. Cited By :421.

[83] A. Vander Straeten, A. Bratek-Skicki, L. Germain, C. D'Haese, P. Eloy, C. . Fustin, and C. Dupont-Gillain. Protein-polyelectrolyte complexes to improve the biological activity of proteins in layer-by-layer assemblies. *Nanoscale*, 9(44):17186–17192, 2017. Cited By :12.

[84] Günter Auernhammer, Hans-Jürgen Butt, and Doris Vollmer. Swelling and water uptake of pah/pss polyelectrolyte multilayers. In *Surface and interfacial forces-from fundamentals to applications*, volume 134. Springer, 2008.

[85] J. Hanania, K. Stenhouse, and J. Donev. Energy education - bandgap [online]. `https://energyeducation.ca/encyclopedia/Band_gap#cite_note-RE2-1`, 2015. Accessed on 2020-24-04.

[86] Inelastic mean free path calculator for electron spectroscopy. `http://electronsoftware.altervista.org/lab/IMFP.html`. Accessed on 2020-24-04.

[87] S. Tanuma, C. J. Powell, and D. R. Penn. Calculation of electron inelastic mean free paths (imfps) vii. reliability of the tpp-2m imfp predictive equation. *Surface and Interface Analysis*, 35(3):268–275, 2003.

[88] G. Lawrie, I. Keen, B. Drew, A. Chandler-Temple, L. Rintoul, P. Fredericks, and L. Grøndahl. Interactions between alginate and chitosan biopolymers characterized using ftir and xps. *Biomacromolecules*, 8(8):2533–2541, 2007. Cited By :585.

[89] AH Robertson. Averaging bacterial counts. *Journal of bacteriology*, 23(2):123, 1932.

[90] V. Prakash, J. S. Lewis, and J. H. Jorgensen. Vancomycin mics for methicillin-resistant staphylococcus aureus isolates differ based upon the susceptibility test method used. *Antimicrobial Agents and Chemotherapy*, 52(12):4528–4528, 2008.

[91] Arjun Ojha Kshetry, Narayan Dutt Pant, Raju Bhandari, Sabita Khatri, Krishma Laxmi Shrestha, Shambhu Kumar Upadhaya, Asia Poudel, Binod Lekhak, and Bijendra Raj Raghubanshi. Minimum inhibitory concentration of vancomycin to methicillin resistant staphylococcus aureus isolated from different clinical samples at a tertiary care hospital in nepal. *Antimicrobial Resistance and Infection Control*, 5, 2016.

[92] European Committee for Antimicrobial Susceptibility Testing (EUCAST) of the European Society of Clinical Microbiology and Infectious Diseases (ESCMID) . Determination of minimum inhibitory concentrations (mics) of antibacterial agents by broth dilution. *Clinical Microbiology and Infection*, 9(8):ix–xv, 2003.

Characterisation of a coating composed of LL-37-heparin complexes and study of its antibacterial activity

Alix Mertens de Wilmars

Nowadays, the rising incidence of prosthetic joint infection after hip replacement surgeries triggers the need to improve the properties of the devices implanted in our body. In this context, an antibacterial coating was developed, with the aim to prevent bacterial adhesion and biofilm formation on the surface of the implant. This coating was constructed by successive adsorption of two oppositely-charged polyelectrolytes, chitosan and heparin, in a layer-by-layer fashion. The LL-37 peptide, which has proved to possess significant antibacterial and antibiofilm activity, was complexed with heparin in a protein-polyelectrolyte complex (PPC) for an optimal integration into the coating.

The objective of this work was to characterise the developed coating, to assess its antibacterial activity and to study the use of the antimicrobial agent LL-37 into the coating set-up. Characterisation methods such as quartz crystal microbalance, ellipsometry and X-ray photoelectron spectroscopy allowed validation of the correct multilayer construction and confirmation of the presence of LL-37.

A bacterial activity test with S. aureus revealed no antibacterial or antibiofilm effect of the coating at this stage. It was suggested that the complexed state of LL-37 and its position in the multilayers might be responsible for a diminished contact of the peptide with bacteria, resulting in a decreased activity. To verify the loss of activity of the peptide upon complexation, the minimal inhibitory concentration of LL-37 was determined. It was shown that even at high concentrations, the peptide complexed with heparin in a PPC did not inhibit bacterial growth. In opposition, the free-standing LL-37 peptide showed bacterial inhibition at concentrations of 140 and 70 g/mL for S. aureus and S. epidermis respectively.

This suggests that the release of LL-37 from its PPC configuration into the immediate environment could potentially enhance the antibacterial activity of the coating. However, this release must be studied and controlled over time. Further research is thus required to obtain an effective antibacterial coating that would be used to prevent biofilm formation on the surface of hip implants.

Université catholique de Louvain
Faculty of Bioscience Engineering
Croix du Sud, 2bte L7.05.01, 1348 Louvain-La-Neuve, Belgique | www.uclouvain.be/agro